Electronic Supplementary Material (ESI) for Dalton Transactions.

Quadratic and Cubic Hyperpolarizabilities of Nitro-phenyl/-naphthalenyl/-anthracenyl Alkynyl Complexes

Jun Du,[a] Mahbod Morshedi,[b] Graeme J. Moxey,[b] Mahesh S. Kodikara,[b] Adam Barlow,[b] Cristóbal Quintana,[b] Genmiao Wang,[b] Robert Stranger,[b] Chi Zhang,[a] Marie P. Cifuentes,[a,b] and Mark G. Humphrey*[a,b]

[a] J. Du, Prof. C. Zhang, Prof. M. P. Cifuentes, Prof. M. G. Humphrey
School of Chemical and Material Engineering, Jiangnan University
Wuxi 214122, Jiangsu Province (P. R. China)

[b] M. S. Kodikara, Dr G. J. Moxey, Dr M. Morshedi, Dr A. Barlow, C. Quintana, Dr G. Wang, Prof. R. Stranger, A/Prof. M. P. Cifuentes, Prof. M. G. Humphrey
Research School of Chemistry, Australian National University,
Canberra, ACT 2601 (Australia)
E-mail: mark.humphrey@anu.edu.au

Contents:

Experimental Section

Materials. All reactions were performed under a nitrogen atmosphere with the use of Schlenk techniques unless otherwise stated. Reaction solvents diethyl ether (sodium/benzophenone), CH_2Cl_2 (CaH_2), and MeOH (Mg/I_2) were dried by standard methods before use, and triethylamine was deoxygenated before use. Petrol refers to a fraction of petroleum spirits with a boiling range 60 – 90 °C. Chromatography was on silica gel (230-400 mesh) or basic alumina. Sodium hexafluorophosphate was recrystallized from acetonitrile prior to use. All commercially available materials were used as received. The following compounds were synthesized by literature procedures: 1-nitro-4-(trimethylsilylethynyl)naphthalene (**1**),[1], 9-bromoanthracene,[2] $[RuCl(dppe)_2]PF_6$,[3] *cis*-$[RuCl_2(dppm)_2]$,[4] $RuCl(PPh_3)_2(\eta^5\text{-}C_5H_5)$,[5] $NiCl(PPh_3)(\eta^5\text{-}C_5H_5)$,[6] $AuCl(PPh_3)$,[7] *trans*-$[Ru(C{\equiv}C\text{-}4\text{-}C_6H_4\text{-}1\text{-}NO_2)Cl(dppe)_2]$ (**6a**),[8] *trans*-$[Ru(C{\equiv}C\text{-}4\text{-}C_6H_4\text{-}1\text{-}NO_2)Cl(dppm)_2]$ (**7a**),[9] $Ru(C{\equiv}C\text{-}4\text{-}C_6H_4\text{-}1\text{-}NO_2)(PPh_3)_2(\eta^5\text{-}C_5H_5)$ (**8a**),[10] $Ni(C{\equiv}C\text{-}4\text{-}C_6H_4\text{-}1\text{-}NO_2)(PPh_3)(\eta^5\text{-}C_5H_5)$ (**9a**),[11] and $Au(C{\equiv}C\text{-}4\text{-}C_6H_4\text{-}1\text{-}NO_2)(PPh_3)$ (**10a**).[12]

Instrumentation. Microanalyses were carried out at the School of Human Sciences, Science Centre, London Metropolitan University, U.K. UV-vis-NIR spectra were recorded as CH_2Cl_2 solutions in 1 cm quartz cells using Cary 5 or Lambda TU1901 spectrophotometers, and are reported as λ_{max} nm (ε 10^4 M^{-1} cm^{-1}). Vibrational spectra were collected on Thermo Fisher Nicolet 6700 ATR IR spectrometer, and are reported in cm^{-1}. ^1H NMR (400 MHz), ^{13}C NMR (101 MHz) and ^{31}P NMR (162 MHz) spectra were recorded using Bruker AVANCE III 400 MHZ FT NMR or Varian Gemini-400 NMR spectrometers, and are referenced to residual chloroform (7.26 ppm), $CDCl_3$ (77.0 ppm), or external 85% H_3PO_4 (0.0 ppm), respectively. Mass spectra were recorded using a Micromass/Waters LCT-ZMD single quadrupole liquid chromatograph-MS (ESI MS, both unit resolution and HR), a VG Quattro II triple quadrupole MS (EI MS, unit resolution), a VG AutoSpec M series sector (EBE), a Micromass/Waters Quattro MicroInstrumentation (ESI-MS), or a Bruker SCIONSQ-456-GC (EI-MS)**.** Mass spectral peaks are reported as *m/z* (relative intensity, assignment).

Synthesis.

4-Ethynyl-1-nitronaphthalene (2): 1-Nitro-4-(trimethylsilylethynyl)naphthalene (0.808 g, 3.00 mmol) was added to a mixture of CH_2Cl_2 and methanol (1:1, 30 mL). K_2CO_3 (0.705 g, 5.1 mmol) was added, and the mixture was stirred for 2 h. Water (10 mL) was added, the product was extracted into CH_2Cl_2, and the organic layer was collected and stirred over anhydrous Na_2SO_4. Following filtration, the solvent volume was reduced under reduced pressure to give **2** as a yellow solid (0.55 g, 2.76 mmol, 92%), identified by comparison of its ^1H NMR spectrum with the reported data.[13] ^1H NMR: δ 8.55 (d, J_{HH} = 8.0 Hz, 1H), 8.50 (d, J_{HH} = 8.0 Hz, 1H), 8.15 (d, J_{HH} = 8.0 Hz, 1H), 7.81 – 7.69 (m, 3H), 3.71 (s, 1H) ppm.

9-Bromo-10-nitroanthracene (3): $NaNO_3$ (0.442 g, 5.20 mmol) was added to a solution of 9-bromoanthracene (1.28 g, 5**.**00 mmol) in a mixture of trifluoroacetic acid (30 mL) and acetic anhydride (50 mL) over a period of 30 min, and the mixture was then stirred for 2 h. The solution was poured into ice water (400 mL) containing conc. H_2SO_4 (3 mL), and the mixture was stirred overnight to hydrolyze the excess acetic anhydride. The resulting solid was collected by filtration, washed repeatedly with water, and then purified by column chromatography, using petrol followed by CH_2Cl_2 as eluant, to give **3** (1.12 g, 3.75 mmol, 75%), identified by comparison of its ^1H NMR spectrum with the reported data.[14] ^1H NMR: δ 8.67 – 8.60 (m, 2H), 7.91 - 7.89 (m, 2H), 7.73 – 7.65 (m, 4H).

9-Nitro-10-(trimethylsilylethynyl)anthracene (4): 9-Bromo-10-nitroanthracene (0.211 g, 0.700 mmol) was added to a mixture of triethylamine and CH_2Cl_2 (1:1, 30 mL). $PdCl_2(PPh_3)_2$ (2.4 mg), CuI (1.2 mg) and trimethylsilylacetylene (0.14 mL, 0.084 g, 1.00 mmol) were added and the reaction was heated to 35 °C and maintained at this temperature overnight. The solution was passed through filter paper, washing with triethylamine, and the solvent was removed from the filtrate. The residue was absorbed onto silica and then passed through a short pad of silica, eluting with petrol:CH_2Cl_2 (4:1). The solvent volume was reduced, affording **4** as a yellow solid (0.160 g, 0.50 mmol, 71%). Elemental analysis calcd (%) for $C_{19}H_{17}NO_2Si$: C 71.44, H 5.36, N 4.38; found: C 71.32, H 5.46, N 4.35. UV-Vis: λ_{max}/nm 414 (1.1), 390 (1.0), 370 (0.7). IR: ν_{max}/cm^{-1} 2159 (C≡C), 1518 (NO_2). ^1H NMR: δ 8.64 – 8.62 (m, 2H), 7.91 - 7.89 (m, 2H), 7.74 – 7.61 (m, 4H), 0.44 (s, 9H) ppm. ^{13}C NMR: δ 145.8, 134.9, 133.5, 130.3, 128.7, 128.6, 123.4, 123.1, 111.3, 101.4, 1.5 ppm. MS (EI): *m*/*z* 319 (M^+, 100%).

10-Ethynyl-9-nitroanthracene (5): 9-Nitro-10-(trimethylsilylethynyl)anthracene (0.160 g, 3.00 mmol) was added to a mixture of CH_2Cl_2 and methanol (1:1, 30 mL). K_2CO_3 (0.705 g, 5.1 mmol) was added, and the mixture was stirred for 1 h. Water (10 mL) was added, and the product was extracted into CH_2Cl_2, drying the extract by stirring over anhydrous Na_2SO_4. Following filtration, the solvent volume was reduced under reduced pressure to give **5** as a yellow solid (0.121 g, 2.91 mmol, 97%). Elemental analysis calcd (%) for $C_{16}H_9NO_2$: C 77.72, H 3.67, N 5.67; found: C 77.70, H 3.59, N 5.74. UV-Vis: λ_{max}/nm 406 (1.0), 385 (0.9). IR: ν_{max}/cm^{-1} 2097 (C≡C), 1506 (NO_2). ^1H NMR: δ 8.68 – 8.65 (m, 2H), 7.93 – 7.90 (m, 2H), 7.71 – 7.65 (m, 4H), 4.13 (s, 1H) ppm. ^{13}C NMR: δ 144.8, 132.5, 128.9, 127.2, 126.9, 126.23, 121.9, 121.7, 120.3, 90.9 ppm. MS (EI): *m*/*z* 247 (M^+, 100%). HRMS: calc for $C_{16}H_9NO_2$: 247.0634, found: 247.0633.

***trans*-[Ru(C≡C-4-$C_{10}H_6$-1-NO_2)Cl(dppe)$_2$] (6b):** $[RuCl(dppe)_2]PF_6$ (0.108 g, 0.100 mmol) and 4-HC≡$CC_{10}H_6$-1-NO_2 (**2**, 0.024 g, 0.12 mmol) were dissolved in CH_2Cl_2 (15 mL) and the resultant solution stirred for 1 h, reduced to a minimal volume of CH_2Cl_2 (5 mL), and then poured into petrol (40 mL). The precipitate was collected and redissolved in CH_2Cl_2. NEt_3 (0.5 mL) was added and the reaction mixture stirred for 15 min, reduced to a minimal volume, triturated with ether (20 mL), and filtered, affording **6b** as a red solid (0.082 g, 0.073 mmol, 73%). Elemental analysis calcd (%) for $C_{64}H_{54}NO_2P_4Ru$: C 68.05, H 4.82, N 1.24; found: C 68.12, H 4.71, N 1.73. UV-Vis: λ_{max}/nm 530 (2.4). IR: ν_{max}/cm^{-1} 2010 (C≡C). ^1H NMR: δ 8.76 (d, J_{HH} = 8.5 Hz, 1H), 8.16 (d, J_{HH} = 8.5 Hz, 1H), 7.70 – 6.70 (m, 43H), 6.47 (d, J_{HH} = 8.5 Hz, 1H), 2.80 (m, 8H) ppm. ^{13}C NMR: δ 139.3, 136.2, 135.8 (m), 134.2, 129.5, 128.8, 128.2, 127.0, 126.5, 125.8, 125.7, 125.4, 123.2, 118.4, 30.2 ppm. ^{31}P NMR: δ 48.3 ppm. MS (ESI): *m*/*z* 1129 (M^+, 25%), 1094 ([M - Cl]$^+$, 100), 898 ([M - C≡$CC_{10}H_6NO_2$ - Cl]$^+$, 10).

***trans*-[Ru(C≡C-4-$C_{10}H_6$-1-NO_2)Cl(dppm)$_2$] (7b)**: A mixture of *cis*-[$RuCl_2$(dppm)$_2$] (200 mg, 0.22 mmol), 4-HC≡C$C_{10}H_6$-1-NO_2 (**2**, 47 mg, 0.24 mmol) and $NaPF_6$ (39 mg, 0.24 mmol) was stirred in CH_2Cl_2 (10 mL) for 3 h at room temperature. NEt_3 (1 mL) was added and the product was immediately absorbed onto alumina and placed on a short chromatography column. Elution with petrol:CH_2Cl_2 (4:1) removed excess acetylene. Subsequent elution with petrol:CH_2Cl_2 (2:3) removed the product. The product was precipitated by removing the CH_2Cl_2 on a rotary evaporator to yield **7b** as a purple powder (104 mg, 0.095 mmol, 43%). Elemental analysis calcd (%) for $C_{62}H_{50}ClNO_2P_4Ru$: C 67.61, H 4.58, N 1.27; found: C 67.46, H 4.62, N 1.25. UV-Vis: λ_{max}/nm 518 (1.9). IR: ν_{max}/cm^{-1} 2023 (C≡C). ^{1}H NMR: δ 8.68 (d, J_{HH} = 8.5 Hz, 1H), 7.92 (d, J_{HH} = 8.5 Hz, 1H), 7.60 – 6.80 (m, 43H), 5.71 (d, J_{HH} = 8.5 Hz, 1H), 5.03 (m, 4H) ppm. ^{13}C NMR: δ 138.9, 136.6, 134.7 (m), 133.4, 129.6, 128.5, 128.4, 127.7, 126.3, 126.2, 125.4, 125.3, 123.0, 50.0 ppm. ^{31}P NMR: δ -7.07 ppm. MS (ESI): *m*/*z* 1101 (M^+, 100%), 1066 ([M - Cl]$^+$, 20).

Ru(C≡C-4-$C_{10}H_6$-1-NO_2)(PPh_3)$_2$(η^5-C_5H_5) (8b): Ru(Cl(PPh_3)$_2$(η^5-C_5H_5) (160 mg, 0.22 mmol) and 4-HC≡C$C_{10}H_6$-1-NO_2 (**2**, 68 mg, 0.34 mmol) were heated in refluxing MeOH (15 mL) for 1 h and the mixture was then cooled. A solution of NaOMe in MeOH (5 mL, 0.102 M) was added, the mixture was stirred, and then the solvent was removed under reduced pressure. Purification by chromatography on a short column of alumina eluting with petrol:CH_2Cl_2 (1:1) afforded **8b** as a red powder (110 mg, 0.123 mmol, 56%). Elemental analysis calcd (%) for $C_{53}H_{41}NO_2P_2Ru$: C 71.77, H 4.66, N 1.58; found: C 71.69, H 4.74, N 1.53. UV-Vis: λ_{max}/nm 498 (1.5). IR: ν_{max}/cm^{-1} 2040 (C≡C). ^{1}H NMR: δ 8.83 (d, J_{HH} = 8.5 Hz, 1H), 8.66 (d, J_{HH} = 8.0 Hz, 1H), 8.29 (d, J_{HH} = 8.5 Hz, 1H), 7.64 (m, 1H), 7.53 – 7.41 (m, 13H), 7.22 (m, 6H), 7.09 (m, 13H), 4.45 (s, 5H) ppm. ^{13}C NMR: δ 139.8, 138.4 (m), 134.8, 133.7 (t, J_{CP} = 5 Hz), 129.0, 128.8, 128.7, 127.4 (t, J_{CP} = 5 Hz), 126.6, 126.2, 125.9, 125.4, 123.5, 117.0, 85.9 ppm. ^{31}P NMR: δ 50.2 ppm. MS (ESI): *m*/*z* 888, (M^+, 58%), 691 ([M - C≡C$C_{10}H_6NO_2$]$^+$, 100). HRMS: calc for $C_{53}H_{42}NO_2P_2Ru$ ([M + H]$^+$): 888.1378, found: 888.1734.

Ni(C≡C-4-$C_{10}H_6$-1-NO_2)(PPh_3)(η^5-C_5H_5) (9b): Ni(Cl(PPh_3)(η^5-C_5H_5) (200 mg, 0.47 mmol), 4-HC≡C$C_{10}H_6$-1-NO_2 (**2**, 103 mg, 0.52 mmol), and CuI (5 mg, 0.03 mmol) were stirred in a mixture of NEt_3 (20 mL) and CH_2Cl_2 (20 mL) for 16 h. The solvent was removed under reduced pressure, and the residue was extracted with CH_2Cl_2 (50 mL) and then passed through a small pad of silica. Petrol (10 mL) and ethanol (2 mL) were added to the eluate, and then the CH_2Cl_2 was removed under reduced pressure, precipitating the microcrystalline product **9b** which was collected by filtration (0.234 g, 0.40 mmol, 86%). Elemental analysis calcd (%) for $C_{35}H_{26}NNiO_2P$: C 72.20, H 4.50, N 2.41; found: C 71.77, H 4.96, N 2.05. UV-Vis: λ_{max}/nm 450 (1.5). IR: ν_{max}/cm^{-1} 2073 (C≡C). ^{1}H NMR: δ 8.54 (d, J_{HH} = 8.5 Hz, 1H), 8.02 (d, J_{HH} = 8.5 Hz, 1H), 7.77 (dd, J_{HH} = 8.0 Hz, J_{HP} = 12.0 Hz, 6H), 7.56 – 7.34 (m, 11H), 7.12 (m, 1H), 6.88 (d, J_{HH} = 8.0 Hz, 1H), 5.32 (s, 5H) ppm. ^{13}C NMR: δ 142.0, 134.4, 133.9 (d, J_{CP} = 11 Hz), 133.5, 133.4 (d, J_{CP} = 48 Hz), 130.5, 128.8, 128.3 (d, J_{CP} = 10 Hz), 128.1, 126.5, 126.2, 125.5, 124.7, 123.0, 108.4, 107.9, 93.04 ppm. ^{31}P NMR: δ 41.5 (PPh_3) ppm. MS (ESI): *m*/*z* 581 (M^+, 13%), 385 ([M - C≡C$C_{10}H_6NO_2$]$^+$, 15). HRMS: calc for $C_{35}H_{26}NNiO_2P$: 581.1055, found: 581.1055.

Au(C≡C-4-$C_{10}H_6$-1-NO_2)(PPh_3) (10b): Au(Cl(PPh_3) (50 mg, 0.10 mmol) and 4-HC≡C$C_{10}H_6$-1-NO_2 (**2**, 24 mg, 0.12 mmol) were stirred in a solution of sodium methoxide in methanol (10 mL, 0.10 M) for 16 h, after which time **10b** had precipitated as a pale yellow solid and was collected by filtration (60 mg, 0.09 mmol, 91%). Elemental analysis calcd (%) for $C_{30}H_{21}NO_2AuP.0.5CH_2Cl_2$: C 52.49, H 3.18, N 2.01; found: C 52.48, H 3.16, N 1.94. UV-Vis: λ_{max}/nm 386 (1.7). IR: ν_{max}/cm^{-1} 2106 (C≡C). ^{1}H NMR: δ 8.80 (d, J_{HH} = 8.0 Hz, 1H), 8.61 (d, J_{HH} = 8.5 Hz, 1H), 8.19 (d, J_{HH} = 8.0 Hz, 1H), 7.83 – 7.38 (m, 19H) ppm. ^{13}C NMR: δ 144.5, 134.9, 134.3 (d, J_{CP} = 14 Hz), 131.7, 130.5, 129.5 (d, J_{CP} = 56 Hz), 129.4, 129.3 (d, J_{CP} = 11 Hz), 128.4, 128.2, 127.4, 125.2, 124.0, 123.2, 100.8, 100.5 ppm. ^{31}P NMR: δ 42.0 ppm. MS (ESI): *m*/*z* 1114 ([M + Au(PPh_3)]$^+$, 18%), 721 ([Au(PPh_3)$_2$]$^+$, 100), 459 ([M - C≡C$C_{10}H_6NO_2$]$^+$, 8).

***trans*-[Ru(C≡C-10-$C_{14}H_8$-9-NO_2)Cl(dppe)$_2$] (6c)**: [RuCl(dppe)$_2$]PF_6 (0.108 g, 0.100 mmol) and 10-HC≡C$C_{14}H_8$-9-NO_2 (**5**, 0.029 g, 0.12 mmol) were reacted as per the synthesis of **6b**, affording **6c** as a red solid (0.085 g, 0.072 mmol, 72%). Elemental analysis calcd (%) for $C_{68}H_{56}ClNO_2P_4Ru.CH_2Cl_2$: C 65.54, H 4.62, N 1.11; found: C 65.47, H 4.21, N 1.56. UV-Vis: λ_{max}/nm 548 (2.1). IR: ν_{max}/cm^{-1} 2001 (C≡C). ^{1}H NMR: δ 7.89 (d, J_{HH} = 8.5 Hz, 2H), 7.70 – 6.70 (m, 44H), 6.68 (m, 2H), 2.92 (m, 8H) ppm. ^{13}C NMR: δ 137.7, 135.2 (m), 134.2, 131.1, 129.6, 128.7, 127.8, 126.9, 124.0, 123.4, 121.0, 116.7, 30.0 ppm. ^{31}P NMR: δ 46.2 ppm. MS (ESI): *m*/*z* 1179 (M^+, 20%), 1144 ([M - Cl]$^+$, 80), 933 ([M - C≡C$C_{14}H_8NO_2$]$^+$, 20).

***trans*-[Ru(C≡C-10-$C_{14}H_8$-9-NO_2)Cl(dppm)$_2$] (7c)**: *cis*-[$RuCl_2$(dppm)$_2$] (200 mg, 0.22 mmol), 10-HC≡C$C_{14}H_8$-9-NO_2 (**5**, 106 mg, 0.43 mmol) and $NaPF_6$ (70 mg, 0.43 mmol) were reacted as per the synthesis of **7b**, yielding **7c** as a purple powder (80 mg, 0.070 mmol, 32%). ^{1}H NMR: δ 7.81 (d, J_{HH} = 8.5 Hz, 2H), 7.70 – 6.70 (m, 44H), 6.59 (m, 2H), 5.15 (m, 4H) ppm. Elemental analysis calcd (%) for $C_{66}H_{52}ClNO_2P_4Ru$: C 68.84, H 4.55, N 1.22; found: C 68.71, H 4.42, N 1.18. UV-Vis: λ_{max}/nm 550 (1.2). IR: ν_{max}/cm^{-1} 2002 (C≡C). ^{13}C NMR: δ 137.4, 133.9 (m), 133.6, 131.0, 129.8, 129.4, 129.1, 127.7, 127.5, 123.8, 123.5, 120.7, 114.3, 49.6 ppm. ^{31}P NMR: δ -7.4 ppm. MS (ESI): *m*/*z* 1151 (M^+, 100%), 1116 ([M - Cl]$^+$, 20), 905 ([M - C≡C$C_{14}H_8NO_2$]$^+$, 10).

Ru(C≡C-10-$C_{14}H_8$-9-NO_2)(PPh_3)$_2$(η^5-C_5H_5) (8c): Ru(Cl(PPh_3)$_2$(η^5-C_5H_5) (160 mg, 0.22 mmol) and 10-HC≡C$C_{14}H_8$-9-NO_2 (**5**, 84 mg, 0.34 mmol) were reacted as per the synthesis of **8b** to give **8c** as a purple powder (106 mg, 0.11 mmol, 50%). Elemental analysis calcd (%) for $C_{57}H_{43}NO_2P_2Ru.0.33MeOH.0.16CH_2Cl_2$: C 71.84, H 4.68, N 1.46; found: C 71.43, H 5.09, N 1.64. UV-Vis: λ_{max}/nm 538 (1.9). IR: ν_{max}/cm^{-1} 2024 (C≡C). ^{1}H NMR: δ 8.70 (d, J_{HH} = 8.5 Hz, 2H), 7.99 (d, J_{HH} = 8.5 Hz, 2H), 7.57 – 7.51 (m, 2H), 7.51 – 7.43 (m, 12H), 7.27 – 7.24 (m, 2H), 7.21 (t, J_{HH} = 7.0 Hz, 6H), 7.07 (t, J_{HH} = 7.0 Hz, 12H), 5.30 (s, 0.32H, 0.16CH_2Cl_2), 4.54 (s, 5H), 3.49 (s, 1H, 0.33CH_3OH) ppm. ^{13}C NMR: δ 148.2, 138.4 (m), 133.7 (t, J_{CP} = 5 Hz), 131.4, 131.2, 129.5, 128.8, 127.5 (t, J_{CP} = 5 Hz), 124.3, 124.2, 121.5, 115.5, 86.1 ppm. ^{31}P NMR: δ 49.9 ppm. MS (ESI): *m*/*z* 937.1 (M^+, 100%). HRMS: calc for $C_{57}H_{44}NO_2P_2Ru$ [M + H]$^+$: 938.1889, found: 938.1891.

Ni(C≡C-10-$C_{14}H_8$-9-NO_2)(PPh_3)(η^5-C_5H_5) (9c): Ni(Cl(PPh_3)(η^5-C_5H_5) (43 mg, 0.10 mmol), 10-HC≡C$C_{14}H_8$-9-NO_2 (**5**, 30 mg, 0.12 mmol), and CuI (2 mg, 0.012 mmol) were reacted as per the synthesis of **9b**, to give **9c** (33 mg, 0.052 mmol, 52%). Elemental analysis calcd (%) for $C_{39}H_{28}NNiO_2P$: C 74.08, H 4.46, N 2.22; found: C 73.53, H 4.73, N 1.8. UV-Vis: λ_{max}/nm 485 (1.6). IR: ν_{max}/cm^{-1} 2075 (C≡C). ^{1}H NMR: δ 8.02 (d, J_{HH} = 8.5 Hz, 2H), 7.83 (dd, J_{HH} = 8.0 Hz, J_{HP} = 12.0 Hz, 6H), 7.78 (d, J_{HH} = 8.5 Hz, 2H), 7.50 – 7.33 (m, 11H), 7.14 (m, 2H), 5.32 (s, 5H) ppm. ^{13}C NMR: δ 140.5, 133.9 (d, J_{CP} = 11 Hz), 133.5 (d, J_{CP} = 48 Hz), 131.3, 130.5, 128.5, 128.3 (d, J_{CP} = 10 Hz), 128.2, 125.0, 122.9, 121.1, 116.9, 100, 93.1 ppm. ^{31}P NMR: δ 41.3 ppm. MS (ESI): *m*/*z* 631 (M^+, 21%), 385 ([M - C≡C$C_{14}H_8NO_2$]$^+$, 42).

Au(C≡C-10-$C_{14}H_8$-9-NO_2)(PPh_3) (10c): AuCl(PPh_3) (50 mg, 0.10 mmol) and 10-HC≡C$C_{14}H_8$-9-NO_2 (**5**, 30 mg, 0.12 mmol) were reacted as per the synthesis of **10b** to give **10c** as a pale yellow solid (60 mg, 0.085 mmol, 85%). Elemental analysis calcd (%) for $C_{34}H_{23}NAuO_2P$: C 57.88, H 3.29, N 1.99; found: C 57.61, H 3.23, N 2.16. UV-Vis: λ_{max}/nm 426 (1.1), 404 (1.0). IR: ν_{max}/cm^{-1} 2086 (C≡C). ^{1}H NMR: δ 8.97 (d, J_{HH} = 8.0 Hz, 2H), 7.90 (d, J_{HH} = 8.5 Hz, 2H), 7.77 – 7.42 (m, 19H) ppm. ^{13}C NMR: δ 142.8, 134.3 (d, J_{CP} = 14 Hz), 132.2, 131.7, 129.4 (d, J_{CP} = 56 Hz), 129.2 (d, J_{CP} = 11 Hz), 128.7, 128.5, 126.33, 124.98, 122.4, 121.4, 98.7 ppm. ^{31}P NMR: δ 42.0 ppm. MS (ESI): *m*/*z* 1164 ([M + Au(PPh_3)]$^+$, 30%), 721 ([Au(PPh_3)$_2$]$^+$, 100), 459 ([M - C≡C$C_{14}H_8NO_2$]$^+$, 15).

Computational Studies. All DFT/TD-DFT calculations were performed using the Gaussian 09 program package.[15] Optimized geometries and TD-DFT calculations were performed using B3LYP[16] and PBE1PBE[17] hybrid DFT methods, respectively. For optimizations, the 6-31G(d) basis set was used, whereas the 6-31+G(d) basis set was employed during TD-DFT calculations. In all cases, pseudo potential of Stuttgart/Dresden and associated SDD basis set[18] was used for the transition metal. To save computational time, appropriate symmetry constraints were imposed on the model complexes: C_s (for **7b'**, **8a'**, **9a'**, and **10a**) and C_{2v} (for **7a'** and **7c'**). Static first hyperpolarizability values were predicted using the same level of theory and basis sets as used in the TD-DFT calculations. The contributions of atoms to the frontier molecular orbitals were analyzed with the GaussSum3.0 program.[19]

NMR spectroscopy

Figure S1. ^{1}H NMR spectrum of 1-nitro-4-(trimethylsilylethynyl)naphthalene (**1**).

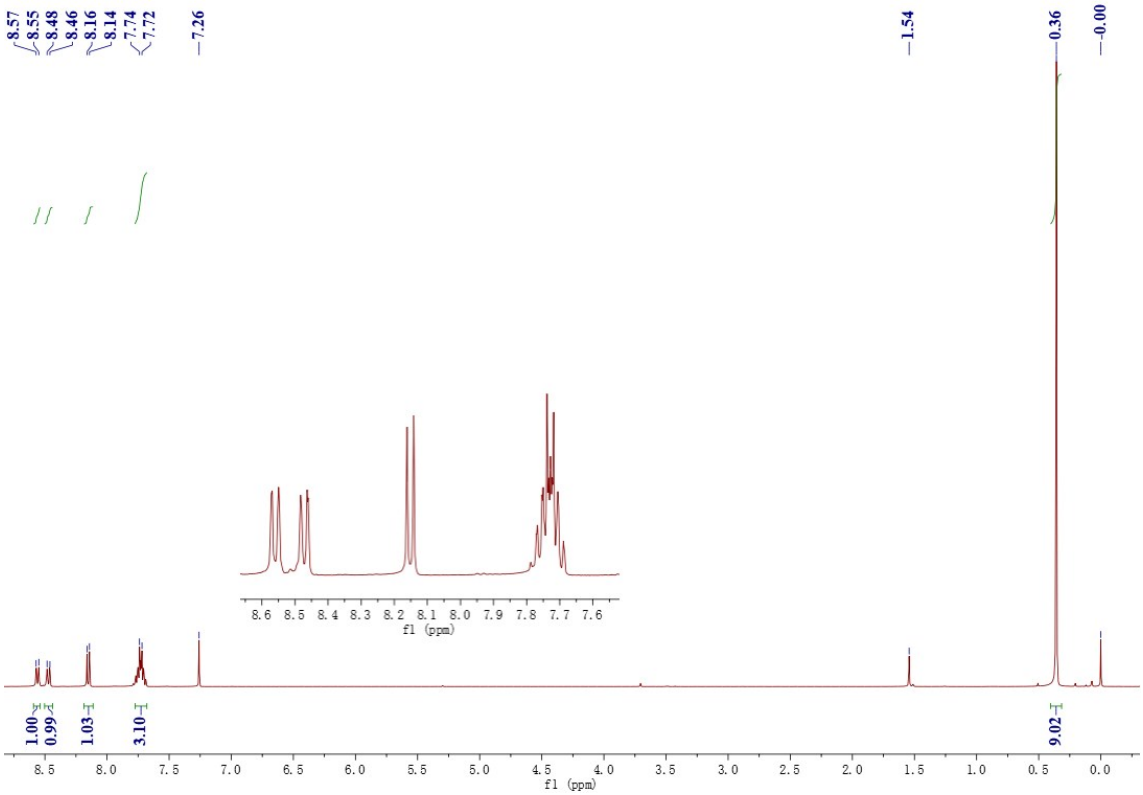

Figure S2. ^{13}C NMR spectrum of 1-nitro-4-(trimethylsilylethynyl)naphthalene (**1**).

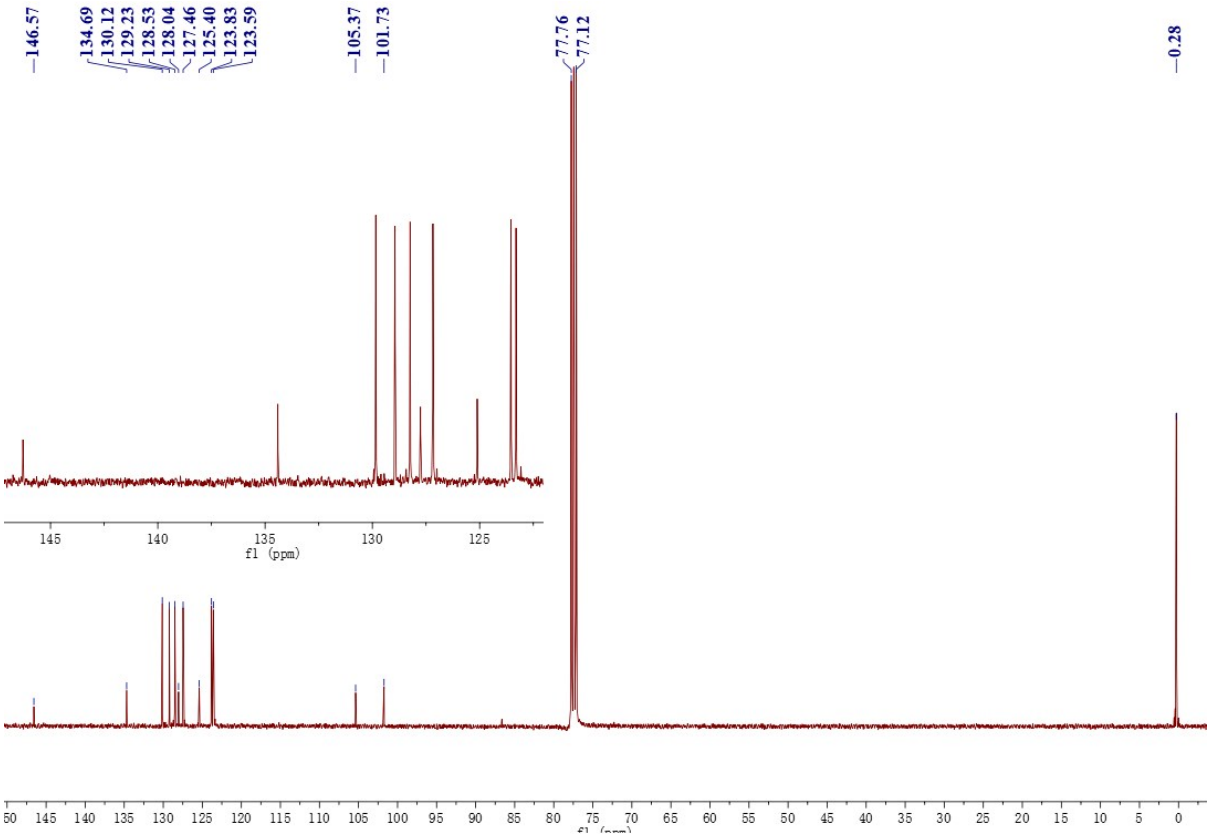

Figure S3. [1]H NMR spectrum of 9-nitro-10-(trimethylsilylethynyl)anthracene ***(4)***.

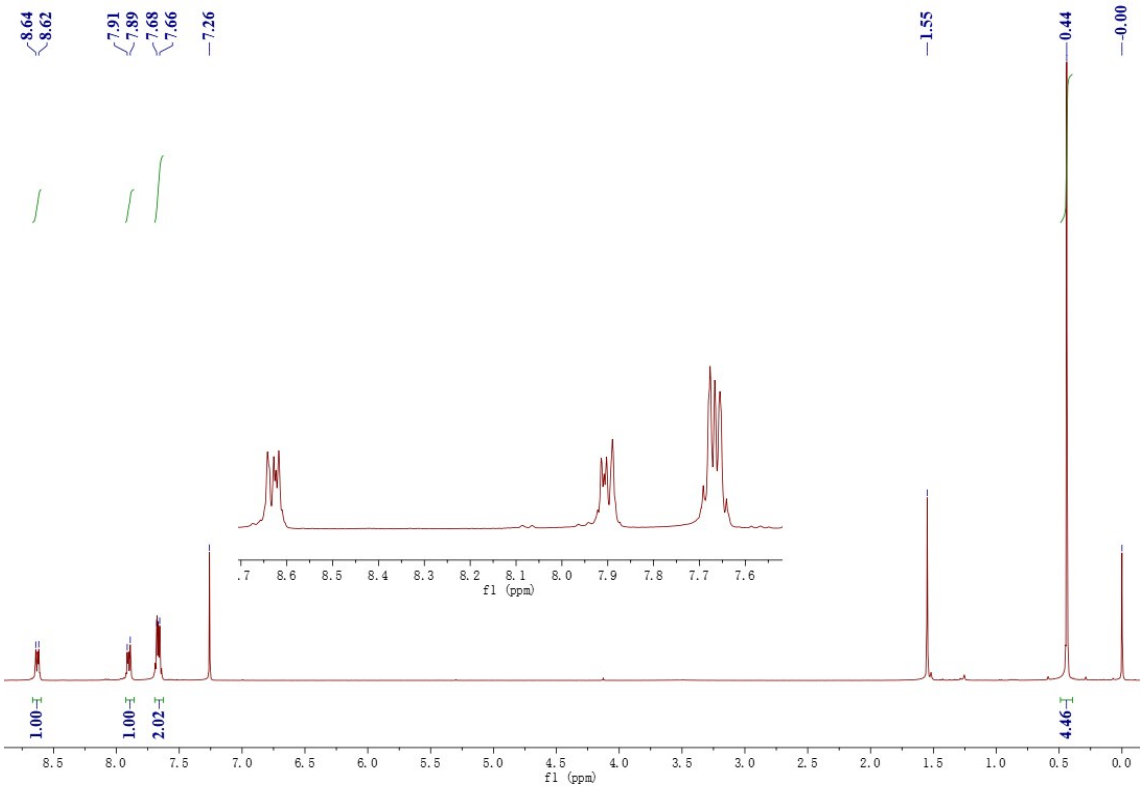

Figure S4. [13]C NMR spectrum of 9-nitro-10-(trimethylsilylethynyl)anthracene ***(4)***.

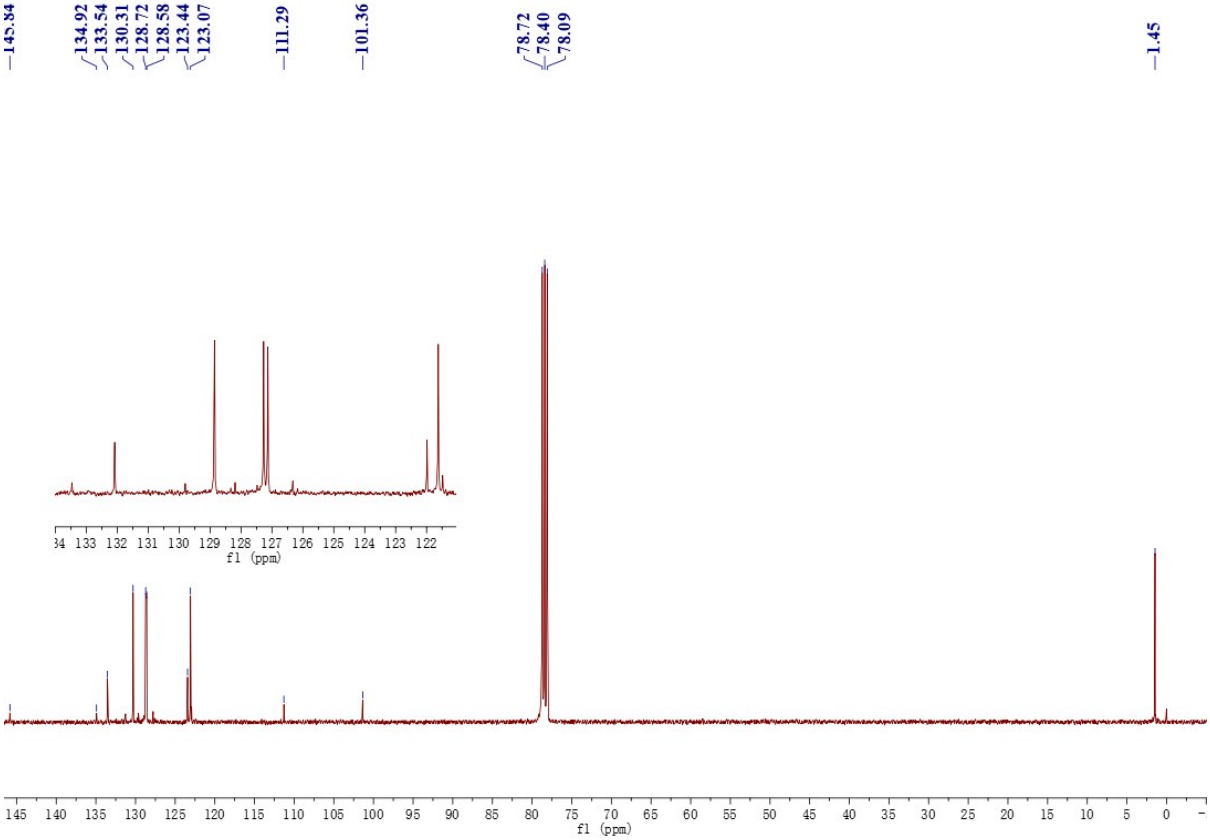

Figure S5. ^{1}H NMR spectrum of 10-ethynyl-9-nitroanthracene (**5**).

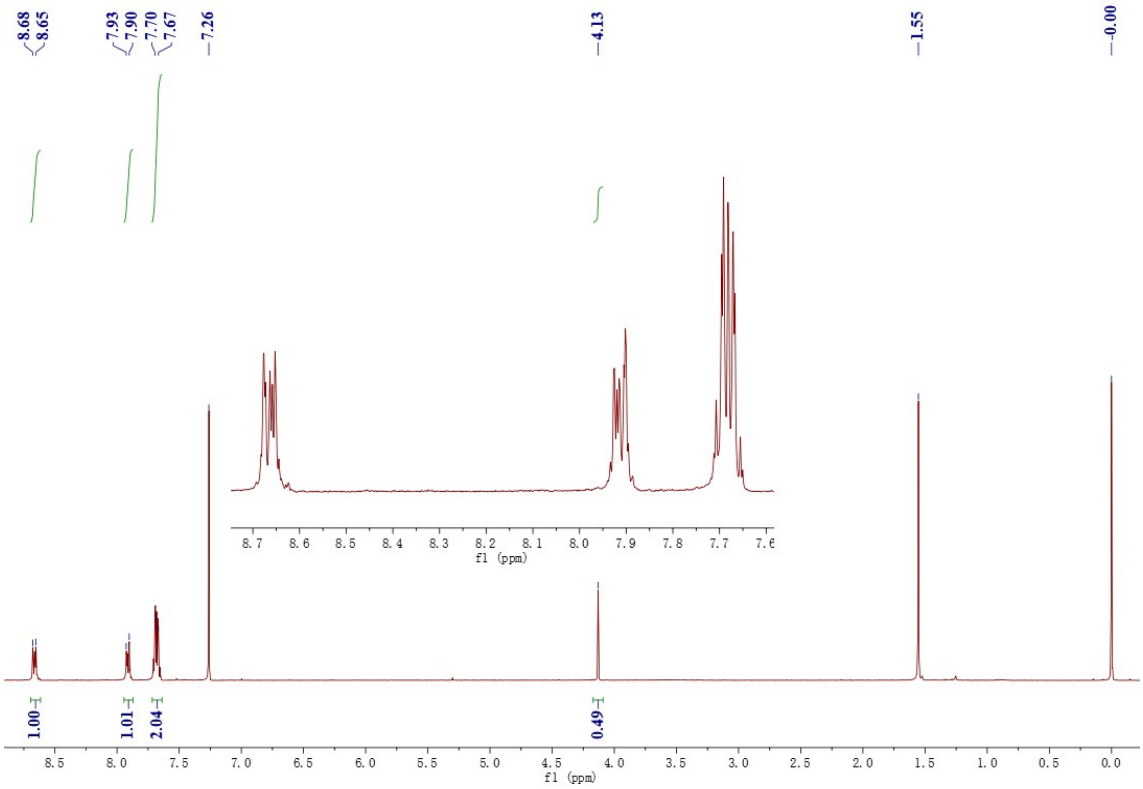

Figure S6. ^{13}C NMR spectrum of 10-ethynyl-9-nitroanthracene (**5**).

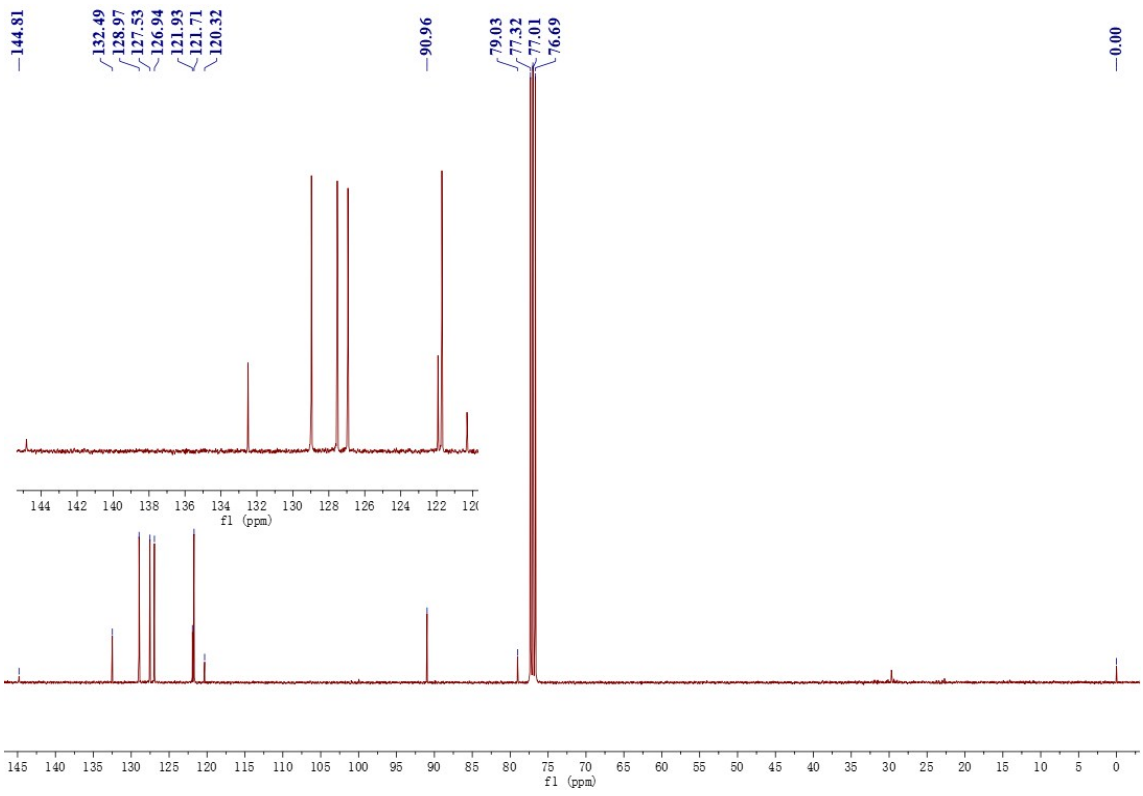

Figure S7. ^{1}H NMR spectrum of *trans*-[Ru(C≡C-4-$C_{10}H_6$-1-NO_2)Cl(dppe)$_2$] (**6b**).

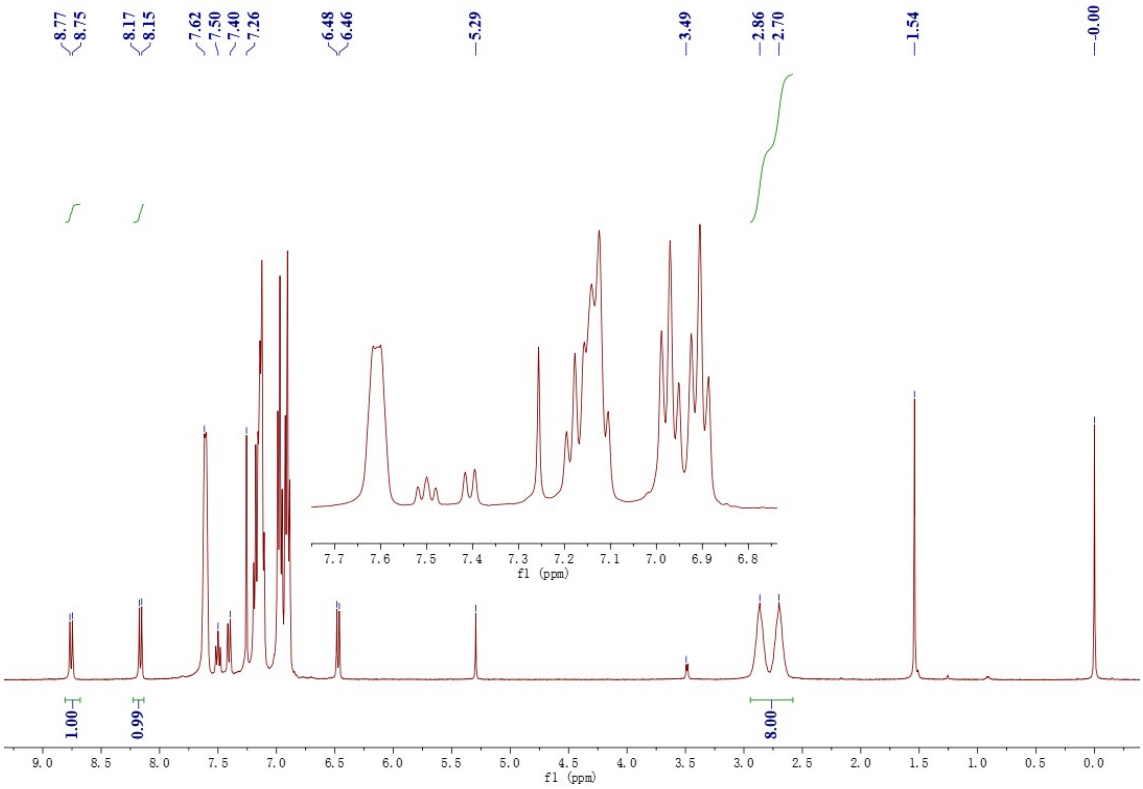

Figure S8. ^{13}C NMR spectrum of *trans*-[Ru(C≡C-4-$C_{10}H_6$-1-NO_2)Cl(dppe)$_2$] (**6b**).

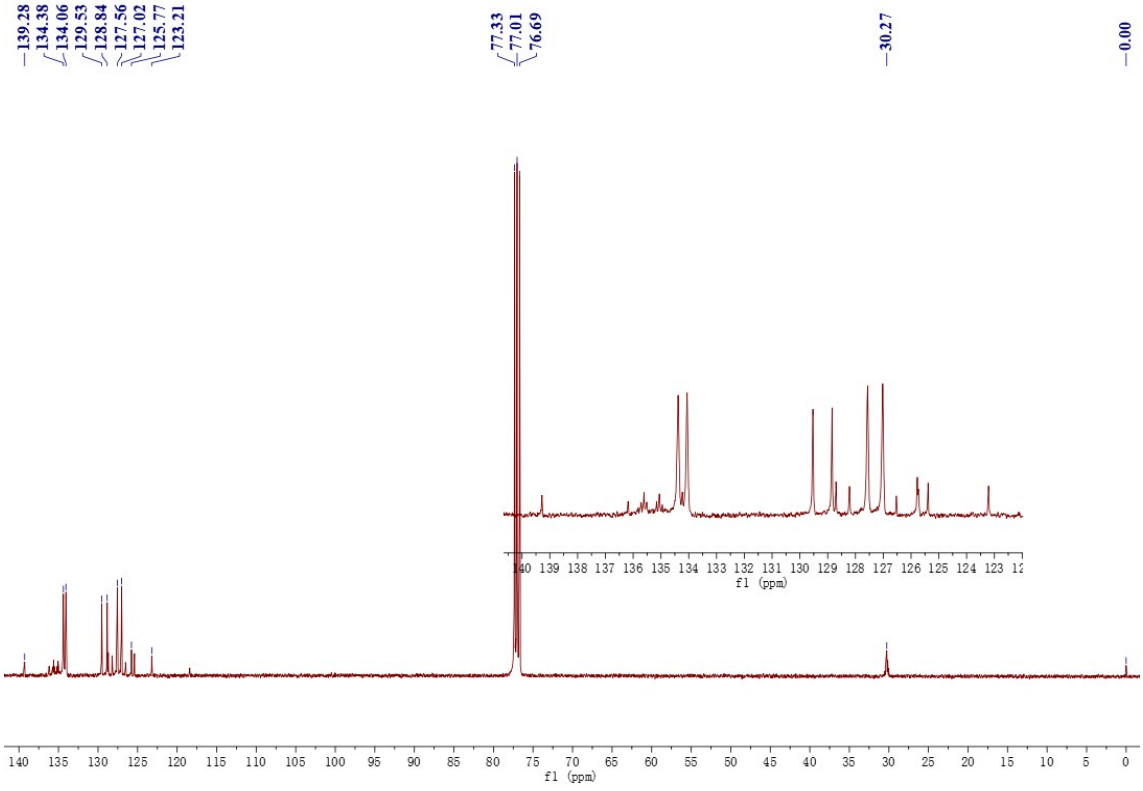

Figure S9. ^{31}P NMR spectrum of *trans*-[Ru(C≡C-4-$C_{10}H_6$-1-NO_2)Cl(dppe)$_2$] (**6b**).

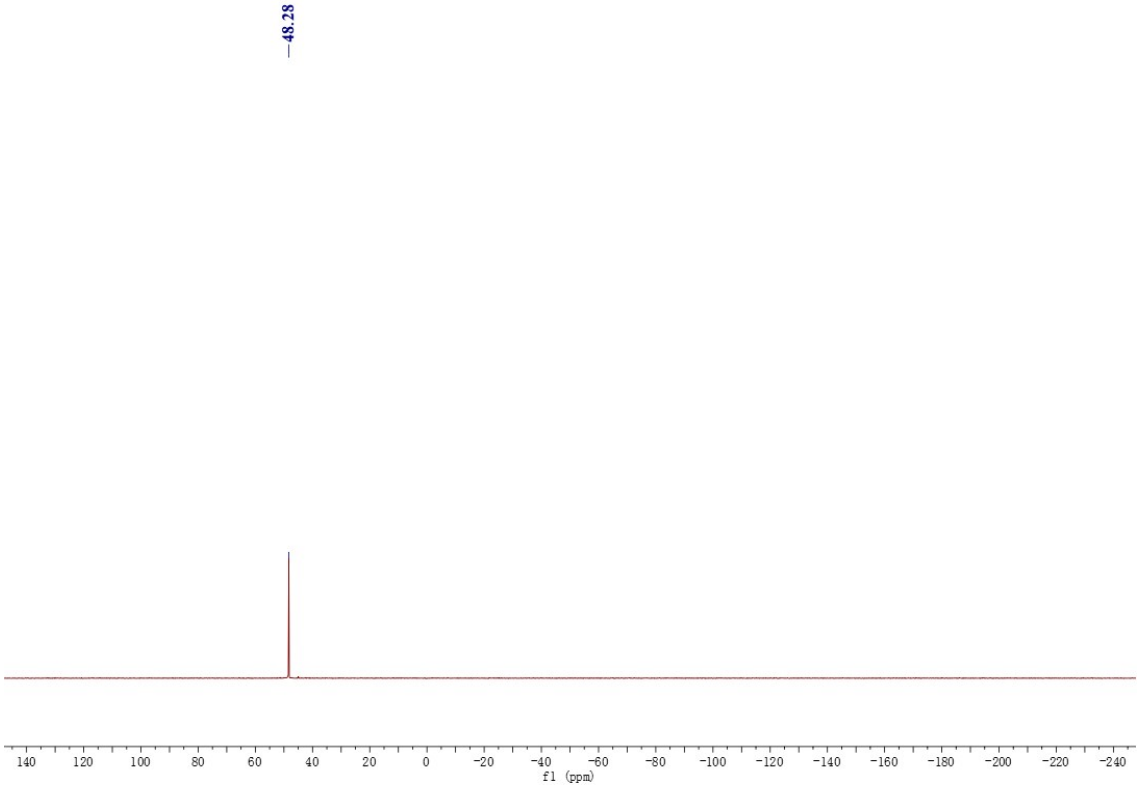

Figure S10. ^{1}H NMR spectrum of *trans*-[Ru(C≡C-4-$C_{10}H_6$-1-NO_2)Cl(dppm)$_2$] (**7b**).

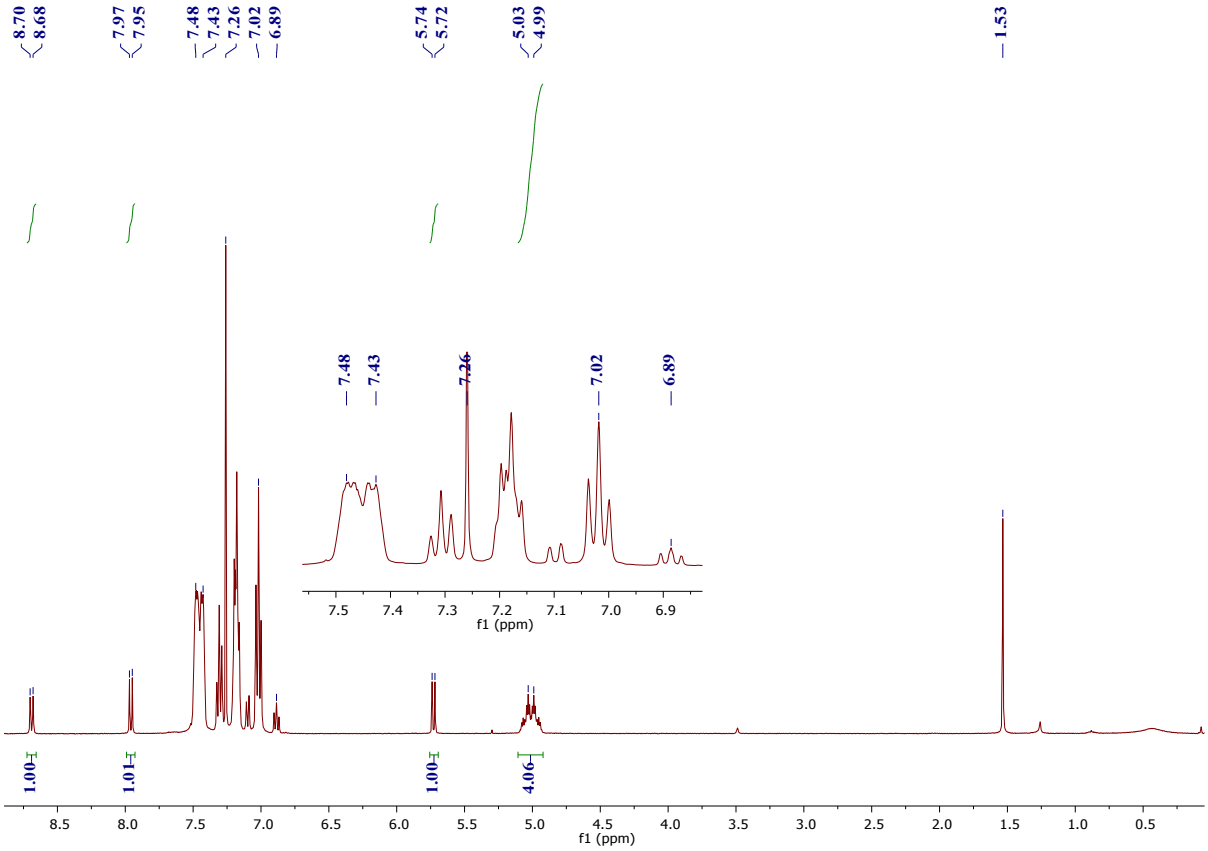

Figure S11. ^{13}C NMR spectrum of *trans*-[Ru(C≡C-4-$C_{10}H_6$-1-NO_2)Cl(dppm)$_2$] (**7b**).

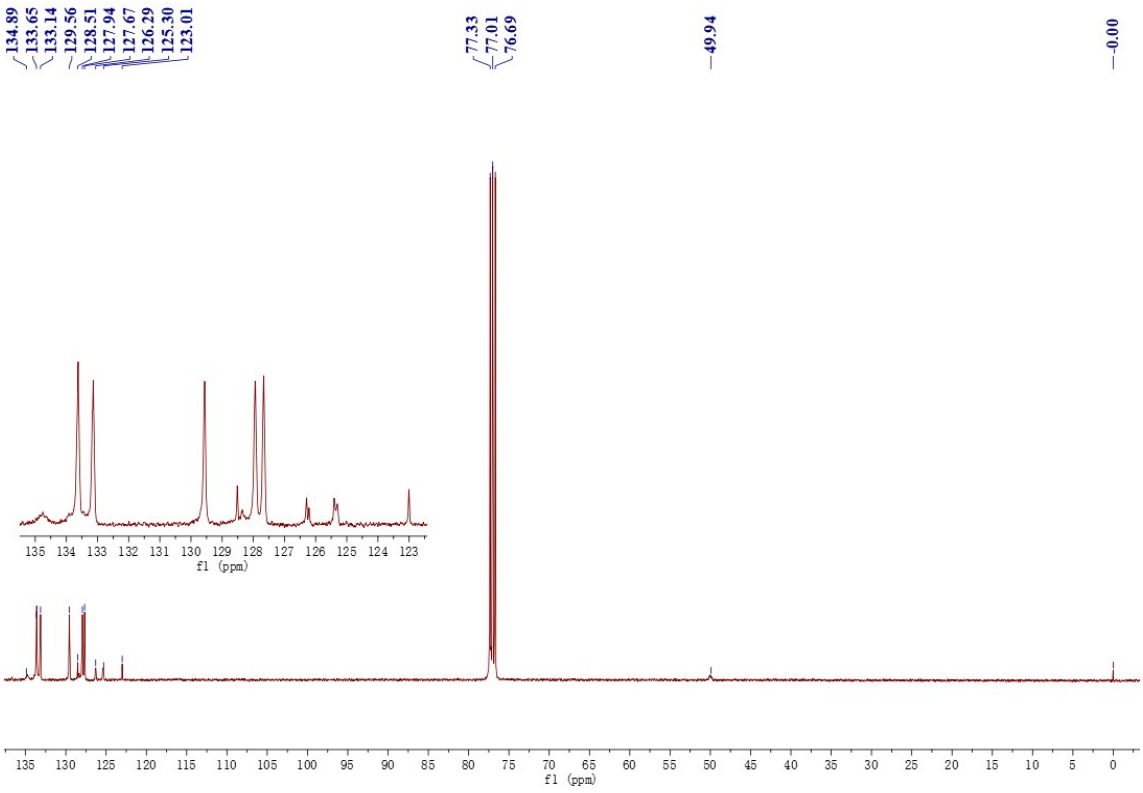

Figure S12. ^{31}P NMR spectrum of *trans*-[Ru(C≡C-4-$C_{10}H_6$-1-NO_2)Cl(dppm)$_2$] (**7b**).

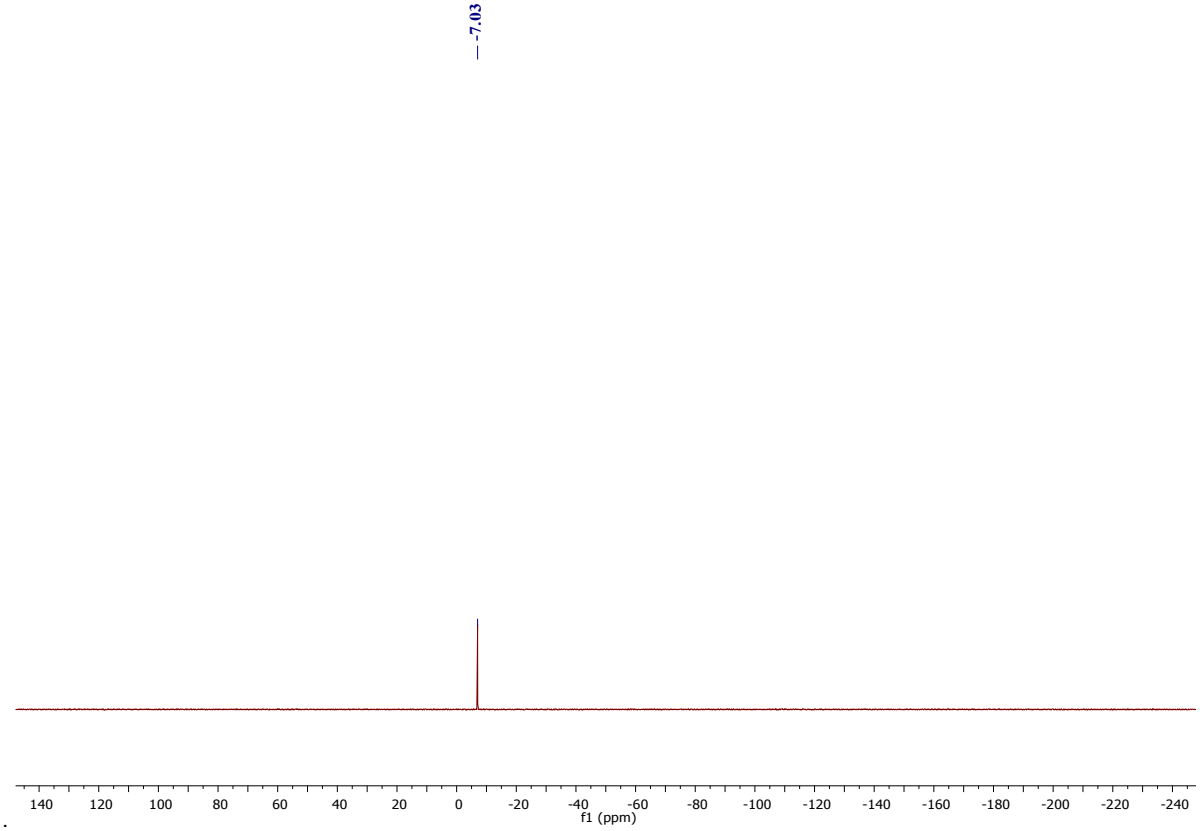

Figure S13. ^{1}H NMR spectrum of Ru(C≡C-4-$C_{10}H_6$-1-NO_2)(PPh_3)$_2$(η^5-C_5H_5) (**8b**).

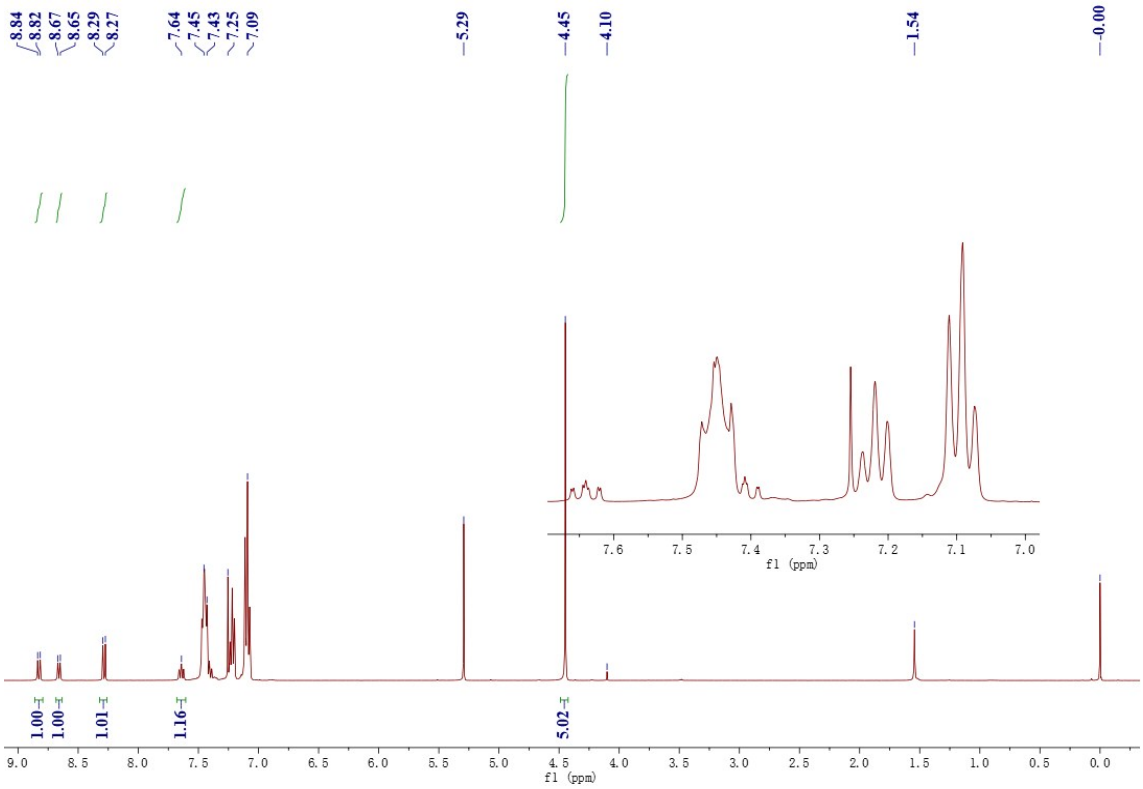

Figure S14. ^{13}C NMR spectrum of Ru(C≡C-4-$C_{10}H_6$-1-NO_2)(PPh_3)$_2$(η^5-C_5H_5) (**8b**).

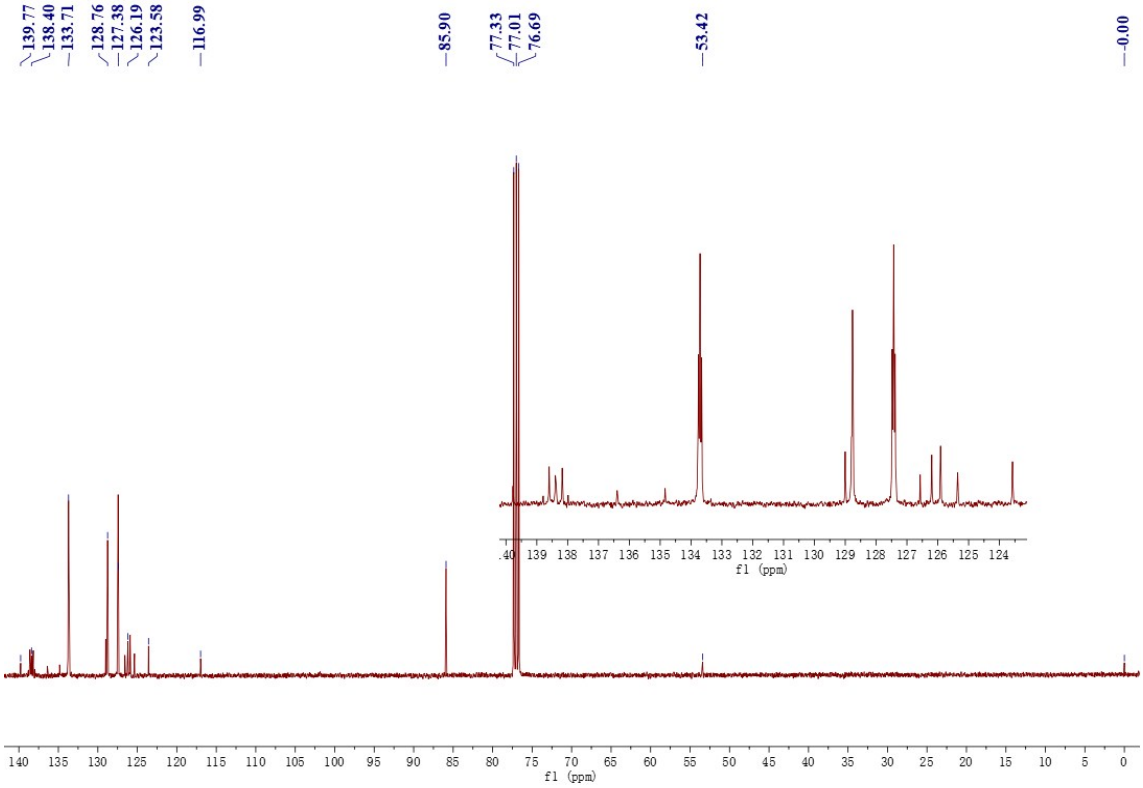

Figure S15. ^{31}P NMR spectrum of Ru(C≡C-4-$C_{10}H_6$-1-NO_2)(PPh_3)$_2$(η^5-C_5H_5) (**8b**).

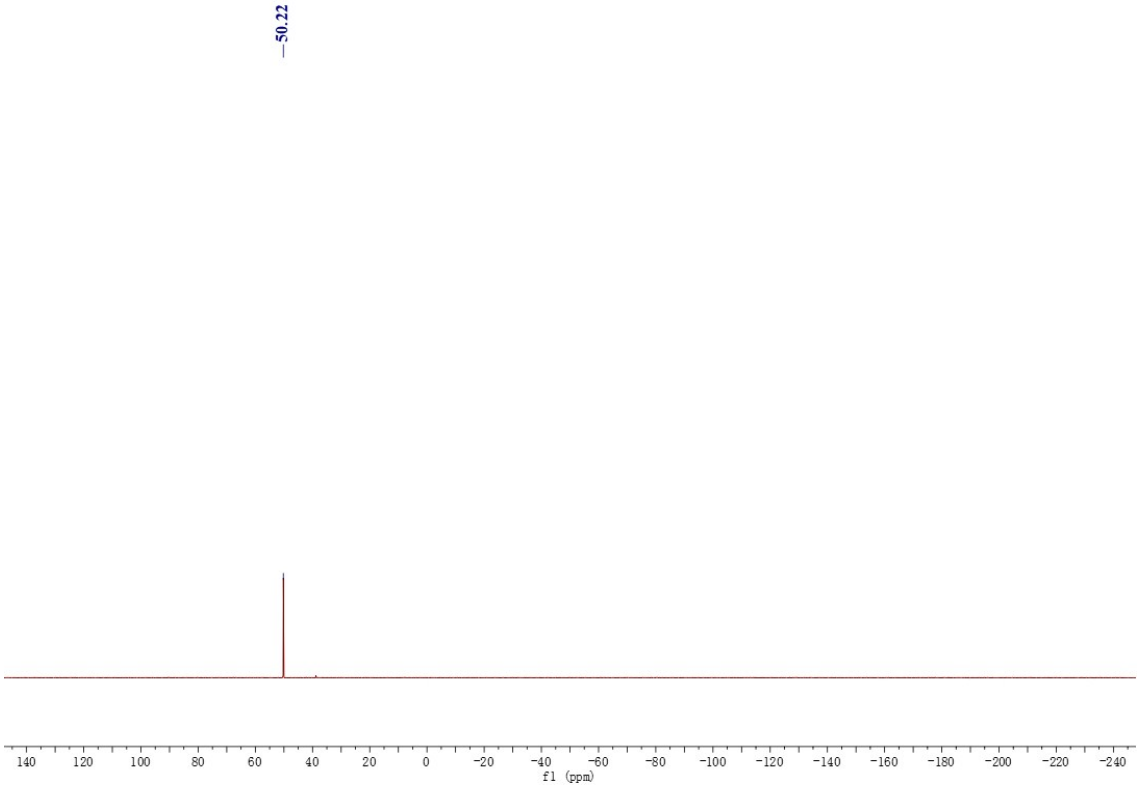

Figure S16. ^{1}H NMR spectrum of Ni(C≡C-4-$C_{10}H_6$-1-NO_2)(PPh_3)(η^5-C_5H_5) (**9b**).

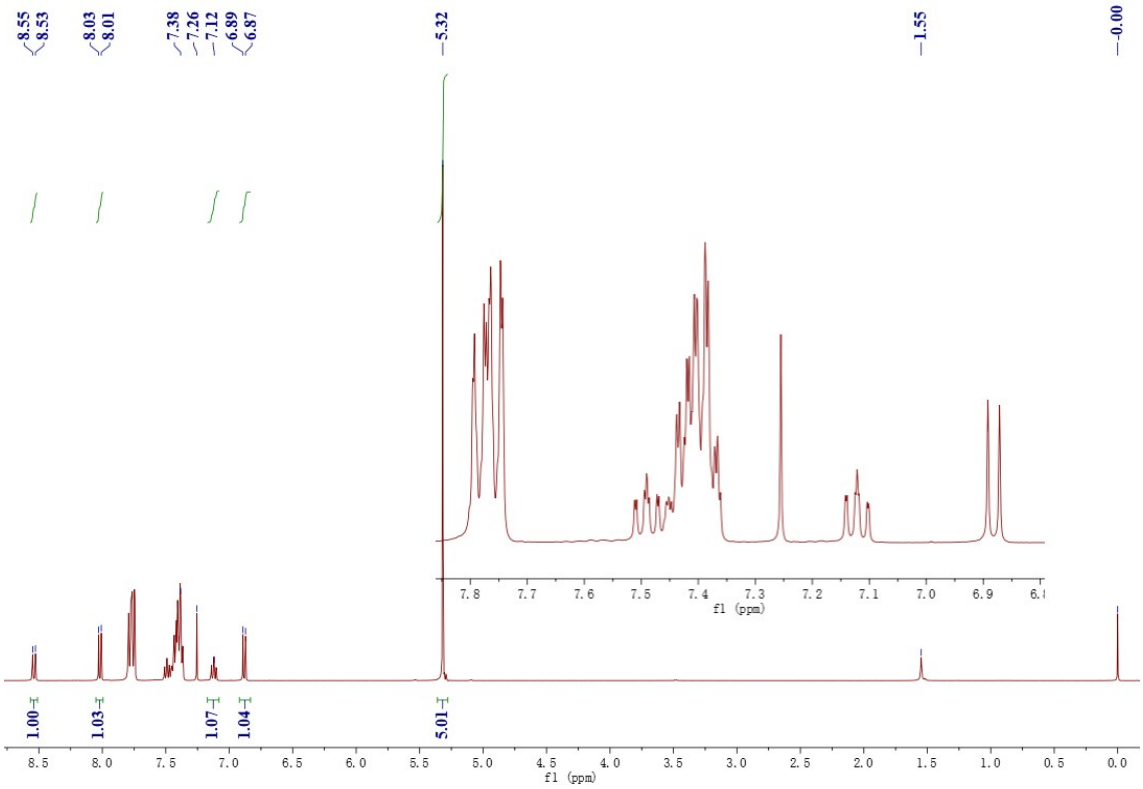

Figure S17. ^{13}C NMR spectrum of Ni(C≡C-4-$C_{10}H_6$-1-NO_2)(PPh_3)(η^5-C_5H_5) (**9b**).

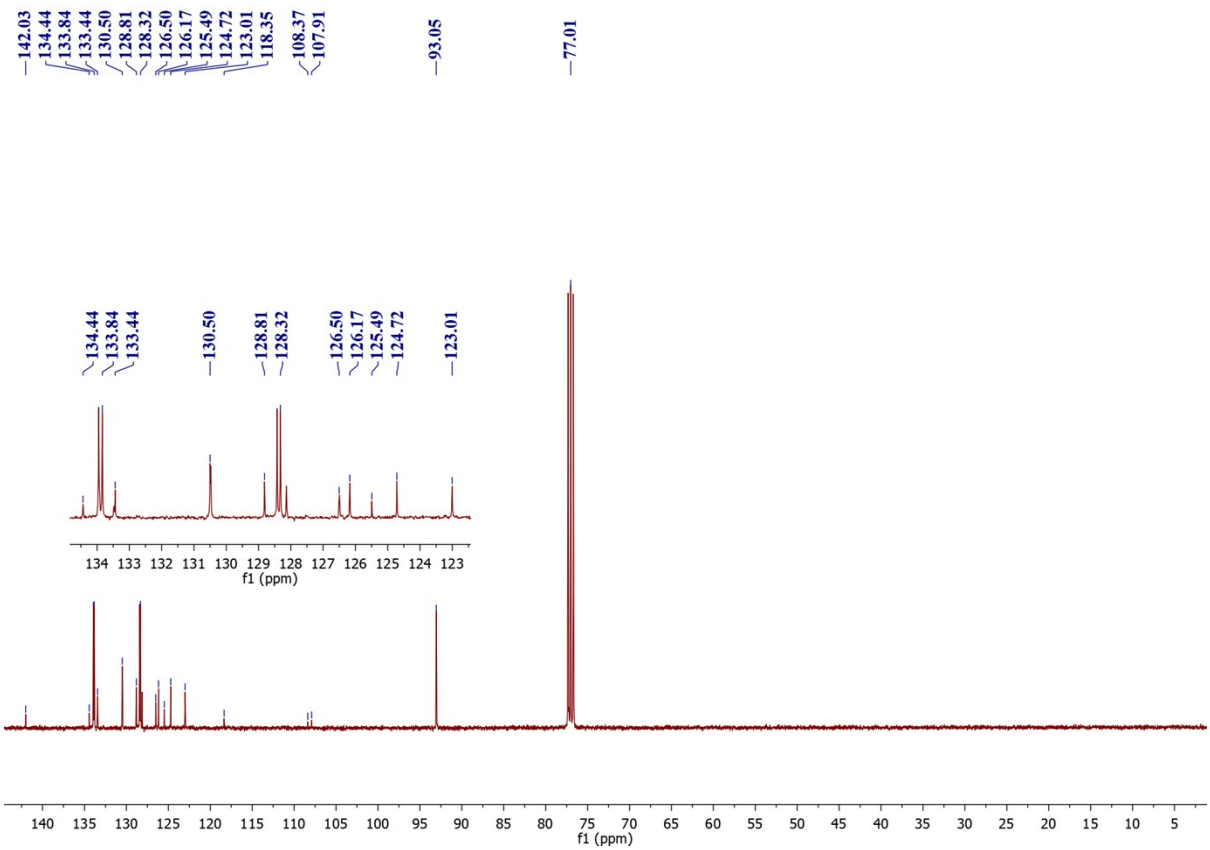

Figure S18. ^{31}P NMR spectrum of Ni(C≡C-4-$C_{10}H_6$-1-NO_2)(PPh_3)(η^5-C_5H_5) (**9b**).

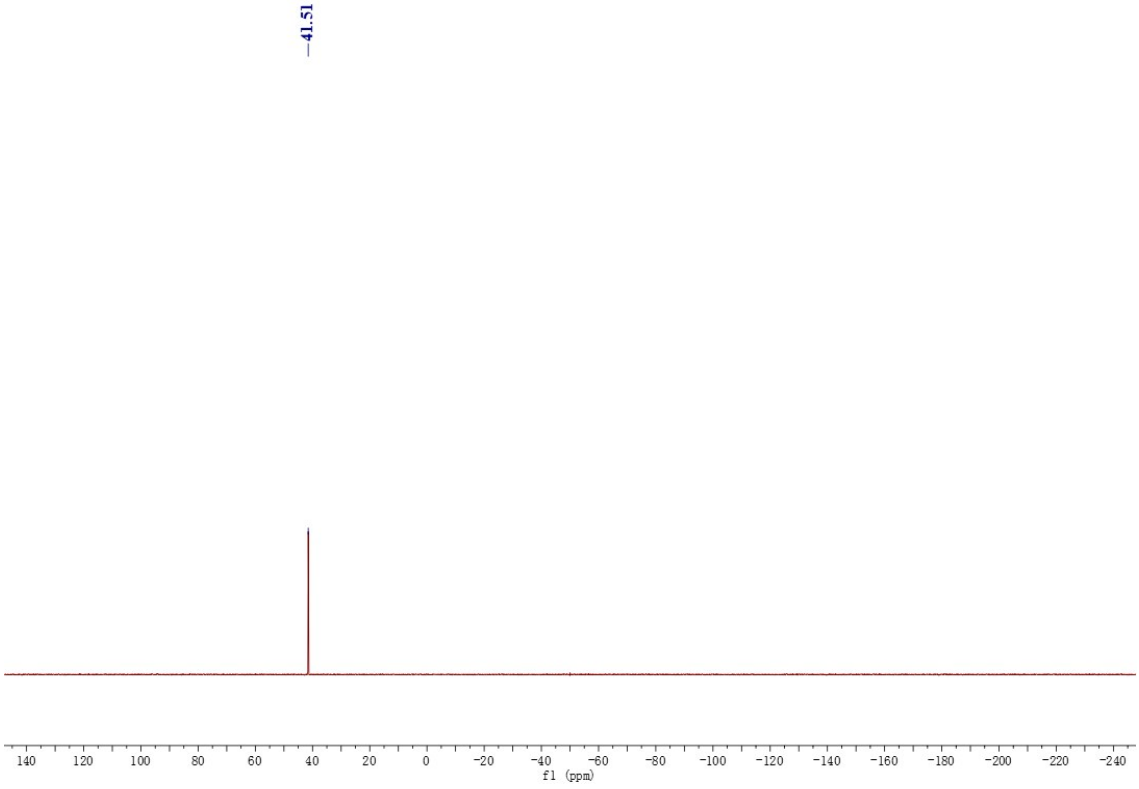

Figure S19. ^{1}H NMR spectrum of Au(C≡C-4-$C_{10}H_6$-1-NO_2)(PPh_3) (**10b***)*.

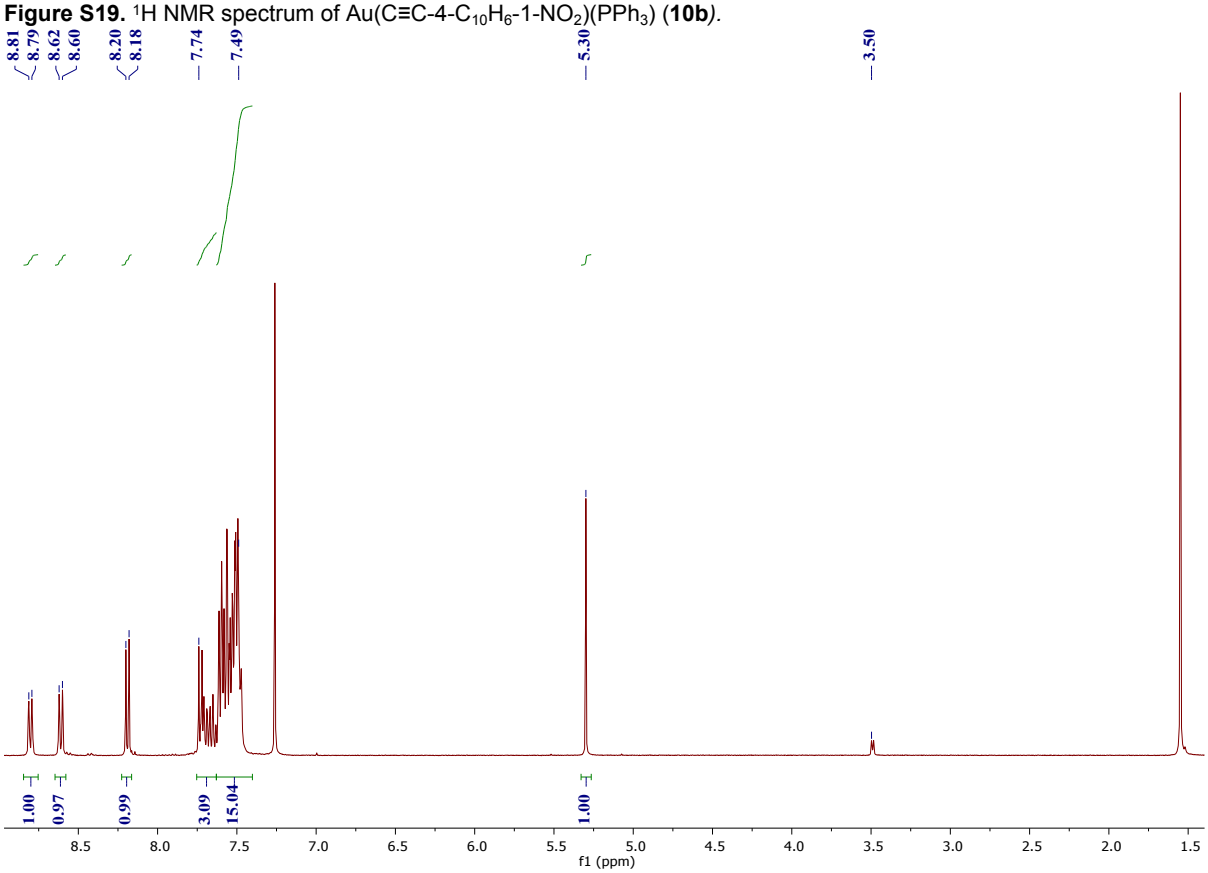

Figure S20. ^{13}C NMR spectrum of Au(C≡C-4-$C_{10}H_6$-1-NO_2)(PPh_3) (**10b**).

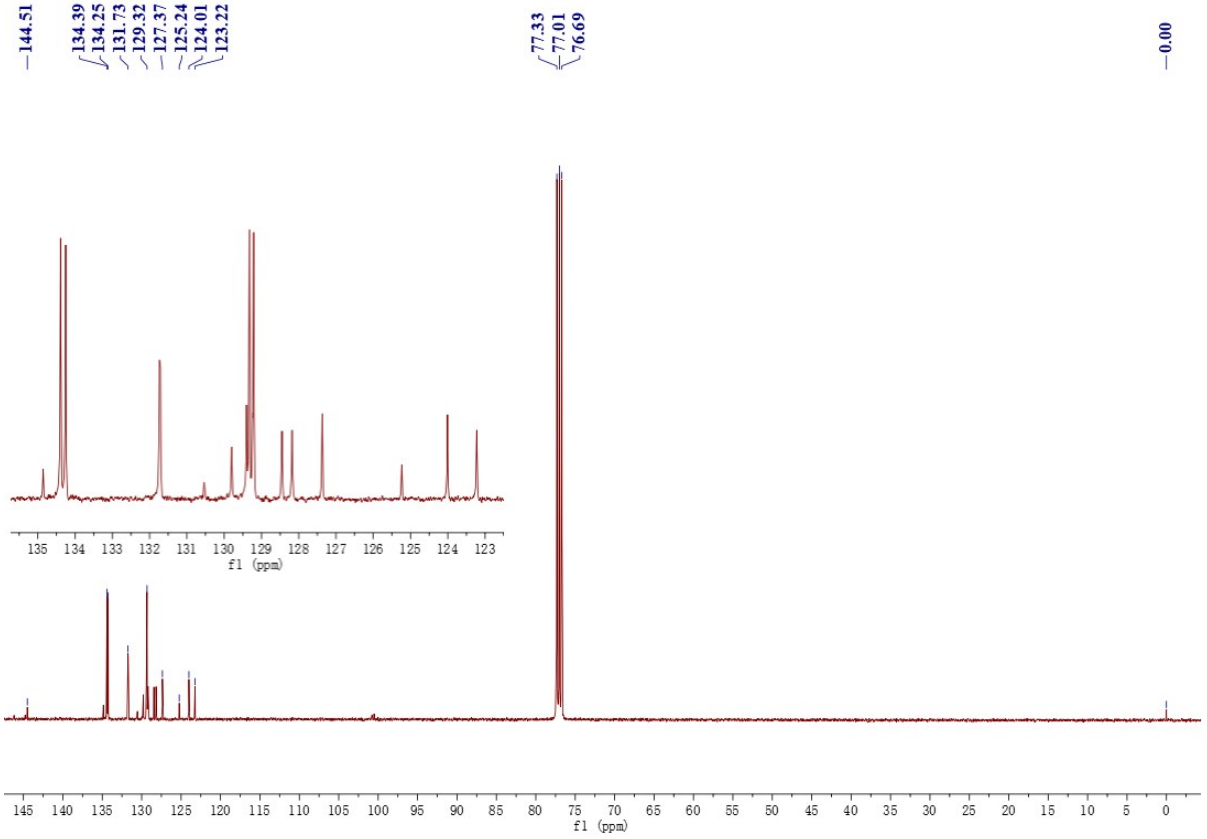

Figure S21. ^{31}P NMR spectrum of Au(C≡C-4-$C_{10}H_6$-1-NO_2)(PPh_3) (**10b**).

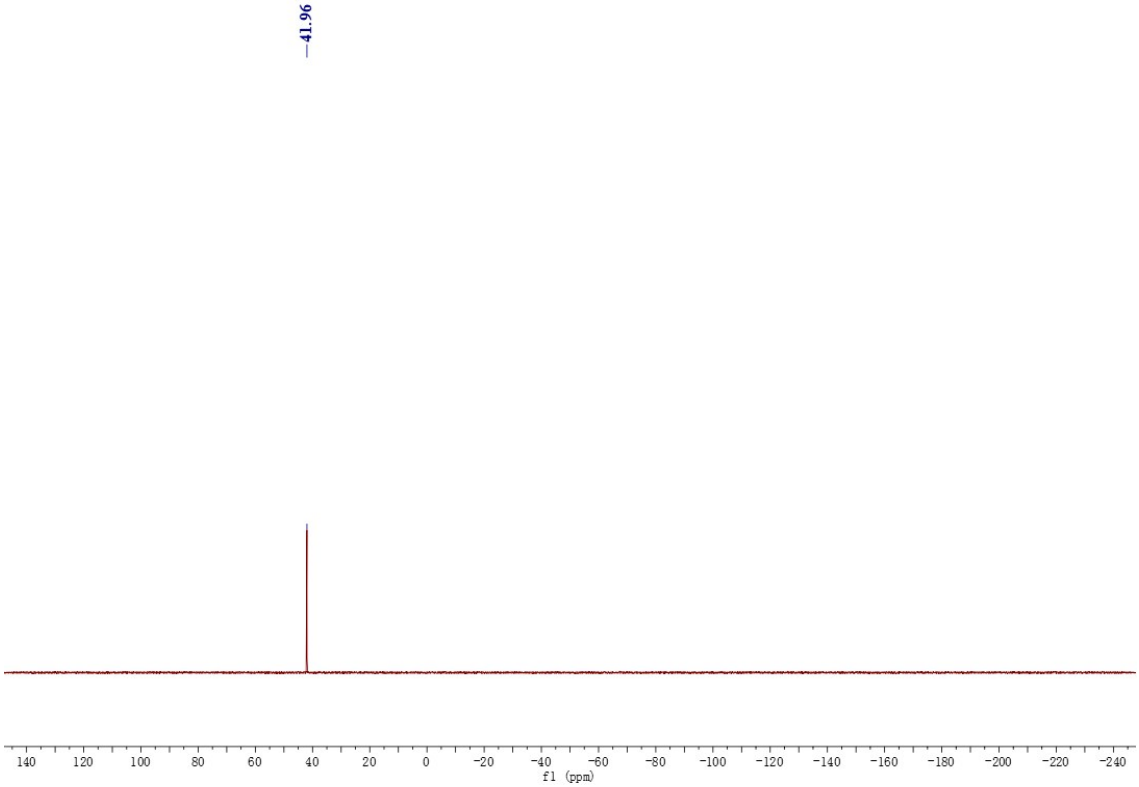

Figure S22. ^{1}H NMR spectrum of *trans*-[Ru(C≡C-10-$C_{14}H_8$-9-NO_2)Cl(dppe)$_2$] (**6c**).

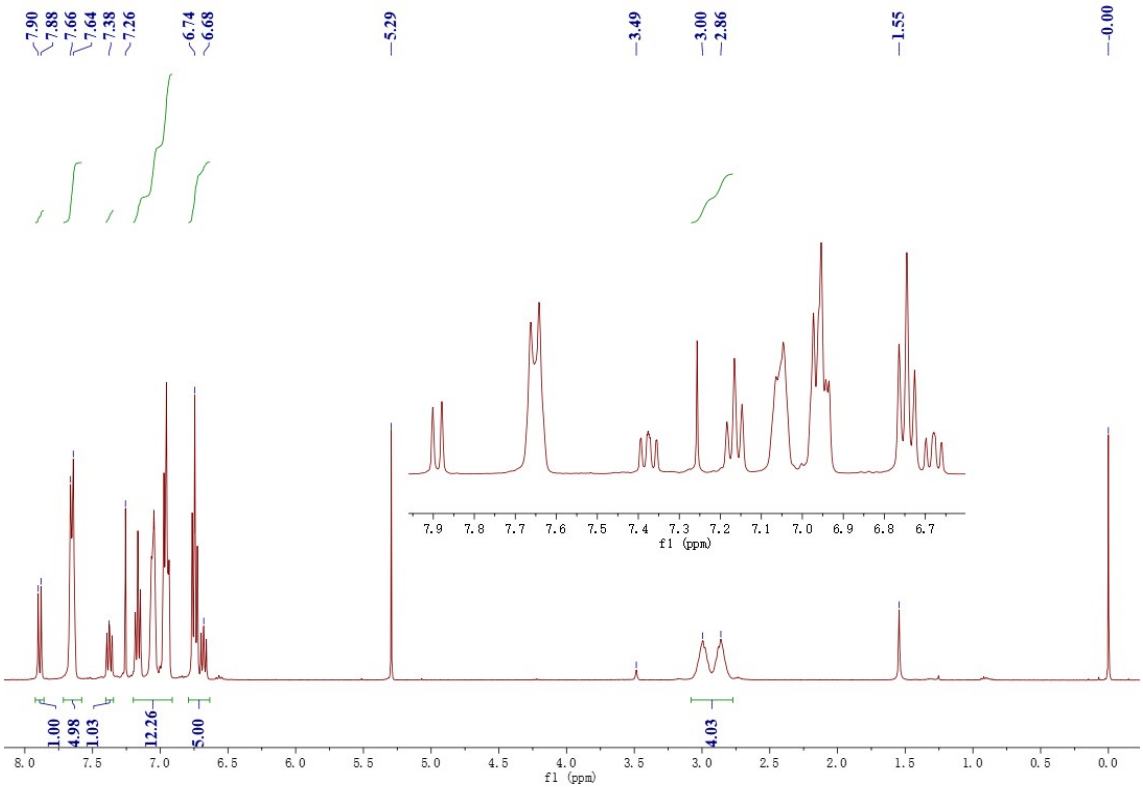

Figure S23. ^{13}C NMR spectrum of *trans*-[Ru(C≡C-10-$C_{14}H_8$-9-NO_2)Cl(dppe)$_2$] (**6c**).

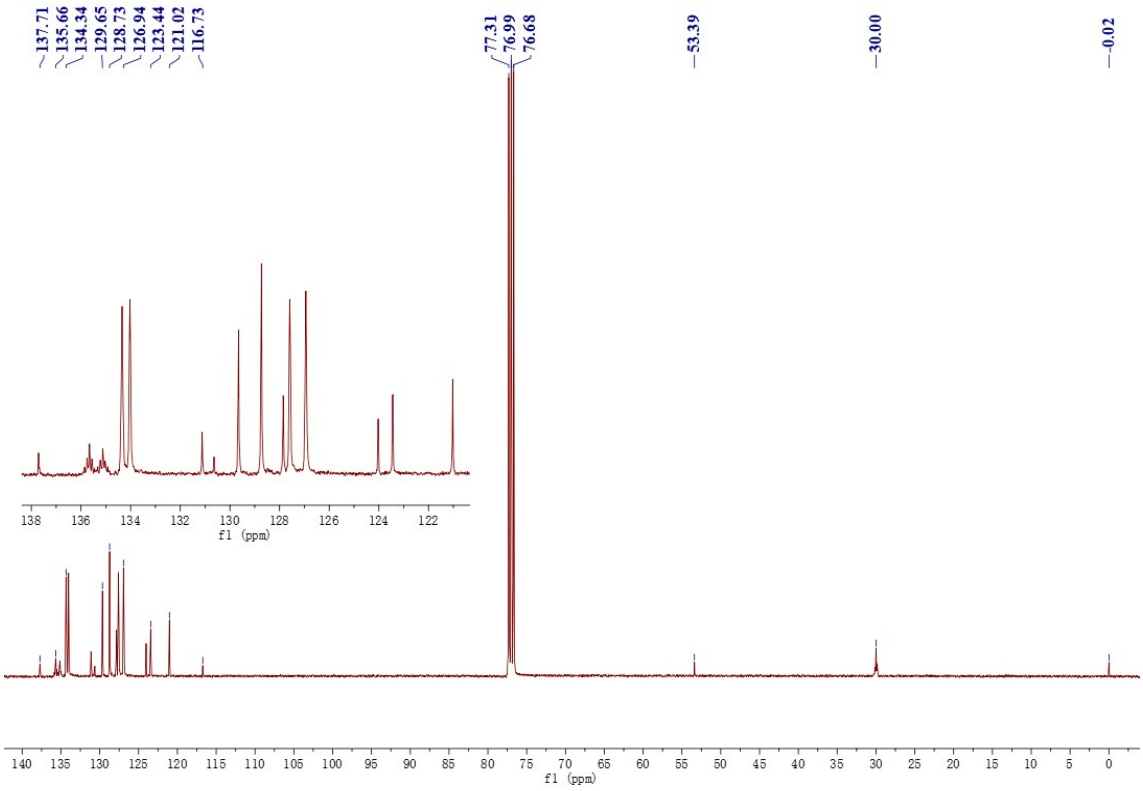

Figure S24. ^{31}P NMR spectrum of *trans*-[Ru(C≡C-10-$C_{14}H_8$-9-NO_2)Cl(dppe)$_2$] (**6c**).

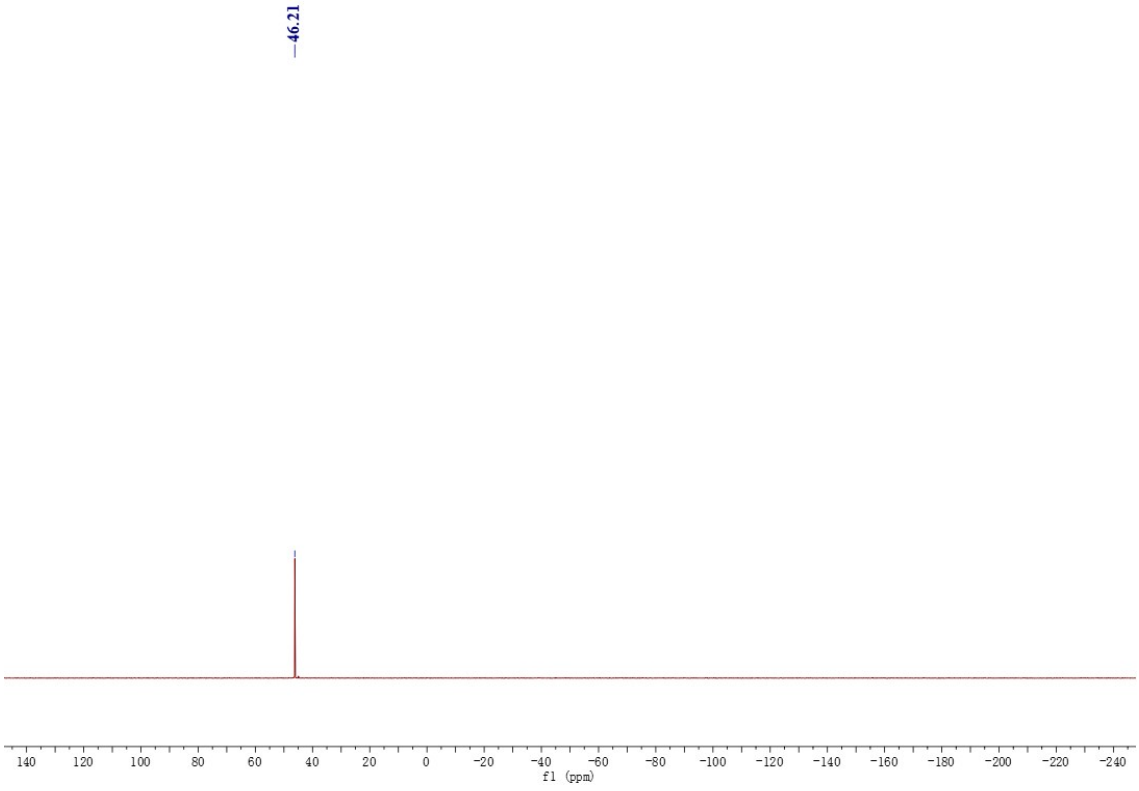

Figure S25. ^{1}H NMR spectrum of *trans*-[Ru(C≡C-10-$C_{14}H_8$-9-NO_2)Cl(dppm)$_2$] (**7c**).

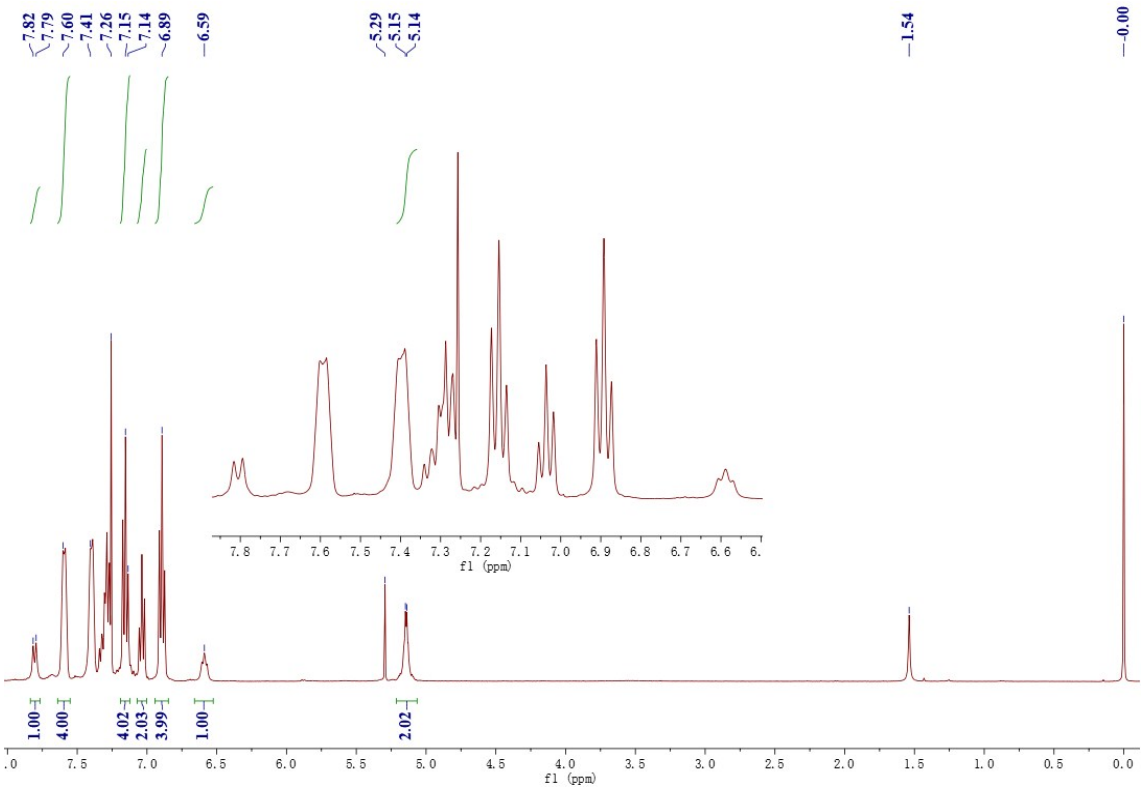

Figure S26. ^{13}C NMR spectrum of *trans*-[Ru(C≡C-10-$C_{14}H_8$-9-NO_2)Cl(dppm)$_2$] (**7c**).

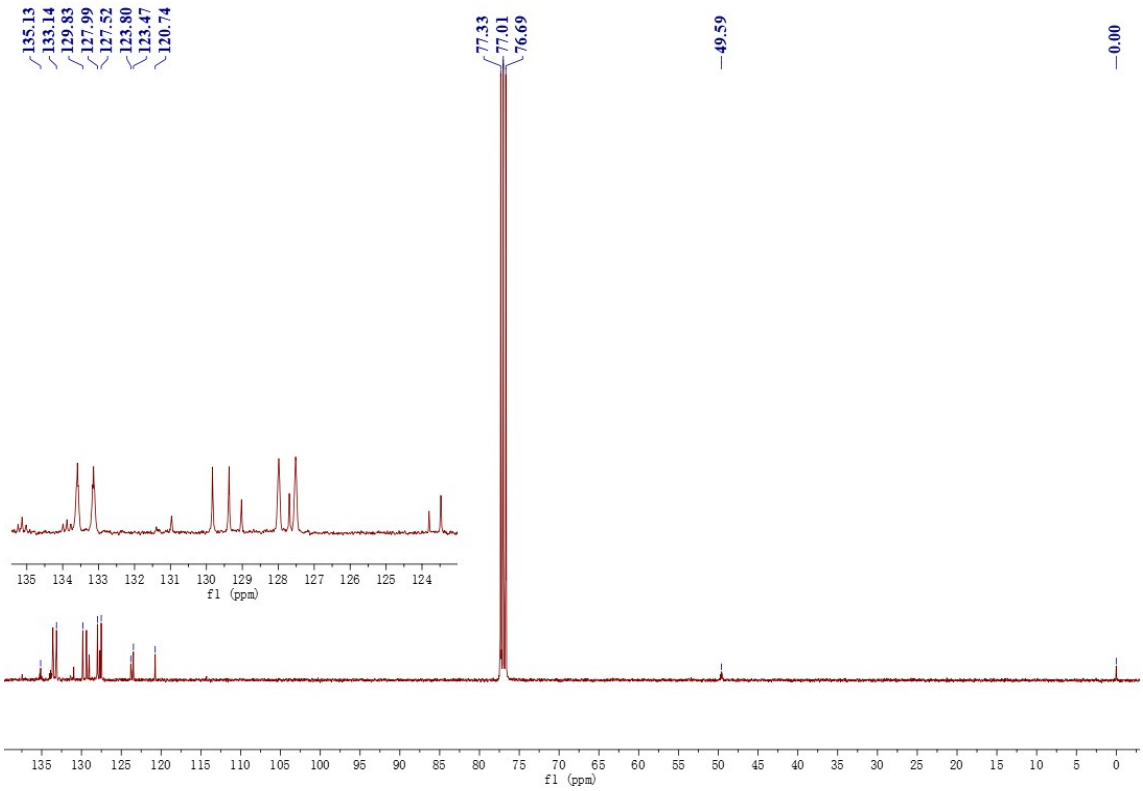

Figure S27. ^{31}P NMR spectrum of *trans*-[Ru(C≡C-10-$C_{14}H_8$-9-NO_2)Cl(dppm)$_2$] (**7c**).

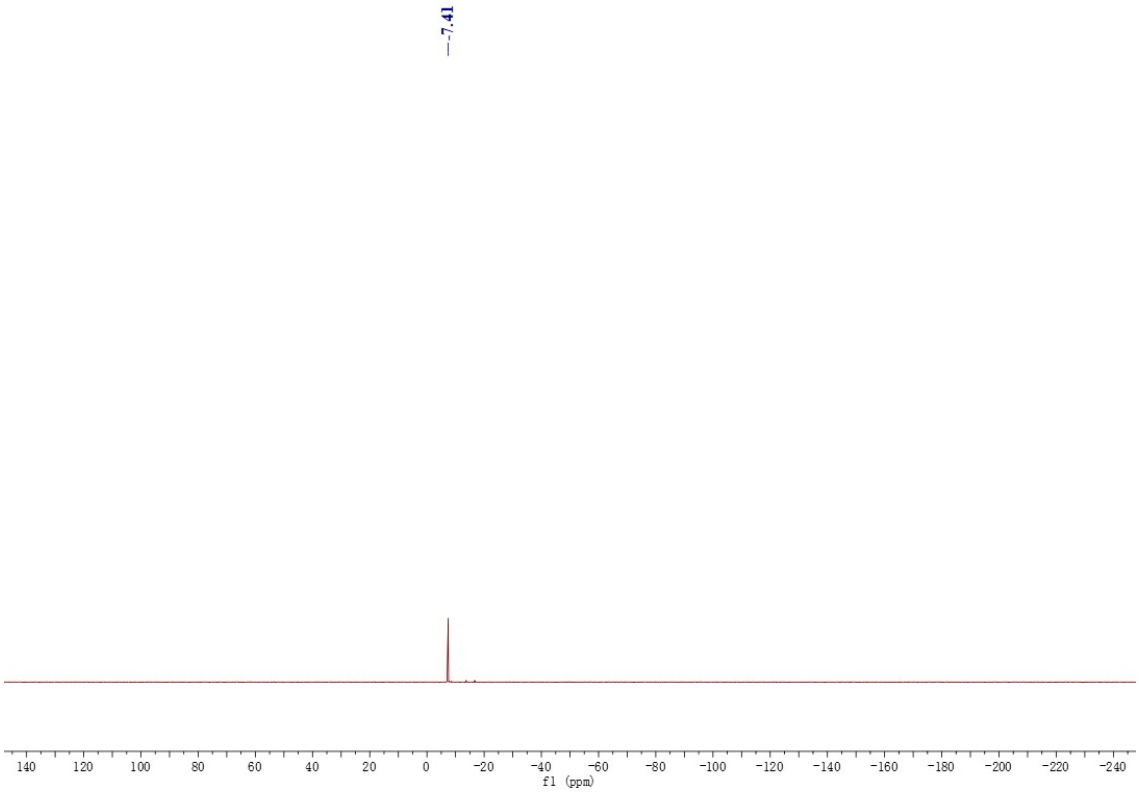

Figure S28. ^{1}H NMR spectrum of Ru(C≡C-10-$C_{14}H_8$-9-NO_2)(PPh_3)$_2$(η^5-C_5H_5) (**8c**).

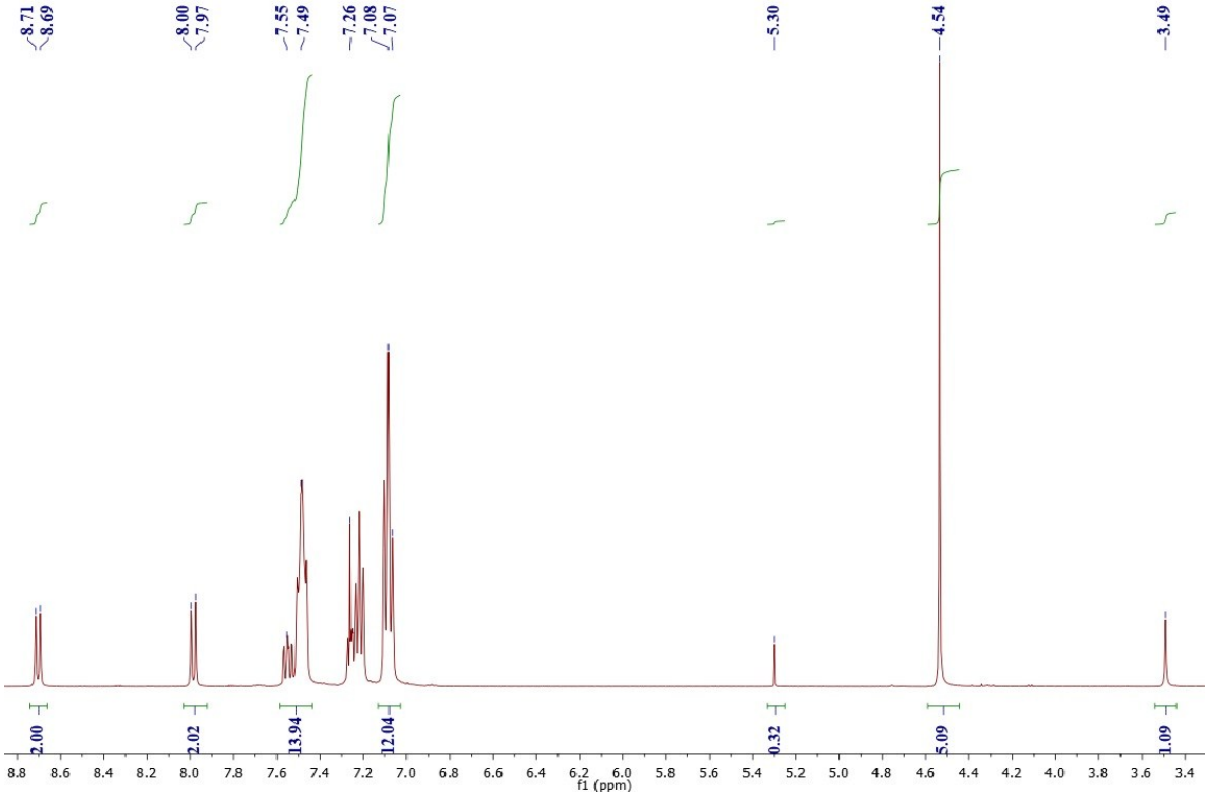

Figure S29. ^{13}C NMR spectrum of Ru(C≡C-10-$C_{14}H_8$-9-NO_2)(PPh_3)$_2$(η^5-C_5H_5) (**8c**).

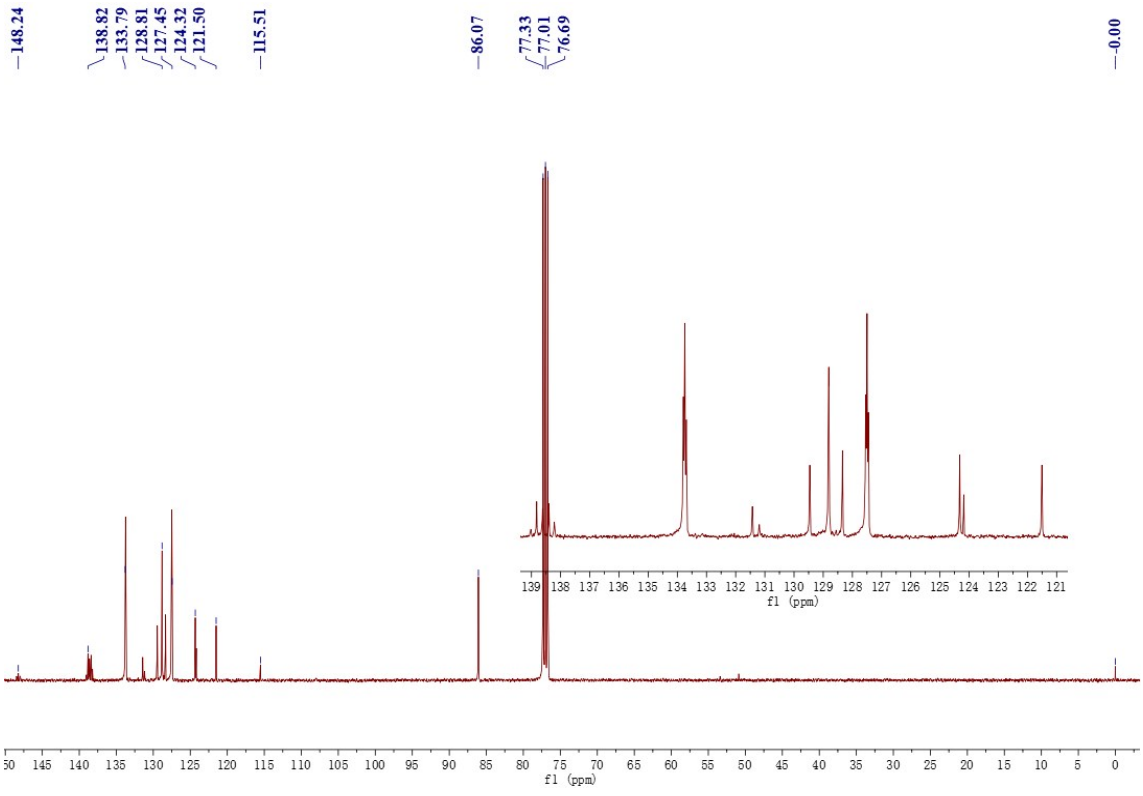

Figure S30. ^{31}P NMR spectrum of Ru(C≡C-10-$C_{14}H_8$-9-NO_2)(PPh_3)$_2$(η^5-C_5H_5) (**8c**).

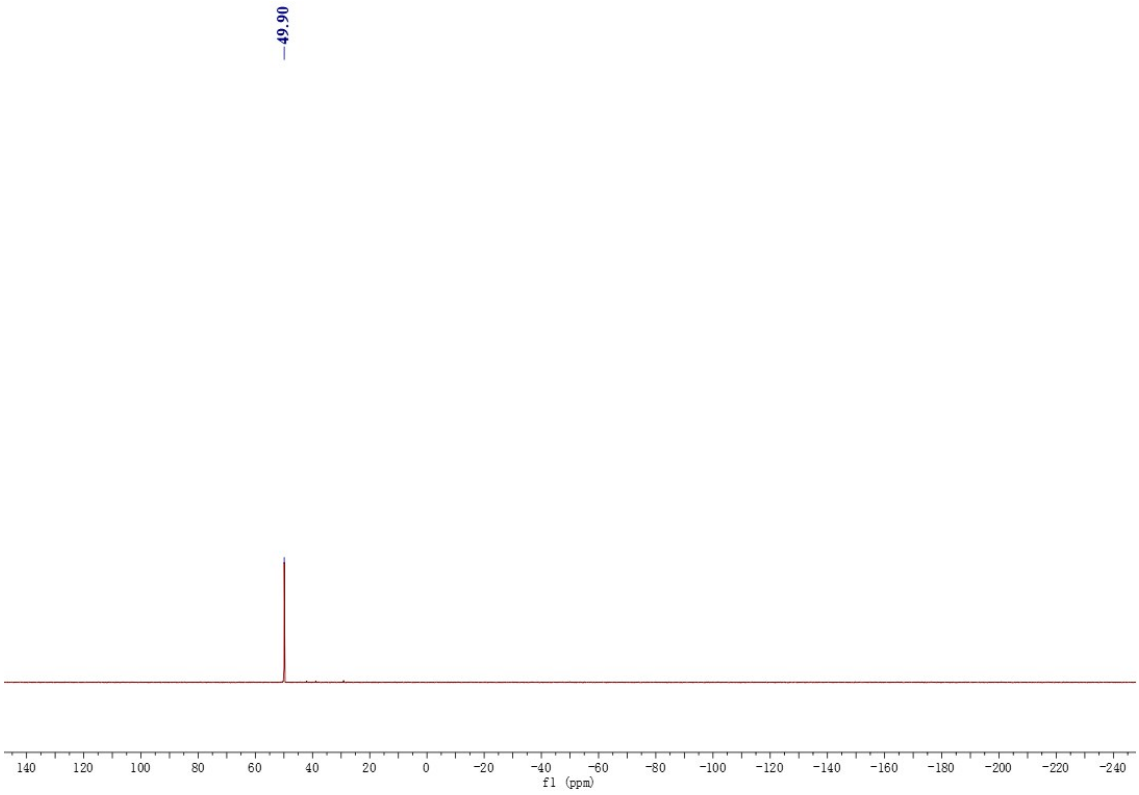

Figure S31. ^{1}H NMR spectrum of Ni(C≡C-10-$C_{14}H_8$-9-NO_2)(PPh_3)(η^5-C_5H_5) (**9c**).

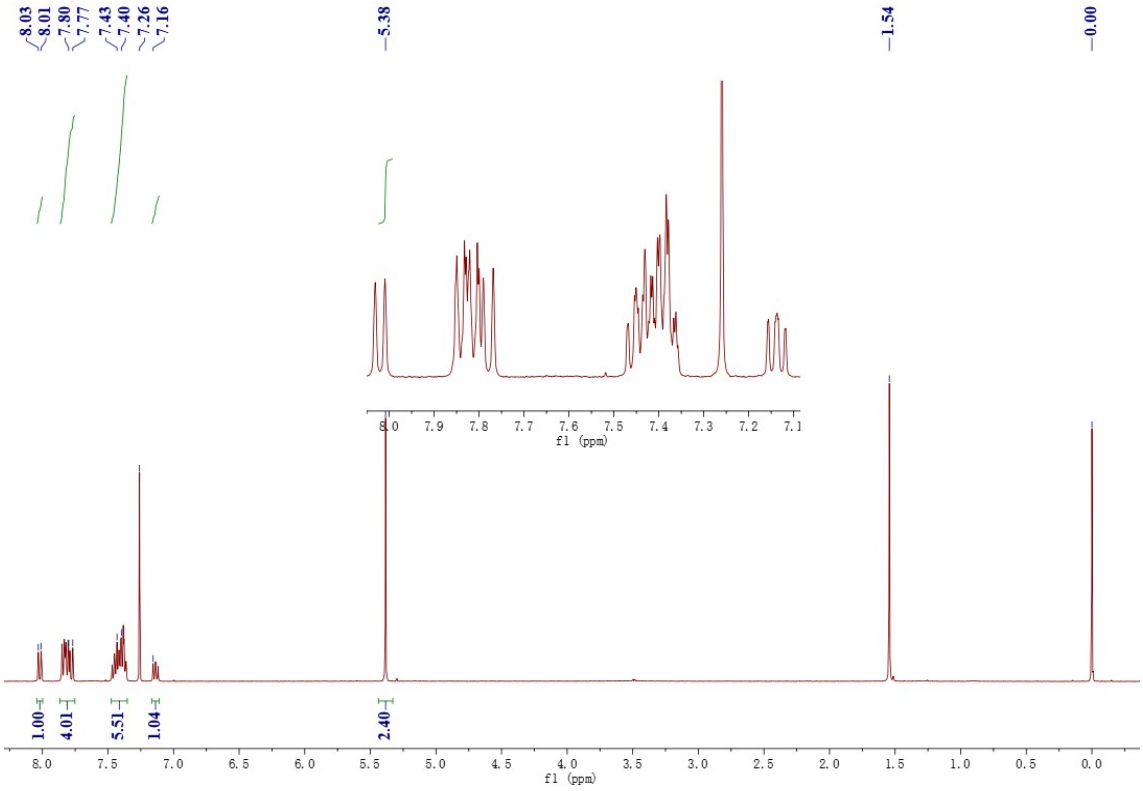

Figure S32. ^{13}C NMR spectrum of Ni(C≡C-10-$C_{14}H_8$-9-NO_2)(PPh_3)(η^5-C_5H_5) (**9c**).

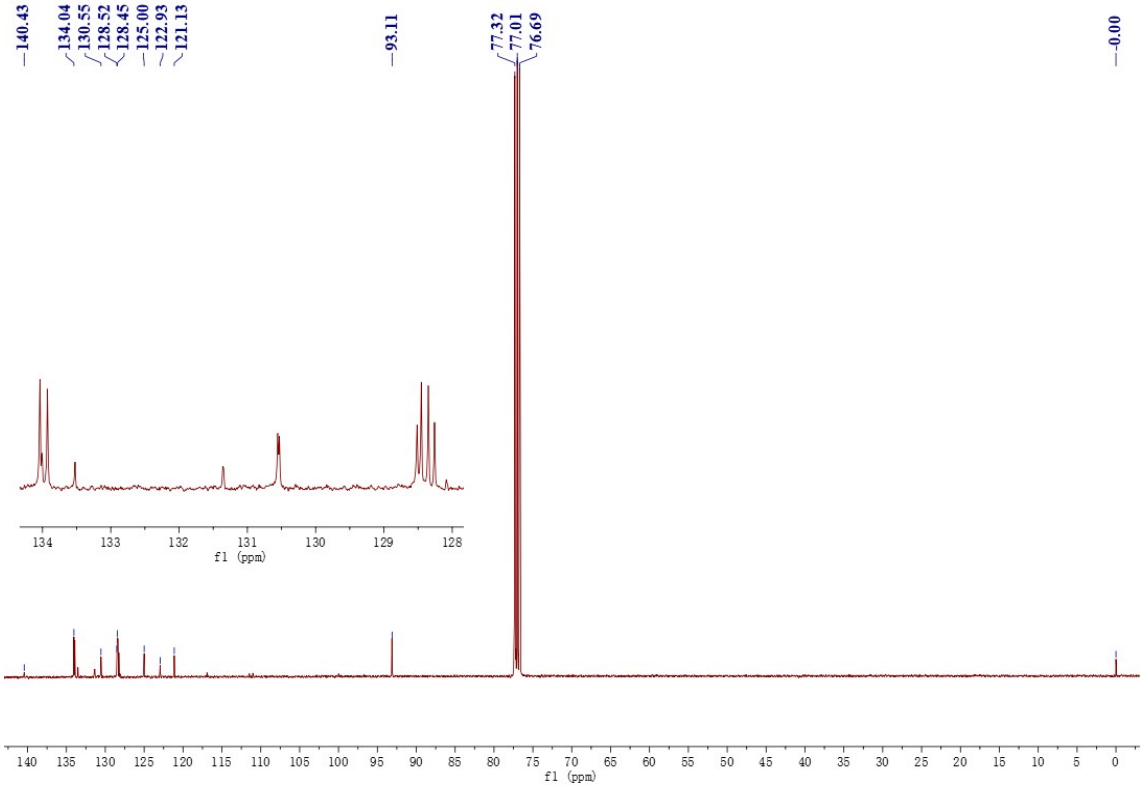

Figure S33. ^{31}P NMR spectrum of Ni(C≡C-10-$C_{14}H_8$-9-NO_2)(PPh_3)(η^5-C_5H_5) (**9c**).

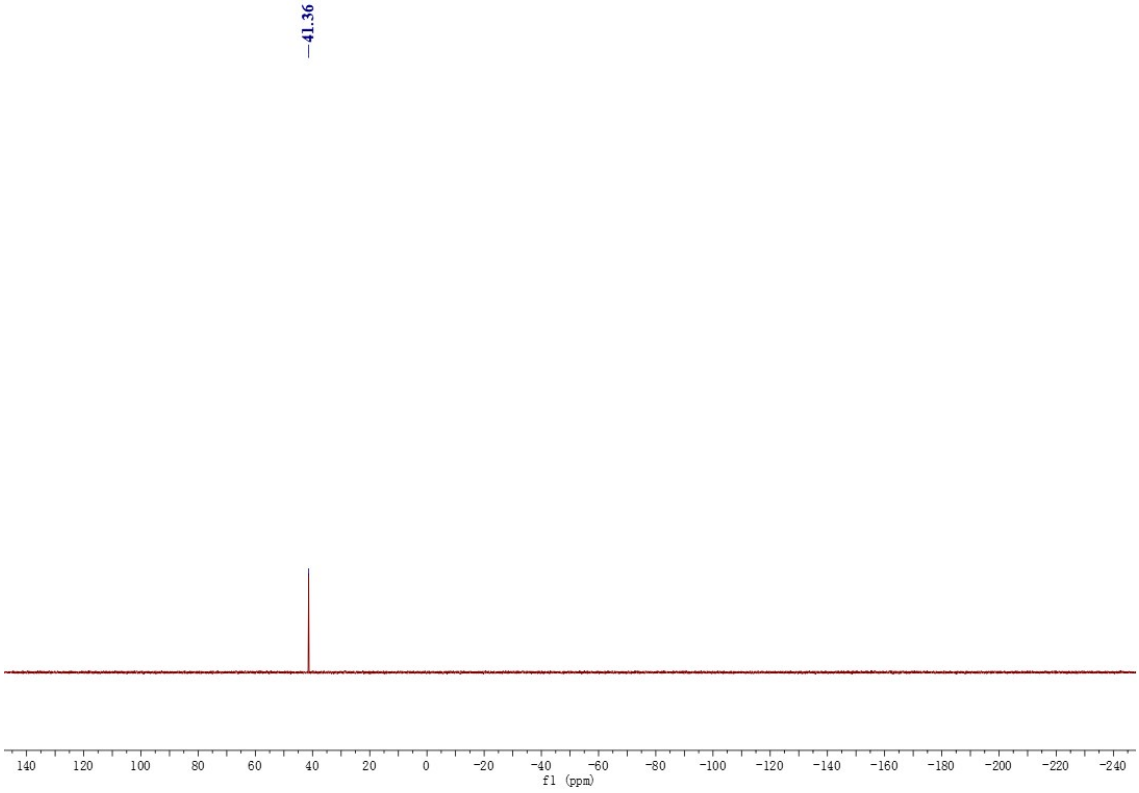

Figure S34. ^{1}H NMR spectrum of Au(C≡C-10-$C_{14}H_8$-9-NO_2)(PPh_3) (**10c**).

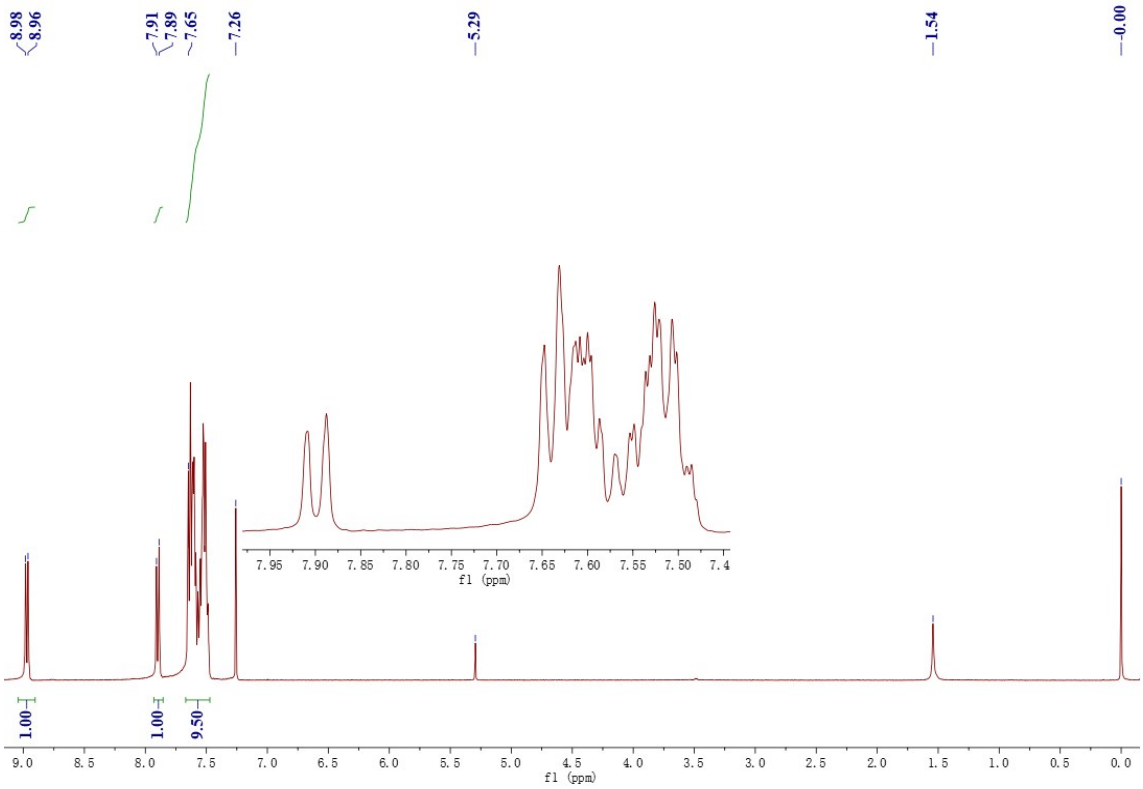

Figure S35. ^{13}C NMR spectrum of Au(C≡C-10-$C_{14}H_8$-9-NO_2)(PPh_3) (**10c**).

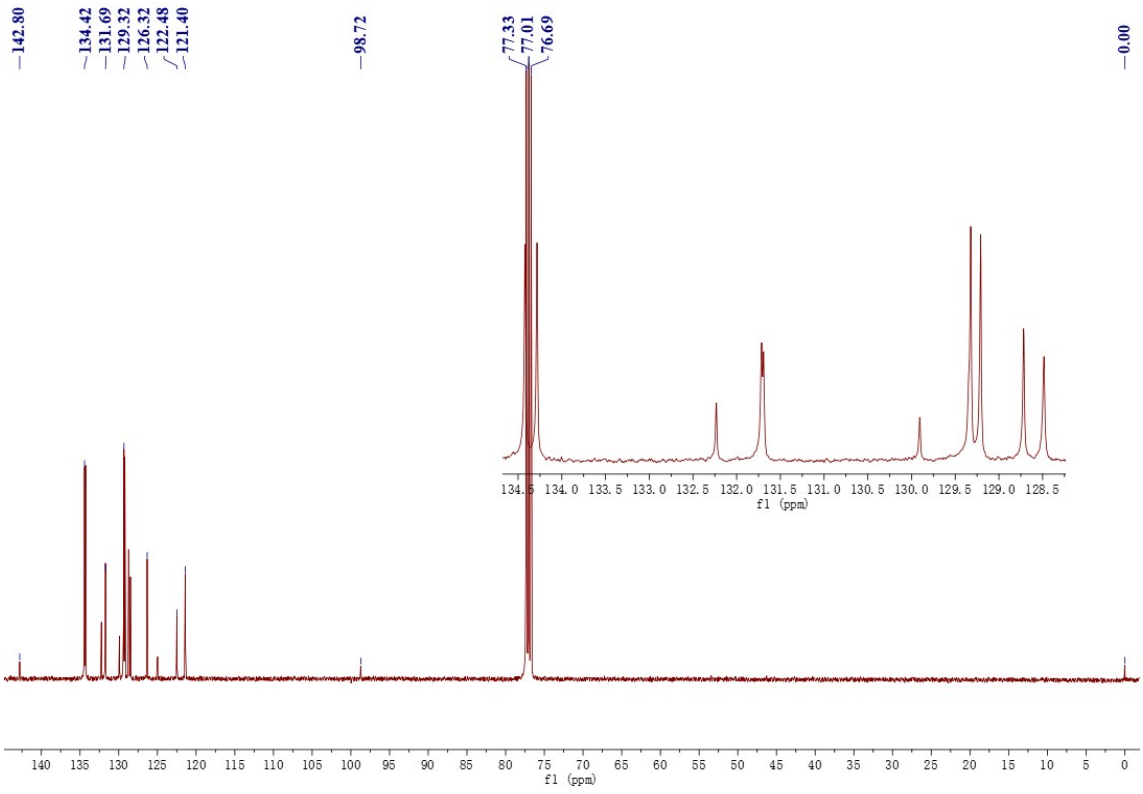

Figure S36. ^{31}P NMR spectrum of Au(C≡C-10-$C_{14}H_8$-9-NO_2)(PPh_3) (**10c**).

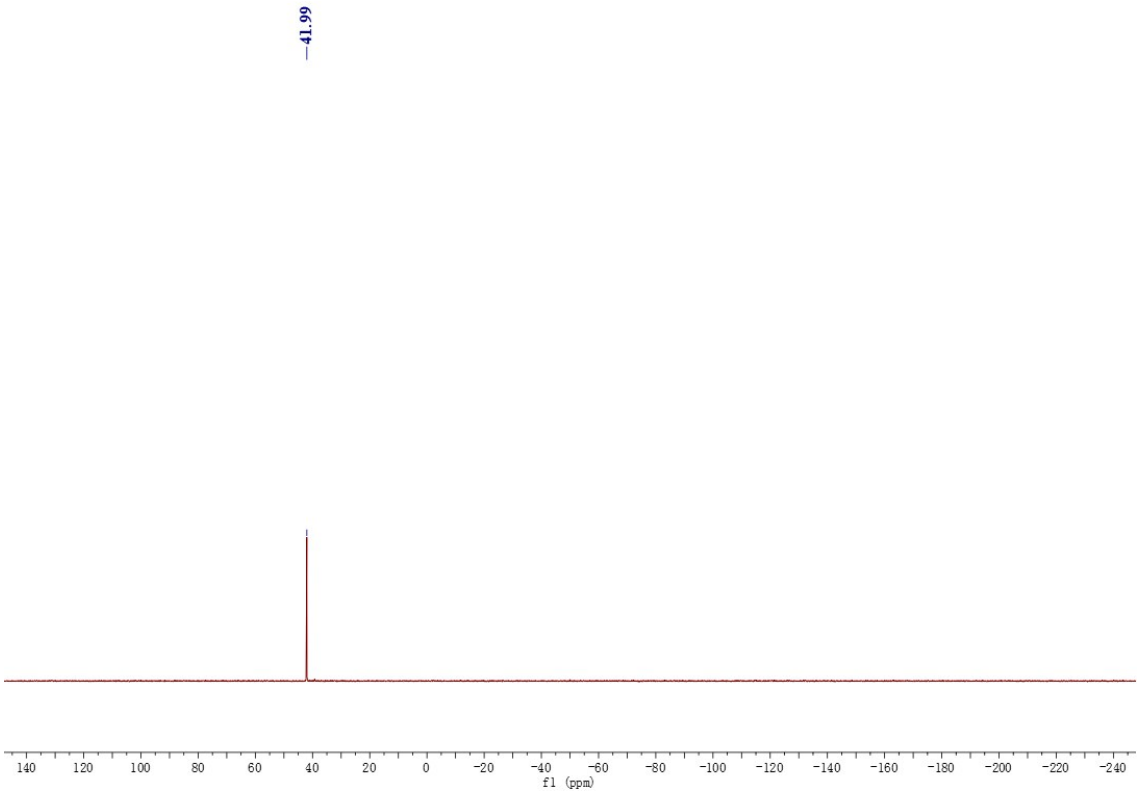

Crystallography

The crystal and refinement data for compounds **4**, **5**, **6a-c**, **7b,c**, **8b,c**, **9b,c**, and **10b,c** are summarized in Table S1. Crystals suitable for the X-ray structural analyses were grown by liquid diffusion of methanol into a dichloromethane solution at 277 K (**4**, **5**, **6b,c**, **7b,c**, **8b,c**, **9b,c**, and **10b,c**) or from a concentrated $CDCl_3$ solution at 298 K (**6a**). Suitable crystals were mounted on MicroMounts (MiTeGen) using Paratone-N oil (Hampton Research) and cooled rapidly to 150 K using an Oxford Cryosystems low-temperature device.[20] Intensity data for **6b,c**, **7b**, **9b,c**, and **10c** were collected on an Agilent XCalibur CCD diffractometer using graphite-monochromated Mo-K_α radiation (λ = 0.71073 Å) and data for **4**, **5**, **6a**, **7c**, **8b,c**, and **10b** were collected on an Agilent SuperNova CCD diffractometer using mirror-monochromated Cu-K_α radiation (λ = 1.54184 Å). N_t (total) reflections were measured by using phi and omega scans and were reduced to N_o unique reflections, with $F_o > 2\sigma(F_o)$ being considered to be observed. The crystals were face-indexed, and Gaussian grid[21] absorption corrections with beam profile corrections were applied. For **6a**, a semi-empirical absorption correction based on symmetry-equivalent and repeat reflections was applied.[22] The structures were solved using direct methods and observed reflections were used in least-squares refinement on F^2, with anisotropic thermal parameters refined for non-hydrogen atoms. Hydrogen atoms were constrained in calculated positions and refined with a riding model. Programs used were CrysAlisPro[23] (control and integration), and SHELXS-97,[24] SHELXL-2014[25] and Olex2[26] (structure solution and refinement and molecular graphics). Crystallographic data for the structural analyses have been deposited with the Cambridge Crystallographic Data Centre, CCDC numbers 1452957-1452969. Copies of this information may be obtained, free of charge, from the Director, CCDC, 12 Union Road, Cambridge CB2 1E2, UK (fax: +44-1223-336033; e-mail: deposit@ccd.cam.ac.uk or www: http://www.ccdc.cam.ac.uk). *Variata*. In **6a**: the 4-nitrophenylethynyl and chloride ligands and lattice $CDCl_3$ molecule are disordered by symmetry over 2 positions, occupancy 0.5:0.5. Restraints were applied to the anisotropic displacements parameters of all atoms on the 4-nitrophenylethynyl and chloride ligands. Atoms C3-C8 of the 4-nitrophenylethynyl ligand were constrained to fit a regular hexagon. In **10b**: rigid bond restraints were applied to the lattice dichloromethane molecule. In **8c**: a lattice dichloromethane molecule could not be successfully modelled, and was therefore removed from the refinement using the smtbx-masks function of Olex2.[26]

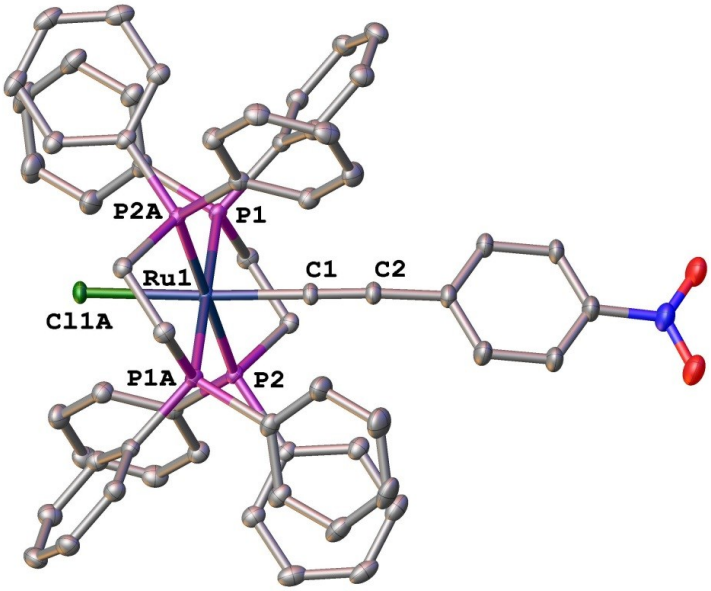

Figure S37. Molecular structure of *trans*-[Ru(C≡C-4-C_6H_4-1-NO_2)Cl(dppe)$_2$] (**6a**), with thermal ellipsoids set at the 40% probability level. Hydrogen atoms, the lattice $CDCl_3$ molecule and disordered components of the 4-nitrophenylethynyl and chloride ligands have been omitted for clarity. Selected bond lengths (Å) and angles (°): Ru1-C1 2.030(7), Ru1-P1 2.3610(5), Ru1-P2 2.3695(5), Ru1-P1A 2.3610(5), Ru1-P2A 2.3695(5), Ru1-Cl1 2.4402(13), C1-C2 1.210(7), P1-Ru1-Cl1A 90.44(4), P1-Ru1-P2 82.852(17), P2-Ru1-Cl1A 99.91(4), P1A-Ru1-Cl1A 89.56(4), P1A-Ru1-P1 180.0, P1A-Ru1-P2 97.148(17), P2A-Ru1-Cl1A 80.09(4), P2A-Ru1-P1 97.147(17), P2A-Ru1-P2 180.0, P2A-Ru1-P1A 82.852(17), C1-Ru1-Cl1A 177.9(2), C1-Ru1-P1 88.0(2), C1-Ru1-P2 81.3(2), C1-Ru1-P1A 92.0(2), C1-Ru1-P2A 98.7(2). Symmetry operation used to generate equivalent atoms A: -x+1, -y+2, -z+1.

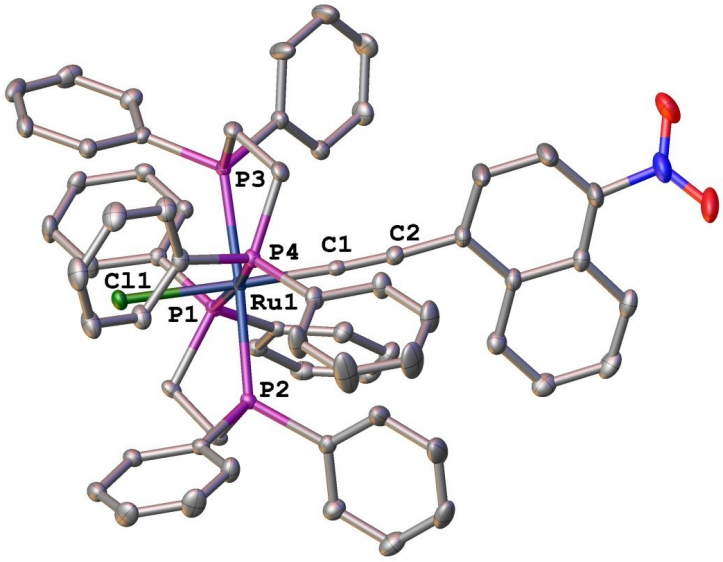

Figure S38. Molecular structure of *trans*-[Ru(C≡C-4-$C_{10}H_6$-1-NO_2)Cl(dppe)$_2$] (**6b**), with thermal ellipsoids set at the 40% probability level. Hydrogen atoms have been omitted for clarity. Selected bond lengths (Å) and angles (°): Ru1-C1 2.002(2), Ru1-P1 2.3751(5), Ru1-P2 2.3753(5), Ru1-P3 2.3732(5), Ru1-P4 2.3687(5), Ru1-Cl1 2.4524(5), C1-C2 1.203(3), P1-Ru1-Cl1 81.097(17), P1-Ru1-P2 81.779(18), P2-Ru1-Cl1 86.780(18), P3-Ru1-Cl1 90.137(18), P3-Ru1-P1 95.728(19), P3-Ru1-P2 176.299(19), P4-Ru1-Cl1 93.063(18), P4-Ru1-P1 173.951(18), P4-Ru1-P2 99.561(19), P4-Ru1-P3 82.637(19), C1-Ru1-Cl1 177.80(5), C1-Ru1-P1 100.52(6), C1-Ru1-P2 94.92(6), C1-Ru1-P3 88.22(6), C1-Ru1-P4 85.28(6).

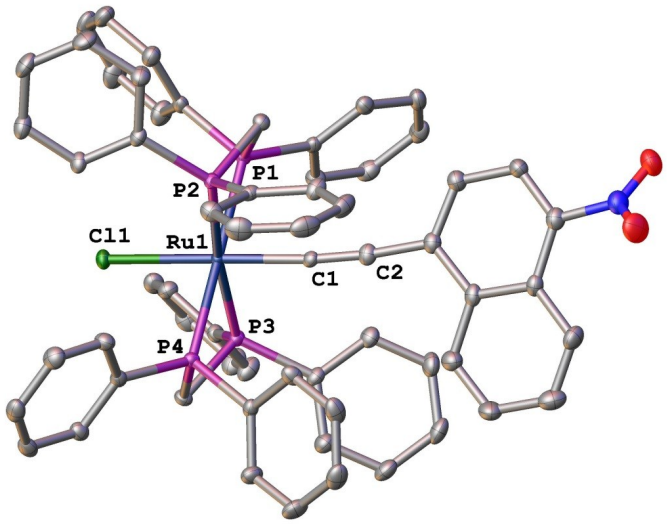

Figure S39. Molecular structure of *trans*-[Ru(C≡C-4-$C_{10}H_6$-1-NO_2)Cl(dppm)$_2$] (**7b**), with thermal ellipsoids set at the 40% probability level. Hydrogen atoms have been omitted for clarity. Selected bond lengths (Å) and angles (°): Ru1-C1 1.985(3), Ru1-P1 2.3360(8), Ru1-P2 2.3624(8), Ru1-P3 2.3550(8), Ru1-P4 2.3395(8), Ru1-Cl1 2.5081(7), C1-C2 1.220(4), P1-Ru1-Cl1 95.86(3), P1-Ru1-P2 70.61(3), P1-Ru1-P3 109.79(3), P1-Ru1-P4 179.45(3), P2-Ru1-Cl1 100.47(3), P3-Ru1-Cl1 86.14(3), P3-Ru1-P2 173.35(3), P4-Ru1-Cl1 83.71(3), P4-Ru1-P2 109.11(3), P4-Ru1-P3 70.55(3), C1-Ru1-Cl1 176.42(9), C1-Ru1-P1 83.38(8), C1-Ru1-P2 82.60(8), C1-Ru1-P3 90.83(8), C1-Ru1-P4 97.06(8).

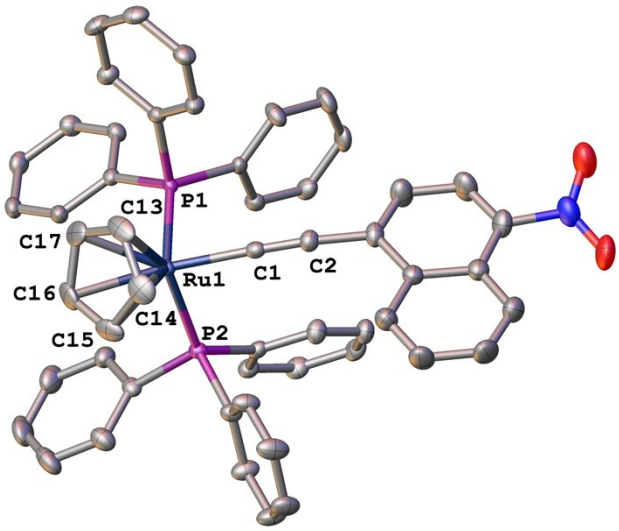

Figure S40. Molecular structure of Ru(C≡C-4-$C_{10}H_6$-1-NO_2)(PPh_3)$_2$(η^5-C_5H_5) (**8b**), with thermal ellipsoids set at the 40% probability level. Hydrogen atoms have been omitted for clarity. Selected bond lengths (Å) and angles (°): Ru1-P1 2.2916(5), Ru1-P2 2.3021(5), Ru1-C1 2.007(2), Ru1-C13 2.218(2), Ru1-C14 2.230(2), Ru1-C15 2.232(2), Ru1-C16 2.247(2), Ru1-C17 2.224(2), C1-C2 1.210(3), P1-Ru1-P2 104.827(19), C1-Ru1-P1 86.38(6), C1-Ru1-P2 87.90(6), C1-Ru1-Cp(centroid) 126.01(8), P1-Ru1-Cp(centroid) 121.82(5), P2-Ru1-Cp(centroid) 121.00(5).

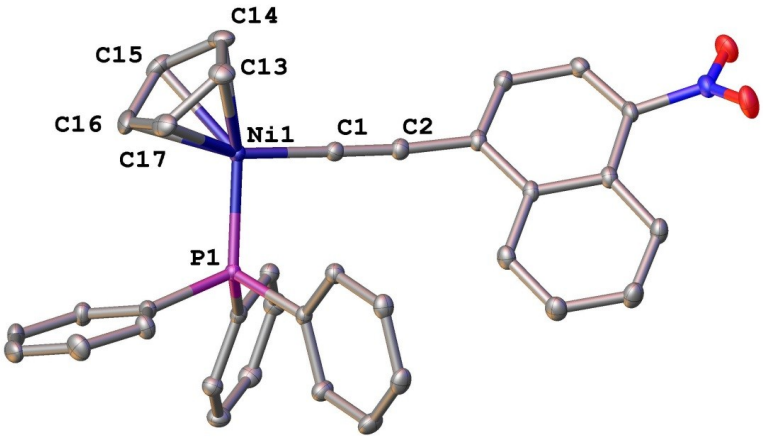

Figure S41. Molecular structure of Ni(C≡C-4-$C_{10}H_6$-1-NO_2)(PPh_3)(η^5-C_5H_5) (**9b**), with thermal ellipsoids set at the 40% probability level. Hydrogen atoms have been omitted for clarity. Selected bond lengths (Å) and angles (°): Ni1-P1 2.1341(4), Ni1-C1 1.8434(13), Ni1-C13 2.1275(14), Ni1-C14 2.0869(14), Ni1-C15 2.1512(15), Ni1-C16 2.0952(14), Ni1-C17 2.1101(14), C1-C2 1.2170(18), C1-Ni1-P1 92.56(4), C1-Ni1-Cp(centroid) 132.76(5), P1-Ru1-Cp(centroid) 133.72(3).

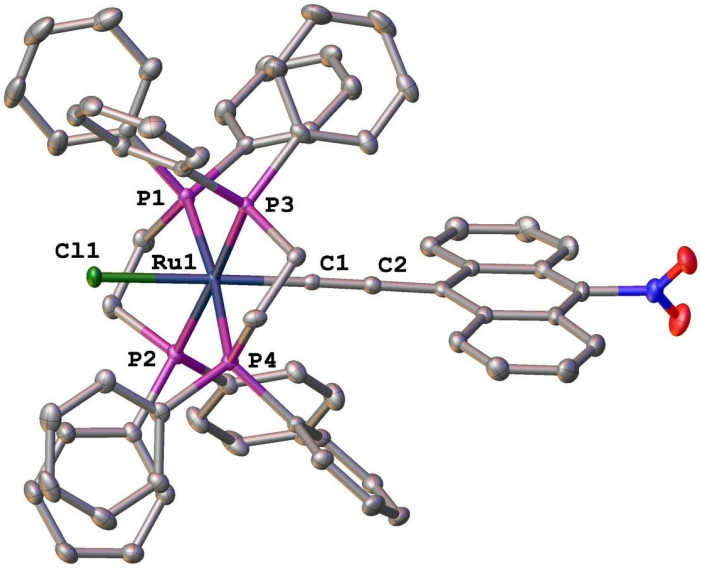

Figure S42. Molecular structure of *trans*-[Ru(C≡C-10-$C_{14}H_8$-9-NO_2)Cl(dppe)$_2$] (**6c**), with thermal ellipsoids set at the 40% probability level. Hydrogen atoms and the lattice dichloromethane molecule have been omitted for clarity. Selected bond lengths (Å) and angles (°): Ru1-C1 2.002(2), Ru1-P1 2.3795(6), Ru1-P2 2.3851(6), Ru1-P3 2.3709(6), Ru1-P4 2.3810(6), Ru1-Cl1 2.4615(5), C1-C2 1.214(3), P1-Ru1-Cl1 85.19(2), P1-Ru1-P2 82.23(2), P2-Ru1-Cl1 81.71(2), P3-Ru1-Cl1 94.91(2), P3-Ru1-P1 98.43(2), P3-Ru1-P2 176.50(2), P4-Ru1-Cl1 88.99(2), P4-Ru1-P1 174.12(2), P4-Ru1-P2 96.11(2), P4-Ru1-P3 82.89(2), C1-Ru1-Cl1 178.48(6), C1-Ru1-P1 96.24(6), C1-Ru1-P2 98.96(6), C1-Ru1-P3 84.41(6), C1-Ru1-P4 89.58(6).

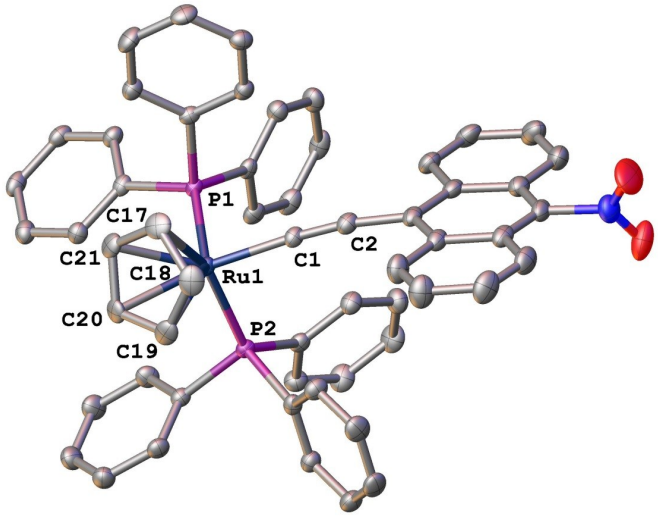

Figure S43. Molecular structure of Ru(C≡C-10-$C_{14}H_8$-9-NO_2)$(PPh_3)_2(\eta^5$-$C_5H_5)$ (**8c**), with thermal ellipsoids set at the 40% probability level. Hydrogen atoms have been omitted for clarity. Selected bond lengths (Å) and angles (°): Ru1-P1 2.2967(8), Ru1-P2 2.2908(8), Ru1-C1 2.002(3), Ru1-C17 2.235(3), Ru1-C18 2.215(3), Ru1-C19 2.233(3), Ru1-C20 2.258(3), Ru1-C21 2.247(3), C1-C2 1.211(5), P1-Ru1-P2 104.57(3), C1-Ru1-P1 88.73(9), C1-Ru1-P2 88.67(9), C1-Ru1-Cp(centroid) 123.13(11), P1-Ru1-Cp(centroid) 122.04(6), P2-Ru1-Cp(centroid) 121.20(6).

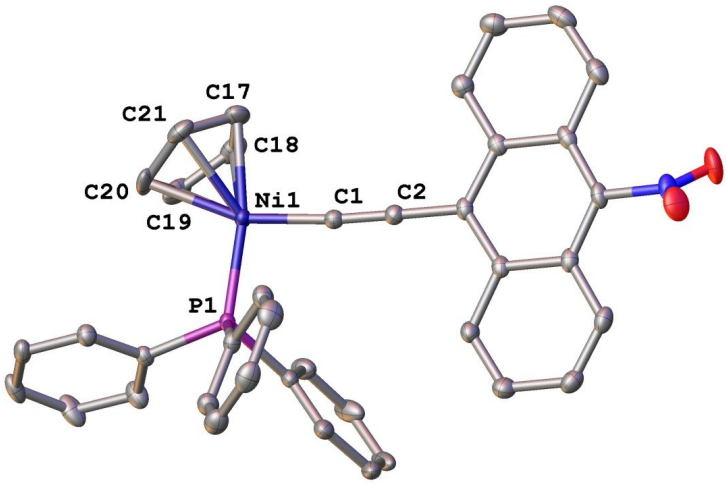

Figure S44. Molecular structure of Ni(C≡C-10-$C_{14}H_8$-9-NO_2)(PPh_3)(η^5-C_5H_5) (**9c**), with thermal ellipsoids set at the 40% probability level. Hydrogen atoms have been omitted for clarity. Selected bond lengths (Å) and angles (°): Ni1-P1 2.1352(6), Ni1-C1 1.8403(19), Ni1-C17 2.065(2), Ni1-C18 2.120(2), Ni1-C19 2.117(2), Ni1-C20 2.075(2), Ni1-C21 2.135(2), C1-C2 1.213(3), C1-Ni1-P1 93.91(6), C1-Ni1-Cp(centroid) 129.31(8), P1-Ru1-Cp(centroid) 136.60(5).

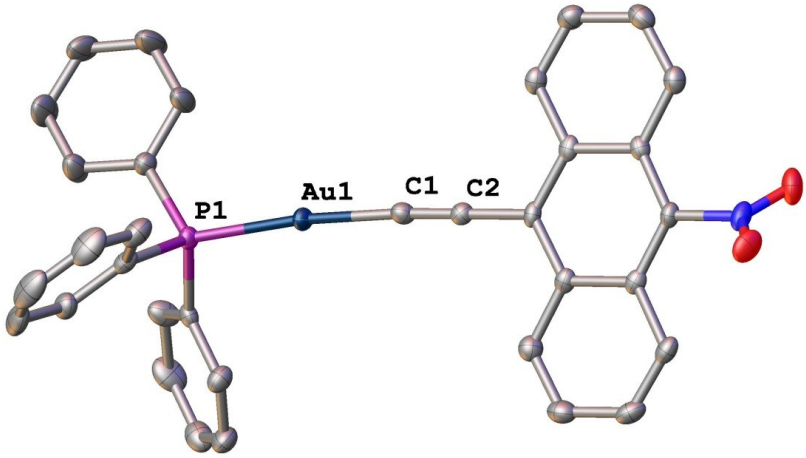

Figure S45. Molecular structure of Au(C≡C-10-$C_{14}H_8$-9-NO_2)(PPh_3) (**10c**), with thermal ellipsoids set at the 40% probability level. Hydrogen atoms have been omitted for clarity. Selected bond lengths (Å) and angle (°): Au1-P1 2.2730(9), Au1-C1 1.991(4), C1-C2 1.199(5), C1-Au1-P1 174.08(10).

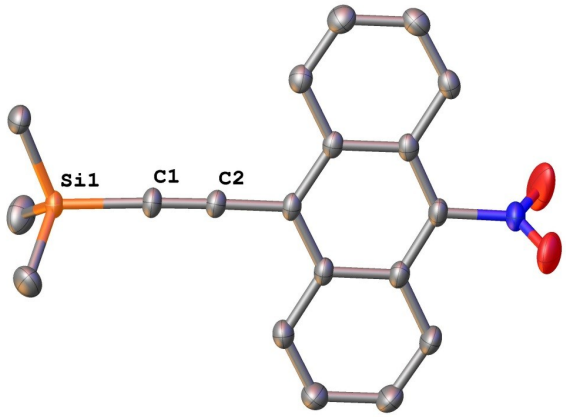

Figure S46. Molecular structure of 9-nitro-10-(trimethylsilylethynyl)anthracene (**4**), with thermal ellipsoids set at the 40% probability level. Hydrogen atoms have been omitted for clarity. Selected bond lengths (Å): Si1-C1 1.841(3), C1-C2 1.208(4), C2-C3 1.429(4), C10-N1 1.470(3), N1-O1 1.249(5), N1-O2 1.191(5).

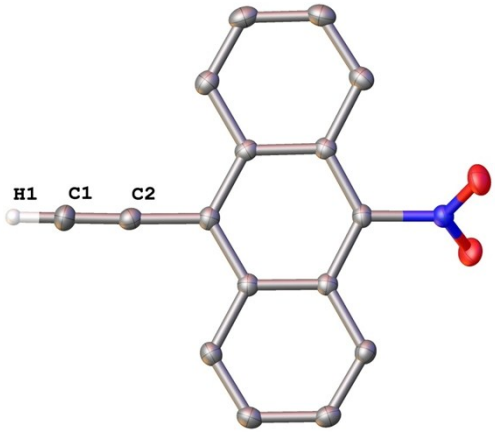

Figure S47. Molecular structure of 10-ethynyl-9-nitroanthracene (**5**), with thermal ellipsoids set at the 40% probability level. Hydrogen atoms, other than H1, have been omitted fpr clarity. Selected bond lengths (Å): C1-C2 1.189(3), C2-C3 1.435(1), C10-N1 1.474(2), N1-O1 1.226(2), N1-O2 1.224(2).

Table S1. Crystal data for **4**, **5**, **6a-c**, **7b,c**, **8b,c**, **9b,c**, and **10b,c**.

	4	**5**	**6a·CDCl$_3$**	**6b**	**6c·CH$_2$Cl$_2$**	**7b**	**7c**
Formula	$C_{19}H_{17}NO_2Si$	$C_{16}H_9NO_2$	$C_{61}H_{53}Cl_4DNO_2P_4Ru$	$C_{64}H_{54}ClNO_2P_4Ru$	$C_{69}H_{58}Cl_3NO_2P_4Ru$	$C_{62}H_{50}ClNO_2P_4Ru$	$C_{66}H_{52}ClNO_2P_4Ru$
FW	319.42	247.24	1200.80	1129.48	1264.46	1101.43	1151.48
Size (mm)	0.18 x 0.04 x 0.03	0.28 x 0.09 x 0.03	0.15 x 0.10 x 0.04	0.26 x 0.15 x 0.14	0.33 x 0.13 x 0.12	0.27 x 0.26 x 0.23	0.28 x 0.23 x 0.15
Crystal system	Triclinic	Monoclinic	Triclinic	Triclinic	Monoclinic	Orthorhombic	Monoclinic
Space group	*P*-1	$P2_1$	*P*-1	*P*-1	$P2_1/c$	$P2_12_12_1$	$P2_1/c$
a (Å)	7.0157(4)	3.86591(12)	9.41766(14)	12.9941(3)	16.08908(17)	16.49656(16)	12.95865(9)
b (Å)	10.2203(5)	16.1913(5)	12.8965(2)	13.3049(3)	20.13082(18)	16.69422(14)	21.29055(15)
c (Å)	12.3017(6)	9.0929(3)	13.5842(3)	17.2440(4)	18.2778(2)	18.18356(14)	20.36872(17)
α (°)	75.910(4)	90	117.477(2)	84.358(2)	90	90	90
β (°)	87.015(4)	100.696(3)	95.3545(14)	82.209(2)	99.7351(10)	90	102.2772(8)
γ (°)	85.358(4)	90	103.8648(14)	63.077(3)	90	90	90
V (Å^3)	852.24(8)	559.27(3)	1380.71(5)	2631.29(13)	3298.8(11)	5007.70(7)	5491.14(7)
Z	2	2	1	2	4	4	4
D_{calc} (g cm^{-3})	1.245	1.468	1.444	1.426	1.439	1.461	1.393
μ (mm^{-1})	1.284	0.796	5.525	0.518	0.564	0.542	4.226
θ_{min} (°)	3.7	5.0	3.9	1.7	1.6	1.7	3.0
θ_{max} (°)	72.2	72.2	72.5	29.7	29.7	29.7	72.3
$N_{collected}$	5764	2219	19019	35106	52553	111509	81679
N_{unique}	3316	1556	5443	12582	14239	13207	10800
$N_{observed}$	2816	1534	5304	10505 ($I > 2\sigma(I)$)	11467 ($I > 2\sigma(I)$)	12309 ($I > 2\sigma(I)$)	9712 ($I > 2\sigma(I)$)
No. of parameters	211	172	391	658	721	640	676
R_1	0.095	0.031	0.032	0.033	0.037	0.030	0.040
wR_2	0.264	0.083	0.085	0.073	0.084	0.066	0.093
S	1.22	1.08	1.04	1.04	1.03	1.07	1.16
$(\Delta/\rho)_{min}$ (e Å^{-3})	-0.42	-0.23	-0.56	-0.67	-1.06	-0.51	-0.47
$(\Delta/\rho)_{max}$ (e Å^{-3})	1.62	0.19	0.97	0.77	0.55	0.73	0.88

Table S1 (continued).

	8b	**8c**	**9b**	**9c**	**2(10b)·CH_2Cl_2**	**10c**
Formula	$C_{53}H_{41}NO_2P_2Ru$	$C_{57}H_{43}NO_2P_2Ru$	$C_{35}H_{26}NNiO_2P$	$C_{39}H_{28}NNiO_2P$	$C_{61}H_{44}Au_2Cl_2N_2O_4P_2$	$C_{34}H_{23}AuNO_2P$
FW	886.88	936.93	582.25	632.30	1395.75	705.47
Size (mm)	0.20 x 0.15 x 0.09	0.22 x 0.18 x 0.15	0.44 x 0.36 x 0.22	0.30 x 0.23 x 0.16	0.09 x 0.07 x 0.04	0.27 x 0.11 x 0.09
Crystal system	Monoclinic	Monoclinic	Triclinic	Triclinic	Monoclinic	Monoclinic
Space group	$P2_1/n$	$P2_1/c$	P-1	P-1	$C2/c$	$P2_1/c$
a (Å)	11.71137(11)	10.87123(14)	9.19956(17)	10.6301(4)	36.1611(8)	13.4643(3)
b (Å)	16.83124(16)	10.86302(14)	10.0055(2)	11.3860(5)	8.77972(5)	12.30268(19)
c (Å)	21.14557(16)	38.6139(5)	15.3374(3)	13.7945(7)	23.3532(5)	16.3775(2)
α (°)	90	90	83.4364(19)	77.211(4)	90	90
β (°)	98.9865(8)	91.7520(11)	72.5673(19)	69.077(4)	135.829(4)	97.0443(16)
γ (°)	90	90	87.4685(17)	75.124(4)	90	90
V (Å^3)	4116.99(6)	4557.96(10)	1338.01(5)	1491.62(13)	5166.3(3)	2692.41(8)
Z	4	4	2	2	4	4
D_{calc} (g cm^{-3})	1.431	1.365	1.445	1.408	1.794	1.740
μ (mm^{-1})	4.162	3.791	0.820	0.742	12.474	5.556
θ_{min} (°)	3.4	4.1	2.0	1.9	3.5	2.1
θ_{max} (°)	72.4	72.4	32.5	29.8	72.3	29.54
$N_{collected}$	80158	32218	66928	12563	80445	14235
N_{unique}	8128	8970	9089	6947	5086	6390
$N_{observed}$	8051 ($I > 2\sigma(I)$)	8696 ($I > 2\sigma(I)$)	7653 ($I > 2\sigma(I)$)	5763 ($I > 2\sigma(I)$)	5047 ($I > 2\sigma(I)$)	5197 ($I > 2\sigma(I)$)
No. of parameters	532	568	361	397	330	352
R_1	0.032	0.043	0.033	0.038	0.020	0.030
wR_2	0.081	0.096	0.074	0.076	0.051	0.051
S	1.07	1.16	1.06	1.05	1.04	1.06
$(\Delta/\rho)_{min}$ (e Å^{-3})	-0.51	-1.04	-0.34	-0.34	-1.51	-0.82
$(\Delta/\rho)_{max}$ (e Å^{-3})	0.99	1.18	0.45	0.38	1.43	0.89

Table S2. Selected bond distances (Å) and angles (^{0}) for complexes **6a-c**, **7a-c**, **8a-c**, **9a-c**, and **10a-c**.

.

Complex [M]	**6a [Ru]**	**6b [Ru]**	**6c [Ru]**	**7a [Ru][b]**	**7b [Ru]**	**7c [Ru]**	**8a [Ru][c]**	**8b [Ru]**	**8c [Ru]**	**9a [Ni][d]**	**9b [Ni]**	**9c [Ni]**	**10a [Au][e]**	**10b [Au]**	**10c [Au]**
[M]-C1	2.030(7)	2.002(3)	2.013(3)	1.998(7) 1.949(6)	1.985(3)	2.002(2)	1.994(5)	2.006(2)	2.002(3)	1.842(6)	1.8434(13)	1.841(2)	1.973(5)	1.999(3)	1.991(4)
C1-C2	1.210(7)	1.203(4)	1.207(4)	1.190(8) 1.201(8)	1.220(4)	1.214(3)	1.202(8)	1.211(3)	1.212(5)	1.207(7)	1.2170(18)	1.213(3)	1.206(6)	1.201(4)	1.199(5)
C2-C3	1.448(6)	1.452(4)	1.430(4)	1.428(8) 1.419(9)	1.434(5)	1.423(3)	1.432(7)	1.462(3)	1.430(5)	1.422(7)	1.4269(18)	1.426(2)	1.446(6)	1.433(3)	1.433(5)
C6-N/C10-N	1.453(4)	1.467(4)	1.473(4)	1.467(9) 1.450(8)	1.446(5)	1.464(3)	1.468(6)	1.474(4)	1.478(4)	1.466(7)	1.4577(17)	1.471(2)	1.492(7)	1.467(3)	1.470(5)
[M]-Cp [a]	-	-	-	-	-	-	-	1.878(10)	1.8836(15)	-	1.7398(7)	1.7316(9)	-	-	-
[M]-C1-C2	174.7(7)	176.47(18)	176.4(3)	176.8(5) 177.6(6)	174.7(3)	176.6(2)	175.9(4)	178.2(2)	173.8(3)	174.5(5)	176.17(12)	174.86(17)	175.1(5)	176.0(2)	175.4(4)
C1-C2-C3	175.4(6)	176.1(2)	177.8(3)	168.4(7) 178.8(7)	173.0(3)	1.797(2)	175.0(9)	168.9(3)	171.8(4)	171.3(7)	173.66(14)	177.8(2)	179.8(6)	179.2(3)	179.9(4)
C1-[M]-Cp [a]	-	-	-	-	-	-	-	125.51(9)	122.13(14)	-	132.76(6)	129.27(9)	-	-	-

[a] Cp centroid, [b] Ref. [27], [c] Ref [10], [d] Ref. [28], [e] Ref. [12].

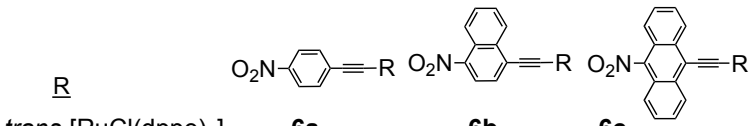

trans-[RuCl(dppe)$_2$]	**6a**	**6b**	**6c**
trans-[RuCl(dppm)$_2$]	**7a**	**7b**	**7c**
Ru(PPh$_3$)$_2$(η-C$_5$H$_5$)	**8a**	**8b**	**8c**
Ni(PPh$_3$)(η-C$_5$H$_5$)	**9a**	**9b**	**9c**
Au(PPh$_3$)	**10a**	**10b**	**10c**

Cyclic Voltammetry

Measurements were recorded using an e-corder 401 potentiostat system from eDaq Pty Ltd. Measurements were carried out at room temperature using Pt disc working-, Pt wire auxiliary-, and Ag/AgCl reference electrodes, such that the ferrocene/ferrocenium redox couple was located at 0.56 V (i_{pc}/i_{pa} = 1, ΔE_p 0.09 V). Scan rates were typically 100 mV s^{-1}. Electrochemical solutions contained 0.1 M $(NBu^n_4)PF_6$ and ca. 10^{-3} M complex in dried and distilled dichloromethane. Solutions were purged and maintained under a nitrogen atmosphere.

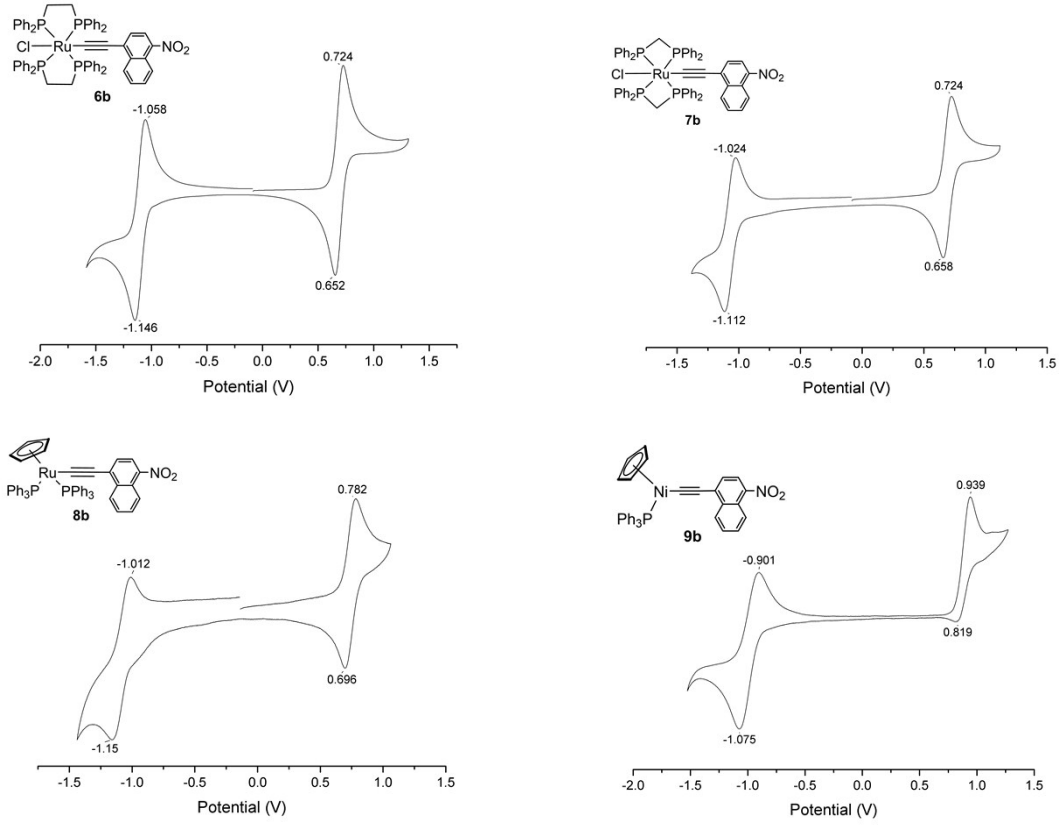

Figures S48 (top left), **S49** (top right), **S50** (bottom left), and **S51** (bottom right). CV traces for compounds **6b**-**9b**.

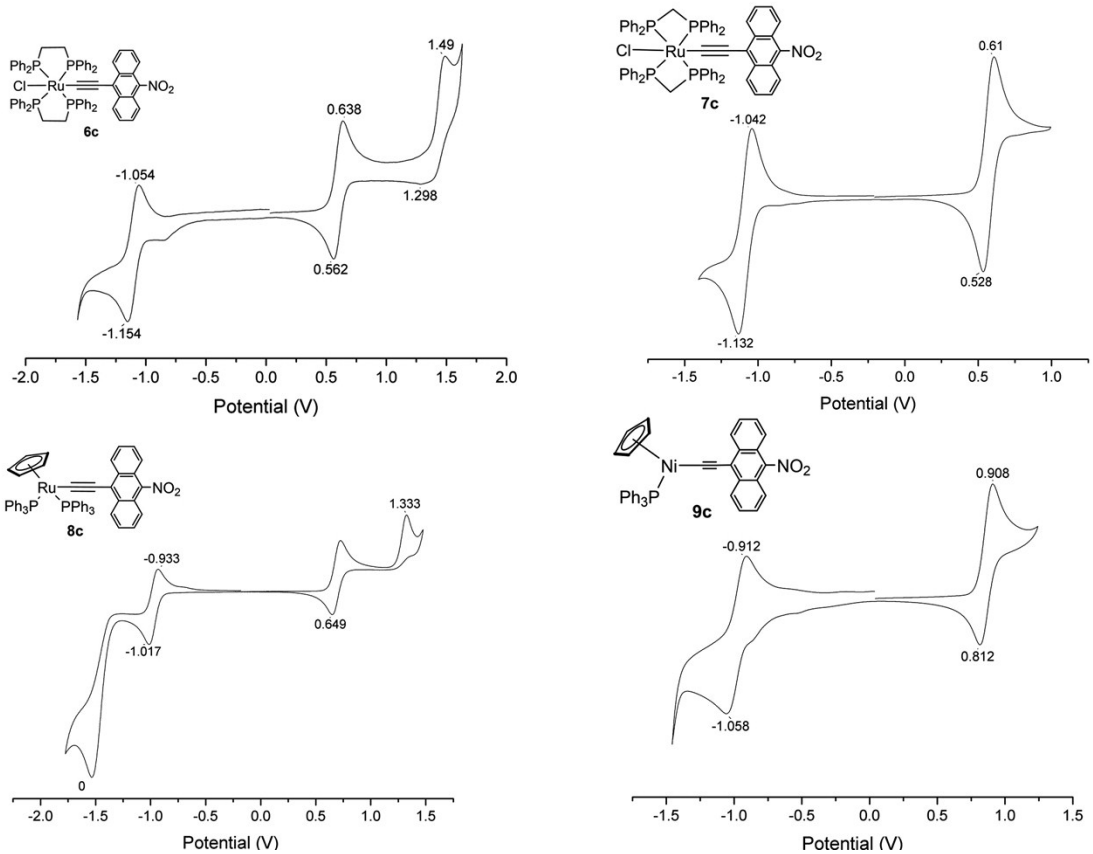

Figures S52 (top left), **S53** (top right), **S54** (bottom left), and **S55** (bottom right). CV traces for compounds **6c**-**9c**.

UV-vis Spectroscopy

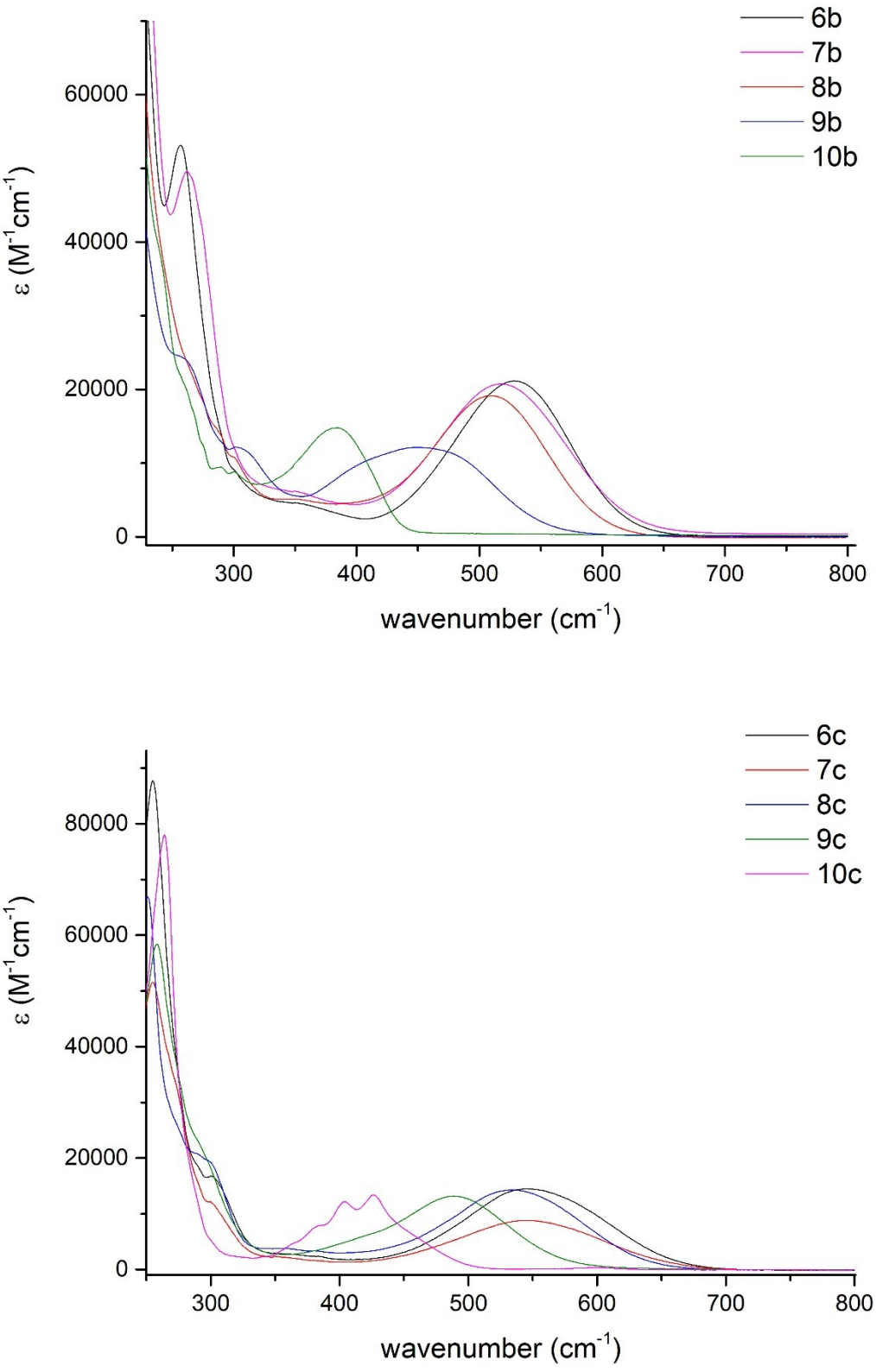

Figure S56. Overlaid UV-vis spectra (CH_2Cl_2) for naphthalenyl complexes **6b**-**10b** (top), and anthracenyl complexes **6c**-**10c** (bottom).

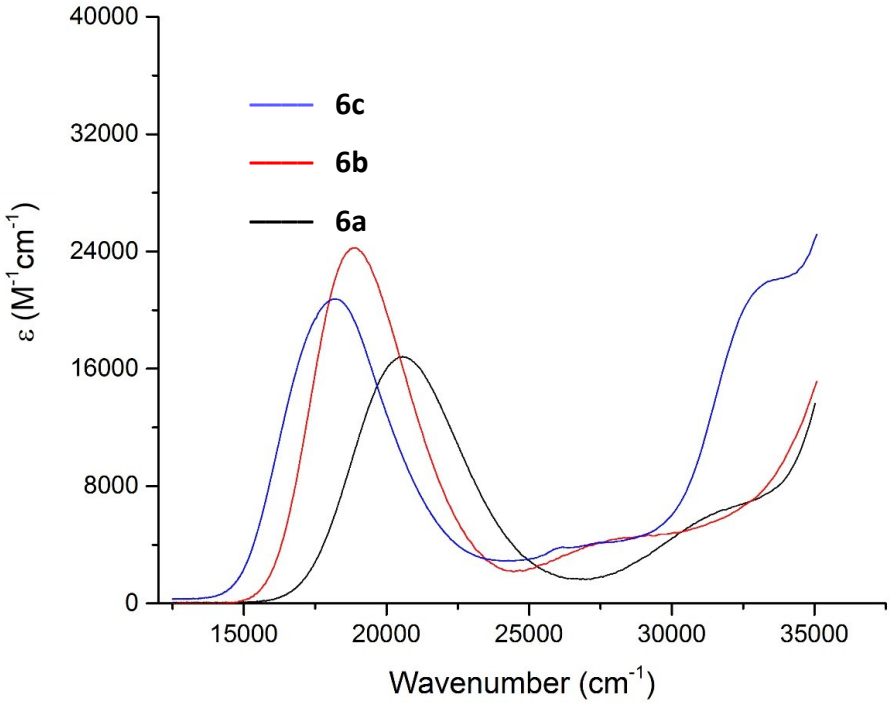

Figure S57. UV-vis spectra for *trans*-[Ru(C≡CR)Cl(dppe)$_2$] complexes **6a-c**.

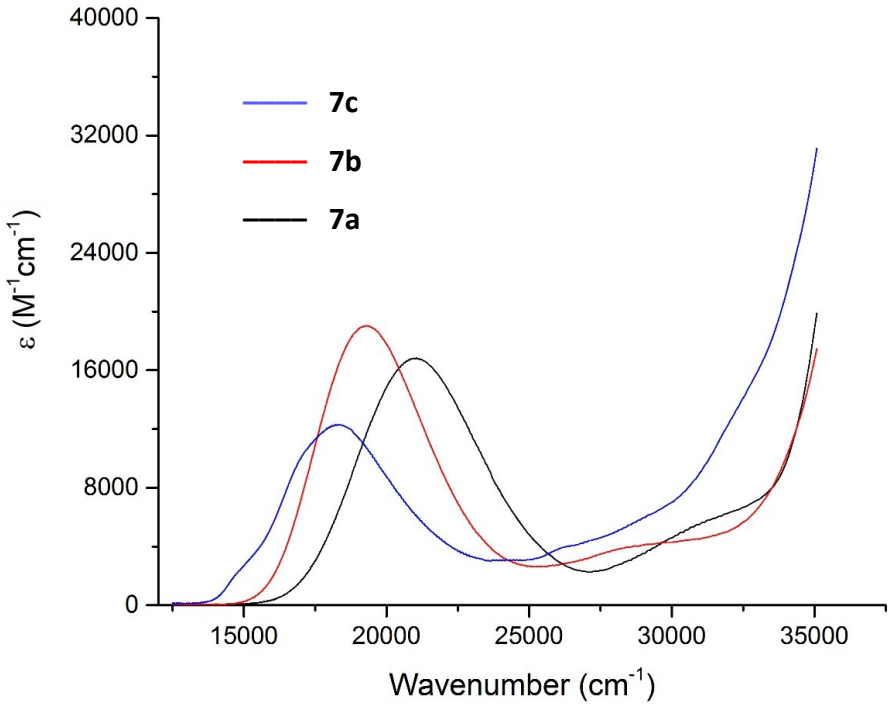

Figure S58. UV-vis spectra for *trans*-[Ru(C≡CR)Cl(dppm)$_2$] complexes **7a-c**.

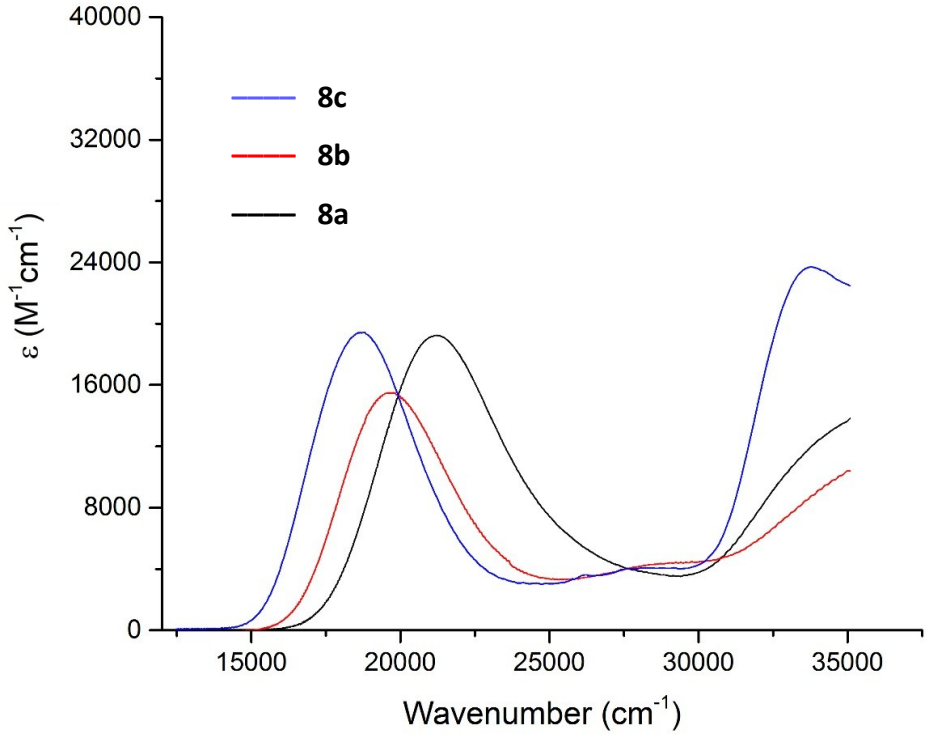

Figure S59. UV-vis spectra for Ru(C≡CR)(PPh$_3$)$_2$(η^5-C$_5$H$_5$) complexes **8a-c**.

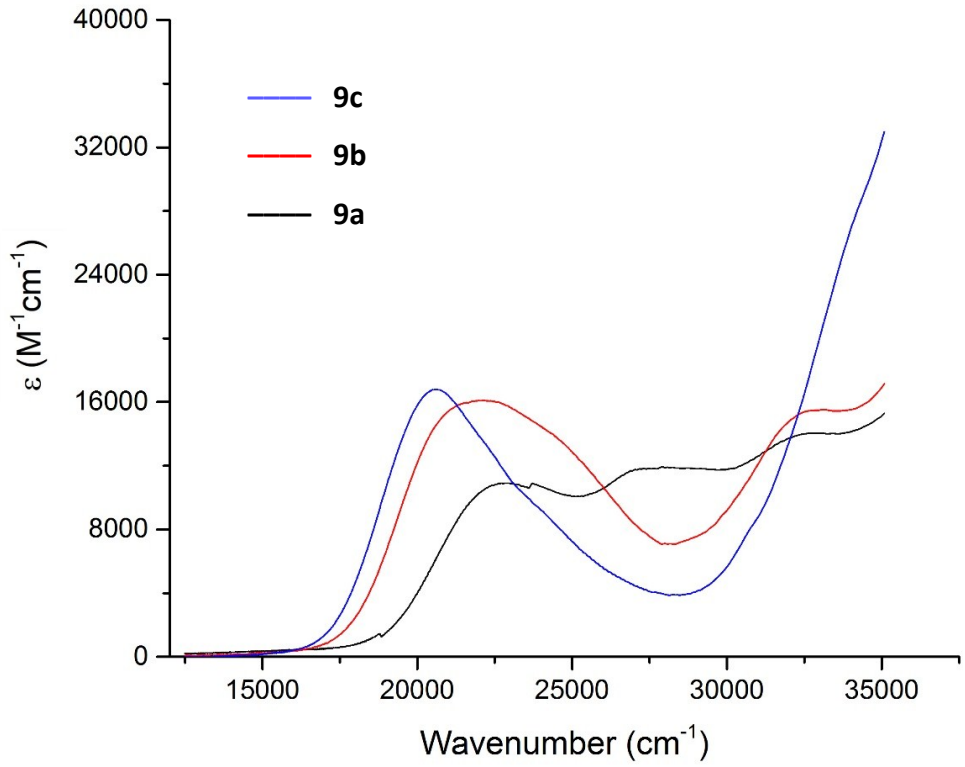

Figure S60. UV-vis spectra for Ni(C≡CR)(PPh$_3$)(η^5-C$_5$H$_5$) complexes **9a-c**.

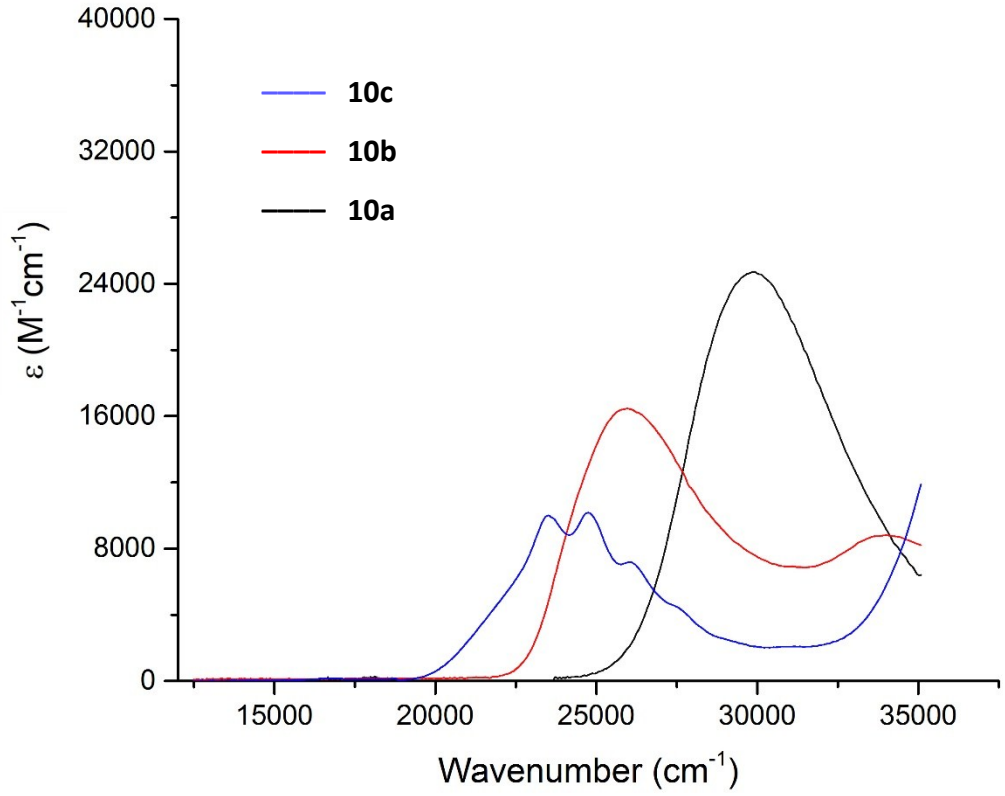

Figure S61. UV-vis spectra for Au(C≡CR)(PPh_3) complexes **10a-c**.

Spectroelectrochemistry

Solution spectra of the oxidized species were obtained at room temperature by electrogeneration using an Autolab III potentiostat and an optically-transparent thin-layer electrochemical (OTTLE) cell constructed using a 0.5 mm path-length optical cuvette with platinum gauze working-, platinum wire counter- and silver wire reference electrodes. Solutions were made up in 0.1 M $(NBu^n_4)PF_6$ in dichloromethane and were purged and maintained under a nitrogen atmosphere. The oxidation potential was set ca. 0.1 V beyond the $E_{1/2}$ measured using cyclic voltammetry, to ensure complete oxidation. The reversibility was tested by applying a reducing potential to the oxidized species.

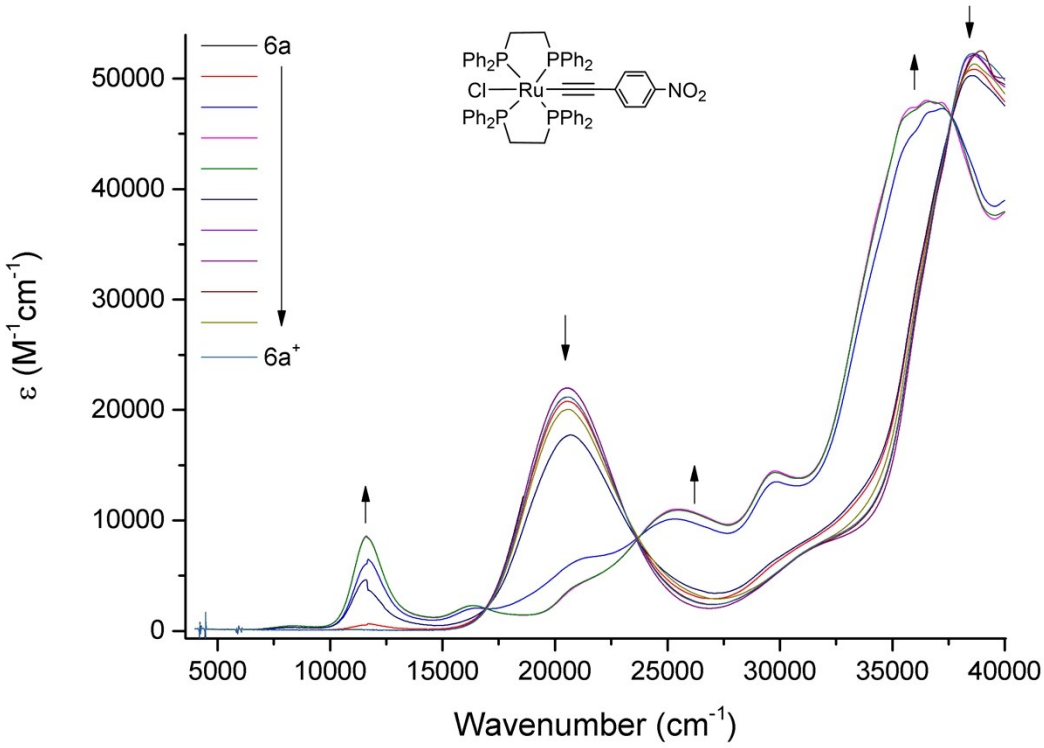

Figure S62. UV-vis-NIR (CH_2Cl_2) spectral progression from oxidation of *trans*-[Ru(C≡C-4-C_6H_4-1-NO_2)Cl(dppe)$_2$] (**6a**).

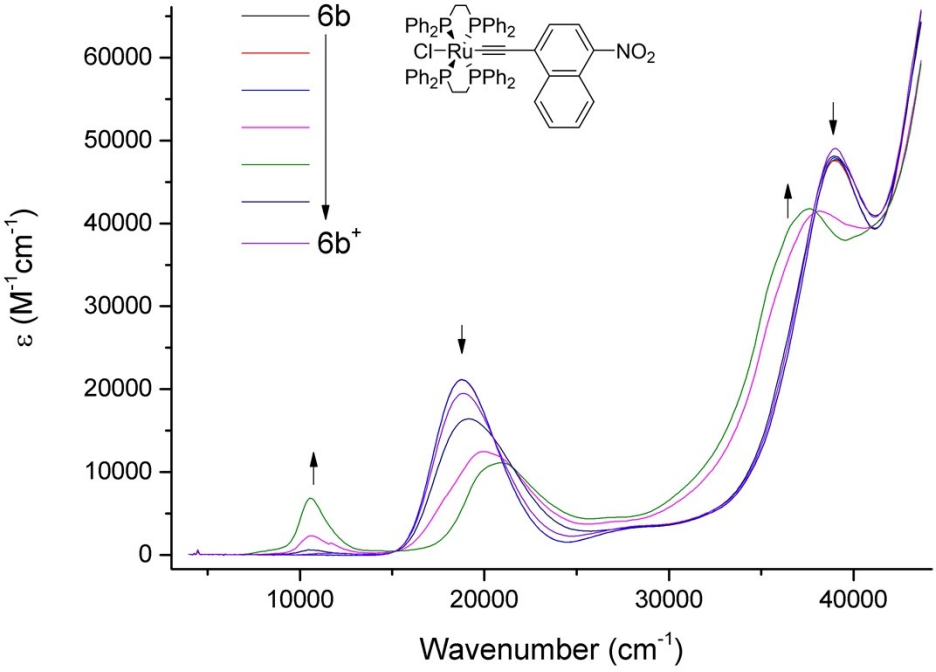

Figure S63. UV-vis-NIR (CH_2Cl_2) spectral progression from oxidation of *trans*-[Ru(C≡C-4-$C_{10}H_6$-1-NO_2)Cl(dppe)$_2$] (**6b**).

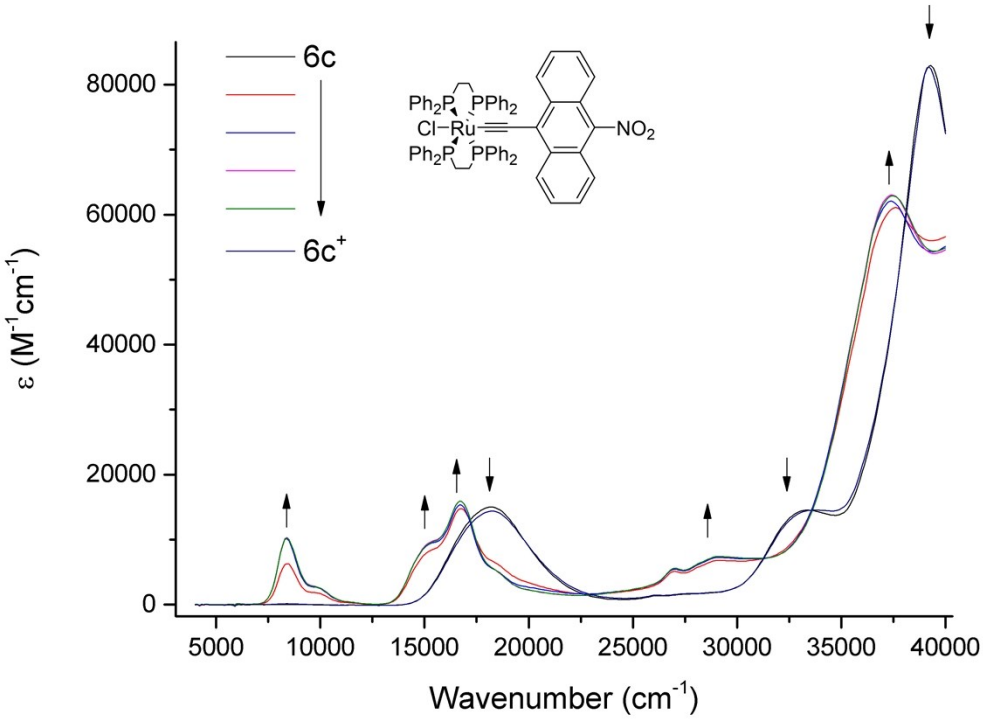

Figure S64. UV-vis-NIR (CH_2Cl_2) spectral progression from oxidation of *trans*-[Ru(C≡C-10-$C_{14}H_8$-9-NO_2)Cl(dppe)$_2$] (**6c**).

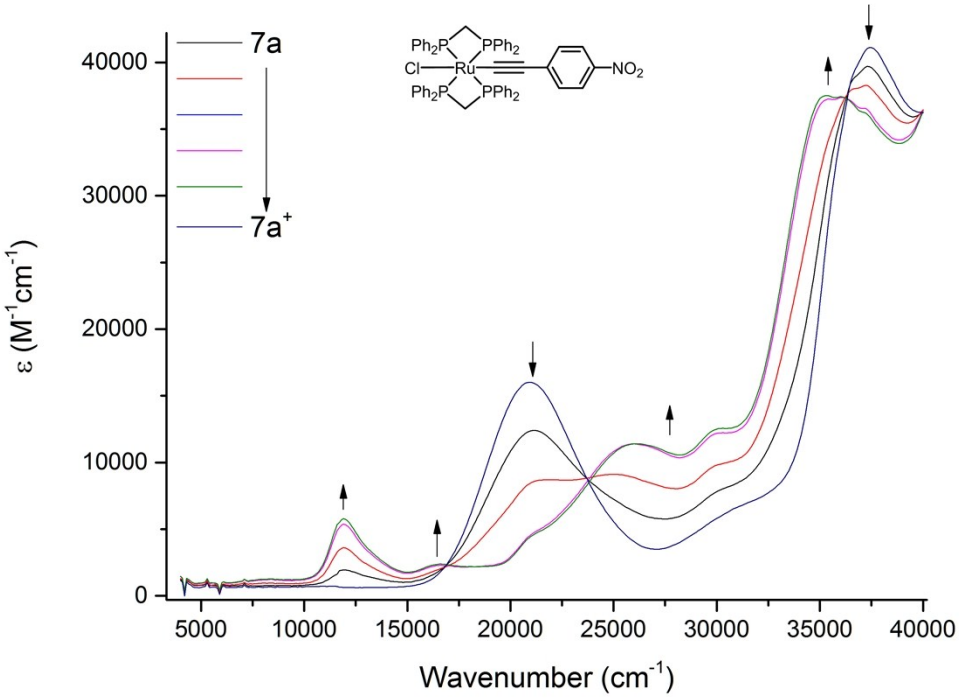

Figure S65. UV-vis-NIR (CH_2Cl_2) spectral progression from oxidation of *trans*-[Ru(C≡C-4-C_6H_4-1-NO_2)Cl(dppm)$_2$] (**7a**).

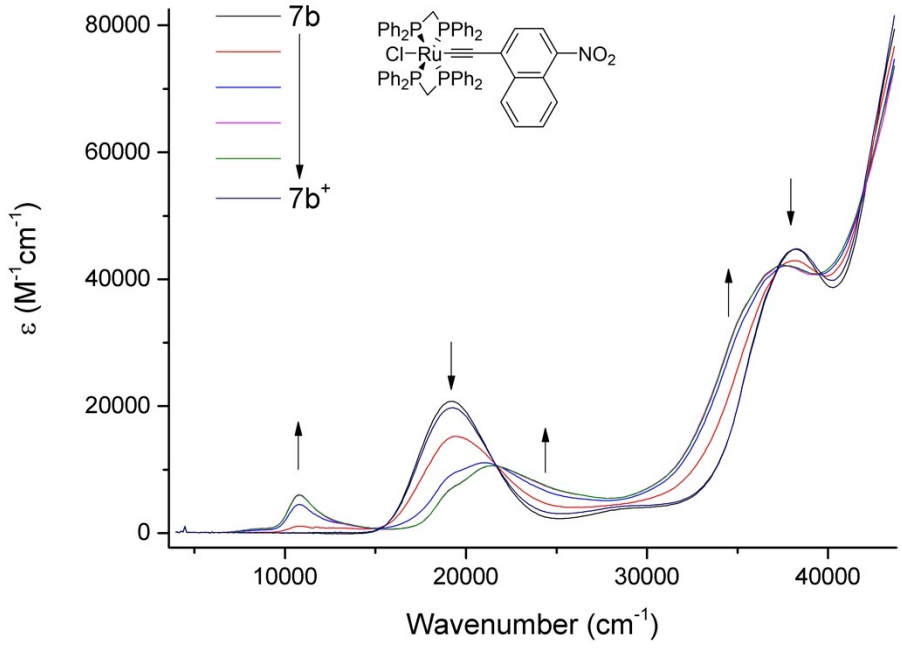

Figure S66. UV-vis-NIR (CH_2Cl_2) spectral progression from oxidation of *trans*-[Ru(C≡C-4-$C_{10}H_6$-1-NO_2)Cl(dppm)$_2$] (**7b**).

Hyper-Rayleigh Scattering

The HRS measurement setup was similar to that reported in the literature.[29] A schematic diagram is shown in Figure S67. The laser used was a pulsed Nd-YAG laser (Spectra-Physics, GCR-150-30) with a maximum pulse energy of 200 mJ at a repetition rate of 30 Hz and at a wavelength of 1064 nm. The pulsed laser passed through a half-wave plate (HW) and a polarizer (P) that together form a beam attenuator (Thorlabs, VBA05-1064). The half-wave plate was mounted on a rotational stage that had a servo motor driver (PRM1MZ8E, Thorlabs). By controlling the rotation of the half-wave plate through a Visual Basic program, we were able to vary the incident laser intensity (or fundamental light intensity), but also to automate the measurement process. After passing the beam attenuator, a small portion of the incident laser light (around 10%) was reflected towards a battery powered Si diode (PD) via a beam splitter (BS: in practice this was a microscope cover-slide). The signal from the Si diode served two purposes: it monitored the incident laser intensity and it provided the trigger signal for the oscilloscope. The majority of the laser beam was reflected by a laser line mirror (NB1-K14, Thorlabs) and subsequently focused via a focusing lens (FL, f = 75 mm, AC254-075-B-ML, Thorlabs) into the sample cell to generate HRS. The sample cell was a rectangular standard fluorometer cell with Teflon stopper (cell dimensions: 45 x 12.5 x 7.5 mm) and was placed so that the focal point of the beam was roughly in the middle of the cell.

To detect HRS, a camera lens (CL, Nikkor 50 mm, Nikon) was placed at 90 degrees to the beam propagation direction to collect the scattered light. A concave mirror (CCM, CM508-038-P01, f = 38.1 mm, Thorlabs) was placed opposite the camera lens at the other side of the sample cell to reflect back the scattered light. The camera lens not only collected all the scattered light, but also focused the light onto the open slit of a monochromator (MNCM, Spex 500M) which acted as a variable filter and allowed only the selected wavelength of light to pass. At the other end of the monochromator, a photomultiplier tube (PMT, R269 Hamamatsu) detected the HRS. The signals from both the Si diode and the PMT were passed to an oscilloscope (TDS2024C, Tektronix) for display and averaging. A dedicated PC with a custom-written Visual Basic program acquired data from the oscilloscope and ran the measurements automatically.

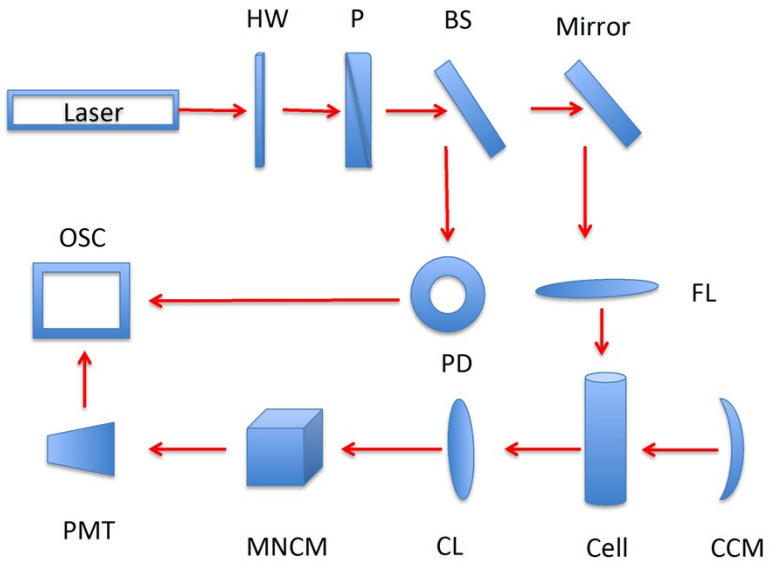

Figure S67. Schematic diagram of the HRS setup. BS: beam splitter, P: polarizer, HW: half-wave plate, OSC: oscilloscope, PD: Si photodiode, FL: focusing lens, PMT: photomultiplier tube, MNCM: monochromator, CL: camera lens, CCM: concave mirror.

We used the internal reference method to measure the first hyperpolarizabilities, $<\beta>$, of the compounds/complexes. Tetrahydrofuran (THF) was chosen as the reference solvent with a known $<\beta>$ value of 0.44 $x10^{-30}$ esu.[30] For any given compound or complex solution, a maximum incident laser intensity was determined, to ensure that there was a reasonable scattering signal at 532 nm (likely HRS), but also that there was no decomposition of the sample. At the same time, at this maximum incident laser intensity, the wavelength setting on the monochromator was scanned at wavelengths around 532 nm to test if there was scattering at other wavelengths. When scattering was only observed at 532 nm, a quick check on a quadratic relationship between the scattering signal and the incident laser intensity was carried out, to confirm that the scattering signal was indeed HRS. Once the HRS signal was confirmed, HRS measurements were carried out by rotating the half-wave plate by means of a computer program, causing the incident light intensity to vary from minimum to maximum or vice versa, and at same time recording both the HRS signal and the incident light intensity. For each sample solution, the HRS measurement was repeated three times to average the large fluctuation of the HRS signals. As an example, Figure S68 shows the measured HRS signal as a function of incident intensity for **9c** at various concentrations.

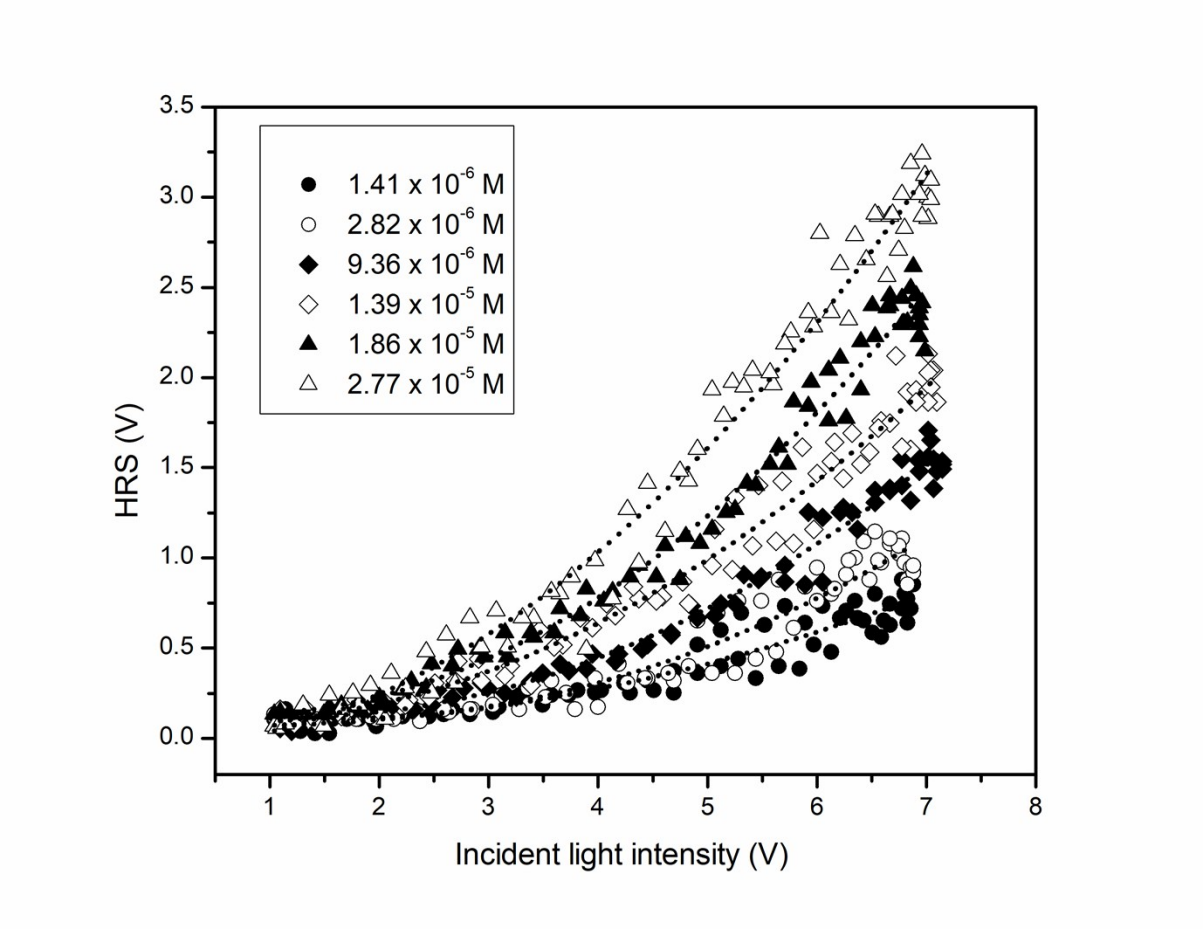

Figure S68. HRS signal of **9c** as a function of incident light intensity and displaying a quadratic relationship.

Sometimes samples not only produce HRS, but also produce broad scattering around 532 nm due to fluorescence, etc. In order to extract the true HRS signal for those samples, a correction is needed for the measured scattering signal at 532 nm to remove the contributions from other sources. HRS is wavelength specific and under our setup with 1064 nm incident light, the HRS signal vanished when the monochromator wavelength was set 1 nm away from 532 nm (see Figure S69). One way to correct is therefore to measure the scattering at 533 nm or 531 nm, and then subtract this from the scattering measured at 532 nm, assuming that the broad scattering from other sources has a similar intensity at 532 nm and 533/531 nm (a reasonable assumption given the proximity of the wavelength). In the case of **10c**, for which the fluorescence was substantial, the quadratic nonlinearity could not be measured,

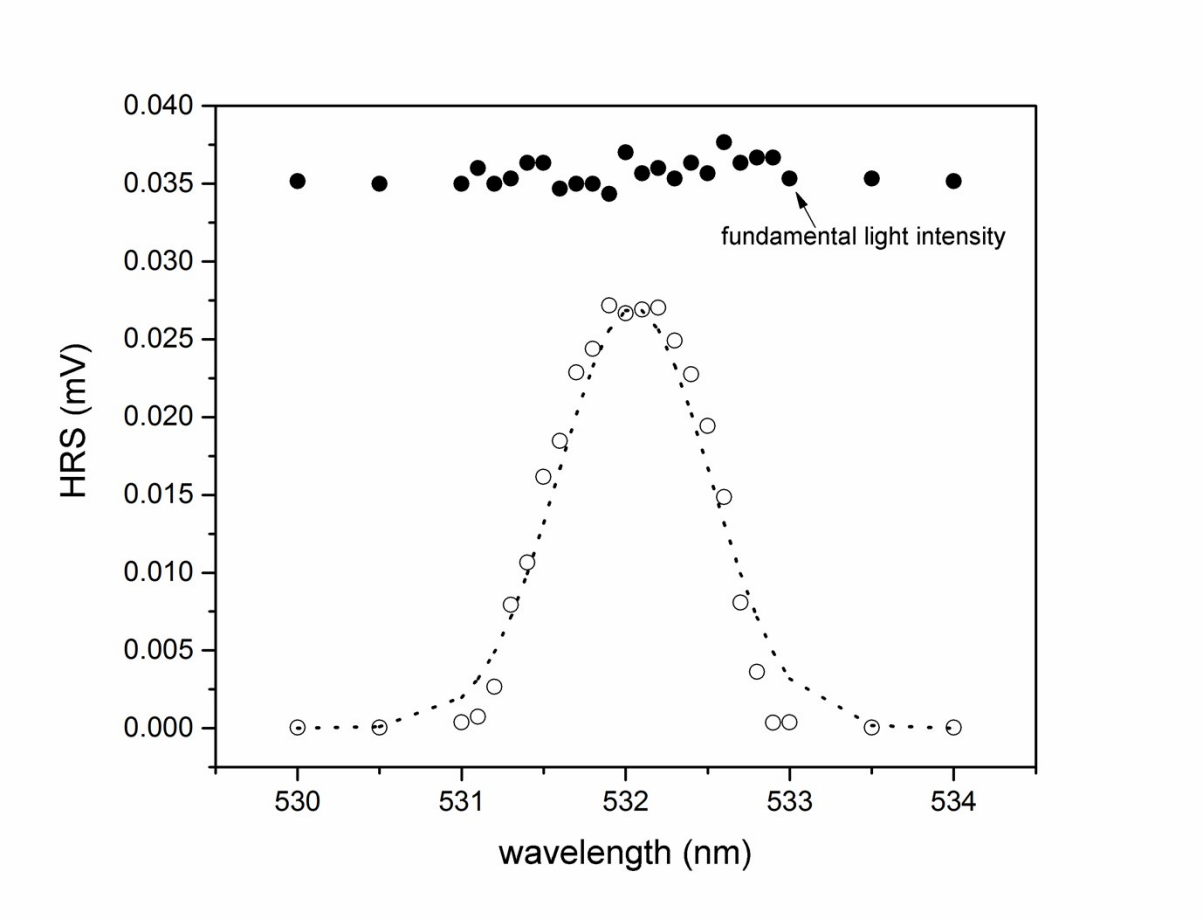

Figure S69. HRS signal as a function of wavelength; the incident light has a wavelength of 1064 nm and its intensity is roughly constant.

For any given compound/complex, a few milligrams of sample were dissolved in THF. The stock solution was then used to form a series of sample solutions with different concentrations (the concentrations were usually low: < 10^{-2} M). HRS measurements were then carried out on each sample solution. When a solute concentration is very low, the solution is sufficiently dilute that the measured HRS can be described as follows:[29]

$$I_{2\omega}/I^2_{\omega} = G[N_{solute}\langle\beta\rangle^2_{solute} + N_{solvent}\langle\beta\rangle^2_{solvent}]$$

where $I_{2\omega}$ is the measured HRS, I_{ω} is the incident light intensity, G is a calibration factor associated with setup and light collection efficiency, N_{solute} and $N_{solvent}$ are the number densities or molar concentrations of the solute and solvent in the solution, and $\langle\beta\rangle^2_{solute}$ and $\langle\beta\rangle^2_{solvent}$ are the first hyperpolarizabilities for the solute and solvent, respectively. A plot of $I_{2\omega}/I^2_{\omega}$ vs molar concentration of solute will yield a straight line (e.g. Figure S70). The slope of the line equals $G\langle\beta\rangle^2_{solute}$ and the intercept is $GN_{solvent}\langle\beta\rangle^2_{solvent}$. Solving for $\langle\beta\rangle_{solute}$, we obtain $\langle\beta\rangle_{solute} = [\text{slope } N_{solvent}\langle\beta\rangle^2_{solvent}/\text{intercept}]^{1/2}$. The $\langle\beta\rangle_{solvent}$ for THF is 0.44 x 10^{-30} esu

and the $N_{solvent}$ is 12.33 M, calculated from the density of 0.8892 g/mL and molecular weight of 72.11. The $<\beta>_{solute}$ can then be calculated for any given slope and intercept (e.g. Figure S70: slope = 1987.5, intercept = 0.0141, $<\beta>$ = 580 x 10^{-30} esu). The $<\beta>$ values are listed in Table 4.

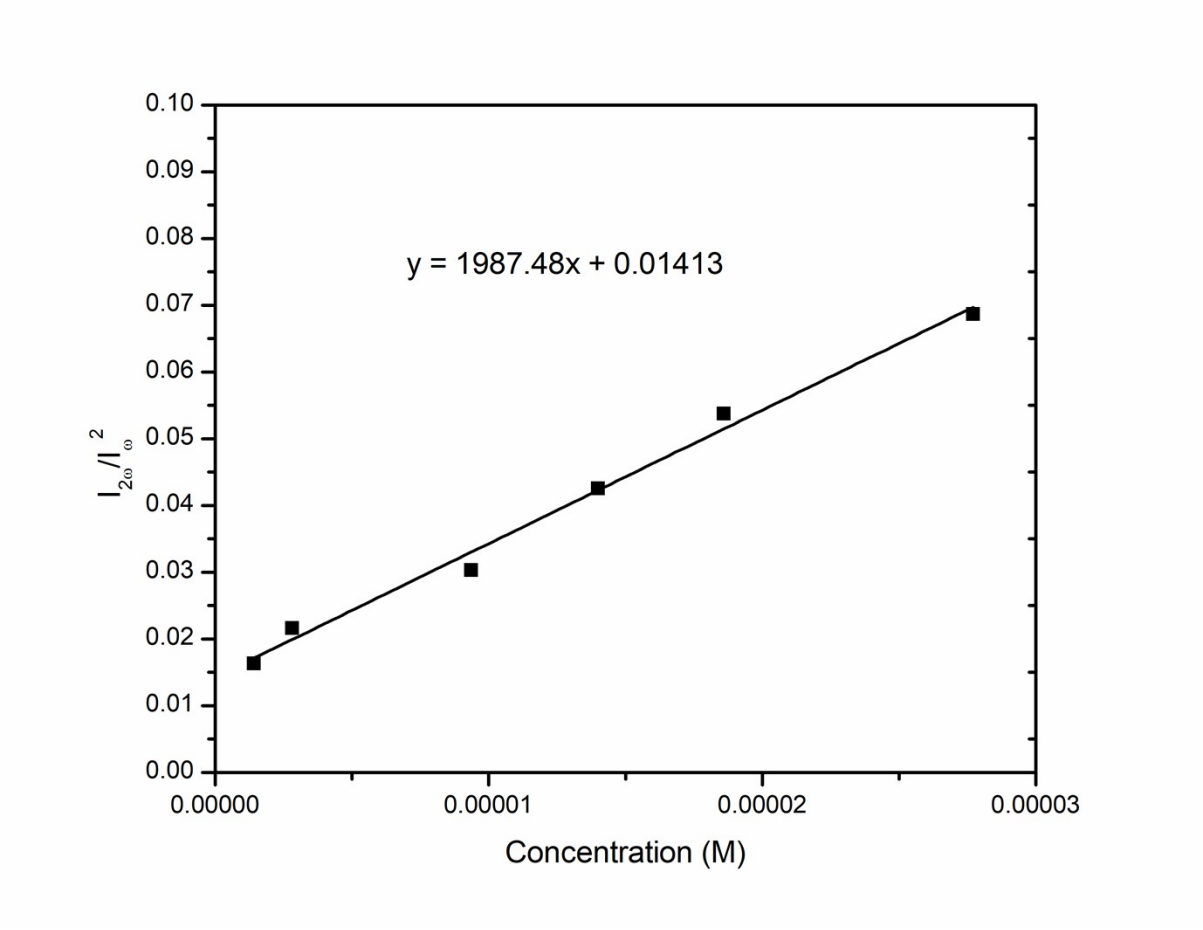

Figure S70. $I_{2\omega}/I^2_{\omega}$ for **9c** as a function of solute concentration.

The $I_{2\omega}/I^2_{\omega}$ data plotted in Figure S70 was the result of examining several incident light intensities. HRS is quadratically related to the incident light intensity, so ideally HRS divided by the square of the incident light intensity, $I_{2\omega}/I^2_{\omega}$, should be a constant. Figure S71 shows a plot of $I_{2\omega}/I^2_{\omega}$ as a function of incident light intensity for one of the HRS measurements in Figure S68 (corresponding to a concentration of 1.399 x 10^{-5} M). The ratio is constant at higher light intensities; the deviation at low incident light intensity is likely due to sources such as background noise and other scatterings that do not follow a quadratic relationship. For this reason, the ratios measured in the higher incident light intensity range were averaged and used in the data analysis.

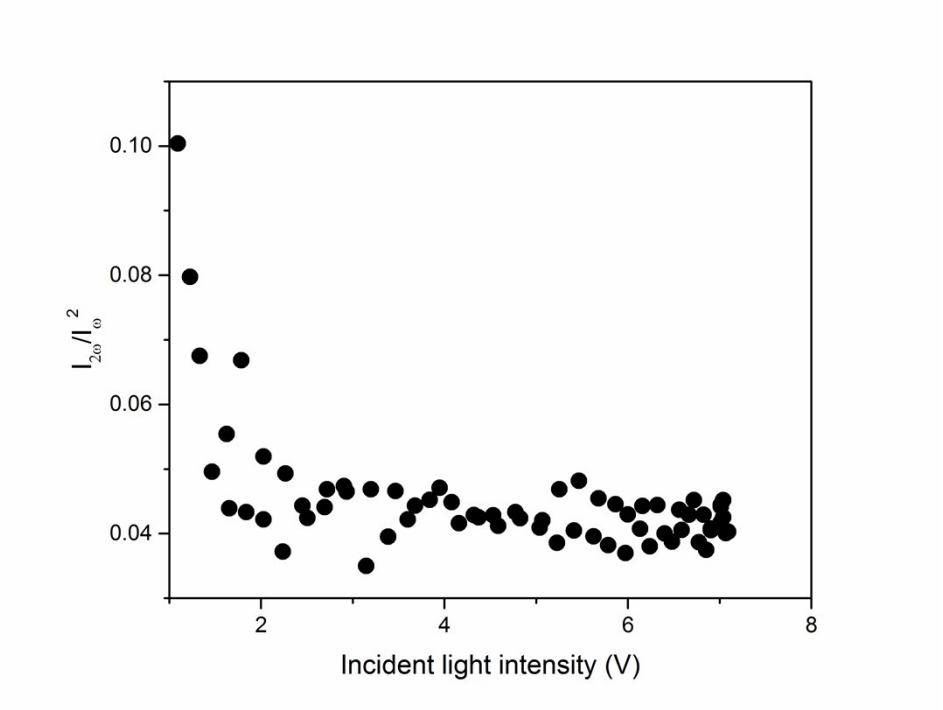

Figure S71. $I_{2\omega}/I^2_{\omega}$ as a function of incident light intensity for **9c** (concentration 1.399 x 10^{-5} M).

Uncertainties in HRS measurements may depend on many factors. Firstly, the HRS signal is partially associated with orientational fluctuations of all molecules in the solution, a random process that causes the HRS signal to fluctuate, so the β value is an average to control for these fluctuations; we averaged the HRS signal over 128 incident pulses (the maximum number of pulses that a Tektronix 2024C oscilloscope can handle). Statistically, the standard deviation for an average over 128 runs is ca. 10%. Secondly, the ratio $I_{2\omega}/I^2_{\omega}$ has a linear relationship with solute concentration when the solute concentration is very low, but when the solute concentration is high, the ratio tends to saturate for various reasons such as self-absorption (see Figure S72), so the lower concentration region should be used or $<\beta>$ may be underestimated. Thirdly, each PMT produces dark current (electronic background noise). For compounds/complexes with large β values, the background signal is usually negligible, but for materials with small β values, a correction for this background signal is necessary and extra error on the HRS result is likely introduced. Fourthly, for materials with broad spectrum scattering around the HRS wavelength, the efficiency in separating the true HRS signal from other sources of scattering impacts the HRS results.

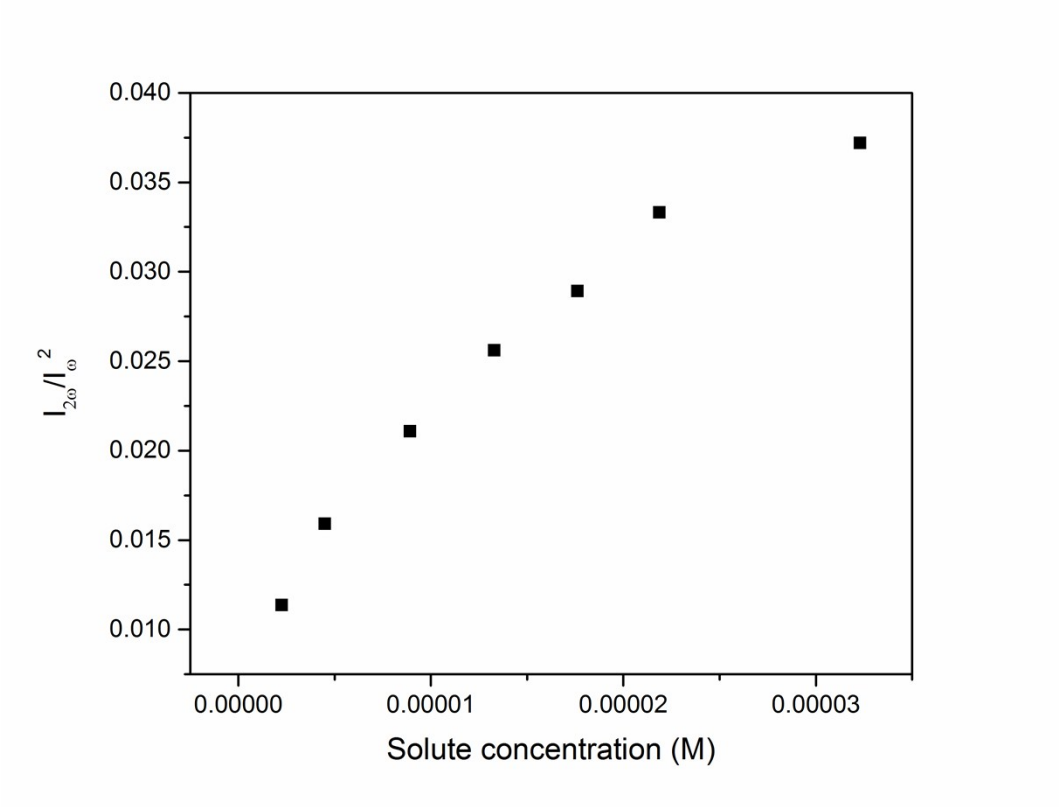

Figure S72. $I_{2\omega}/I^2_{\omega}$ for **6c**, plotted as a function of solute concentration showing a plateauing effect at high concentration.

Two samples were run twice, with the <β> values varying only by a few per cent, so we believe that a 10-15% uncertainly in the HRS measurement (a level often reported in the literature) is reasonable.

Fluorescence Spectroscopy

The samples were assessed for fluorescence as discussed above. The fluorescence spectrum was measured on a Varian Cary Eclipse Fluorescence Spectrometer in CH_2Cl_2 at 20 °C, excitation and emission slits 5, scan rate 600 nm min^{-1}.

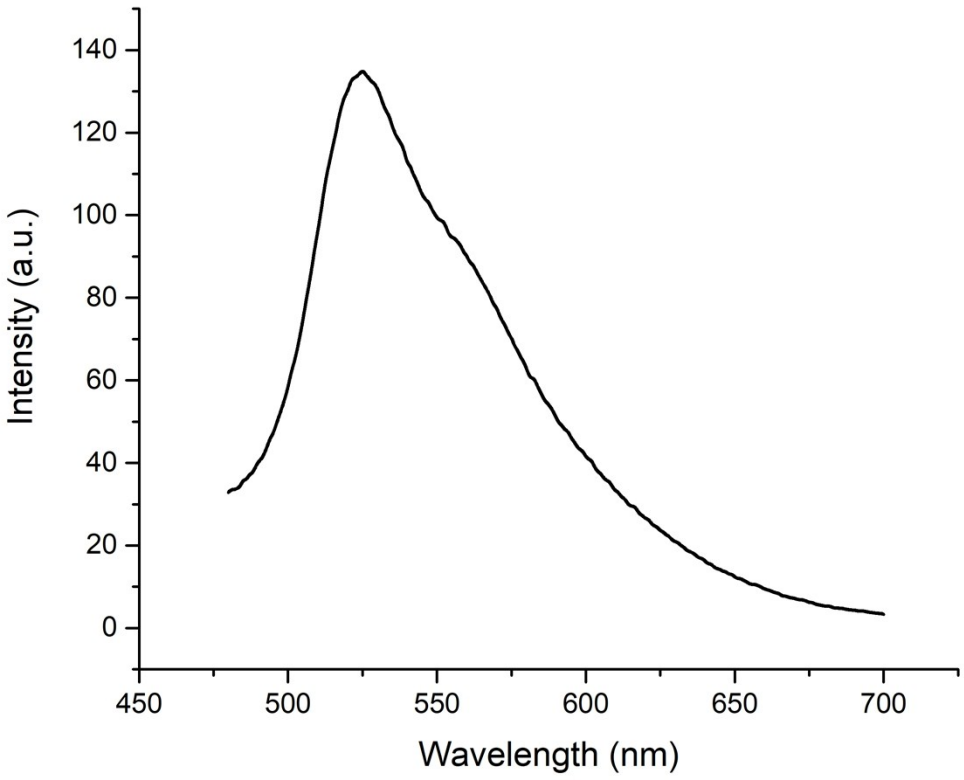

Figure S73. Fluorescence spectrum of **10c.**

Z-scan

Third-order nonlinear optical (NLO) properties were investigated on a laser system consisting of a Quantronix Integra-C3.5F pumping a Quantronix Palitra-FS optical parametric amplifier, tuneable over a wavelength range from 500 to 1600 nm. The output wavelength was confirmed using an Ocean Optics USB2000+ spectrometer (500-1000 nm) or an Ocean Optics NIR-Quest spectrometer (1000-1800 nm). The output delivered 130 fs pulse with a 1 kHz repetition rate. Coloured glass filters and a Thorlabs polarizing filter were used to remove unwanted wavelengths, and the power adjusted by use of neutral density filters to obtain nonlinear phase shifts between 0.2 to 1.3 rad. The focal length of the lens used in the experiment was 75 mm, which gave 25-40 μm beam waists resulting in Rayleigh lengths longer than that of the sample thickness. Measurements were made in 1 mm optical cells, such that the total thickness was ≤3 mm including the glass walls, so results could safely be treated using the thin sample approximation. Samples travelled down the Z-axis on a Thorlabs motorized stage between -20 and +20 mm (where 0 was the laser focus). Data were collected by three Thorlabs photodiodes, 500-900 nm with Si-based detectors, 900-1300 nm with InGaAs detectors, and 1300-2000 nm with amplified InGaAs detectors. Data from the detectors were collected by a Tektronix oscilloscope feeding a custom-written LabVIEW program providing a curve fitting of a theoretical trace that used equations derived by Sheik-Bahae *et al*.[31] All measurements were calibrated against closed-aperture Z-scans of the solvent, as well as a 3 mm thick silica plate. The real and imaginary components of the second hyperpolarizability (γ) of the materials were calculated assuming additivity to these reference samples. Solutions contained 0.2-0.3 w/w% of the compound in deoxygenated and distilled CH_2Cl_2.

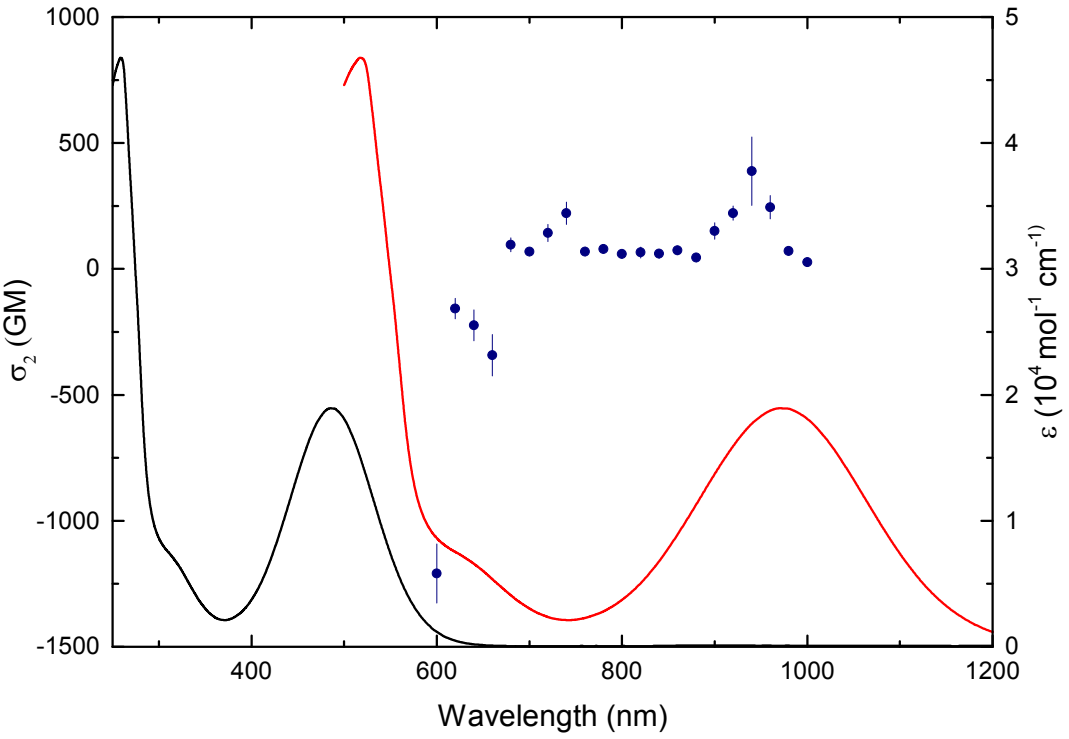

Figure S74. Plot of σ_2 (blue) for *trans*-[Ru(C≡C-4-C_6H_4-1-NO_2)Cl(dppe)$_2$] (**6a**) overlaid on the UV-visible spectrum (black), and including a plot of the UV-visible spectrum at twice the wavelength (red).

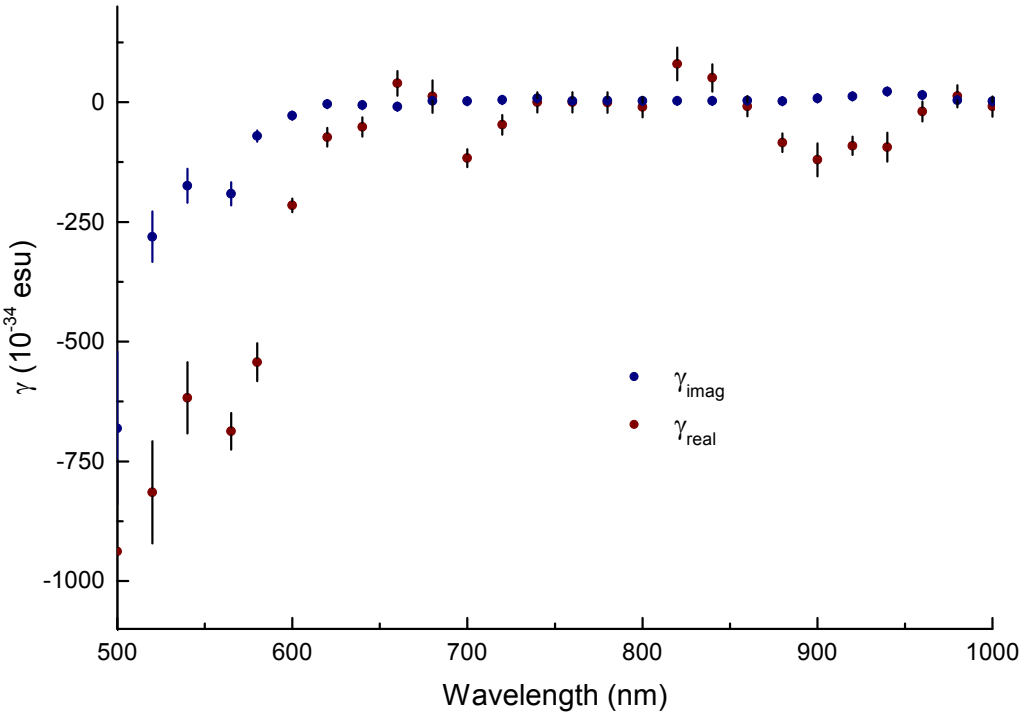

Figure S75. Plot of the real (red) and imaginary (blue) parts of the third-order hyperpolarizability of **6a**.

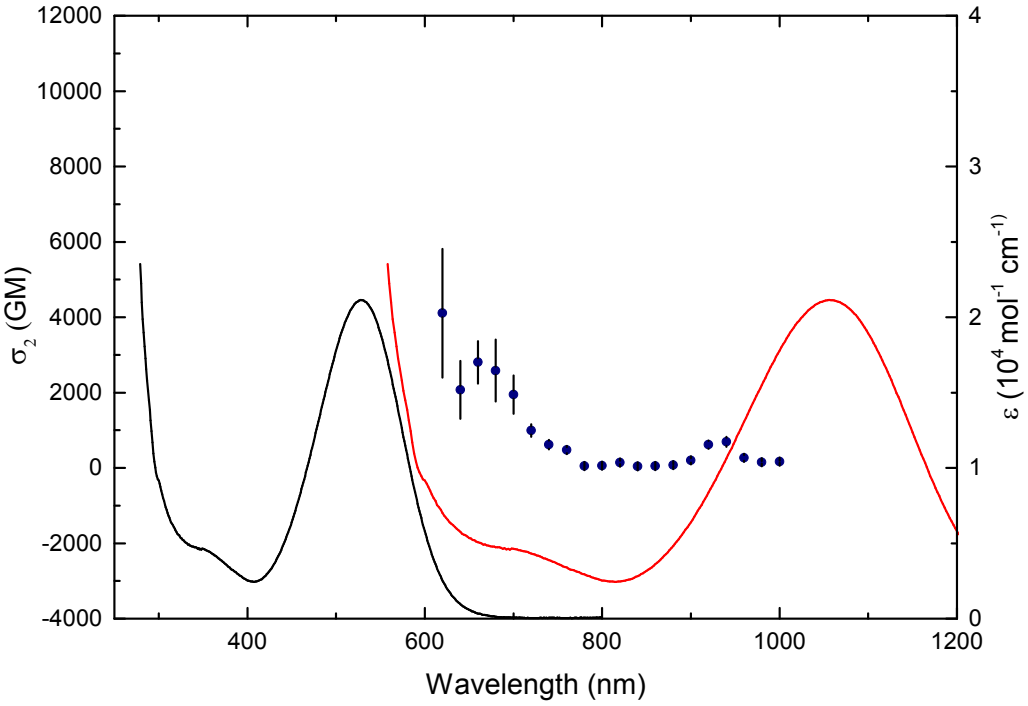

Figure S76. Plot of σ_2 (blue) for *trans*-[Ru(C≡C-4-$C_{10}H_6$-1-NO_2)Cl(dppe)$_2$] (**6b**) overlaid on the UV-visible spectrum (black), and including a plot of the UV-visible spectrum at twice the wavelength (red).

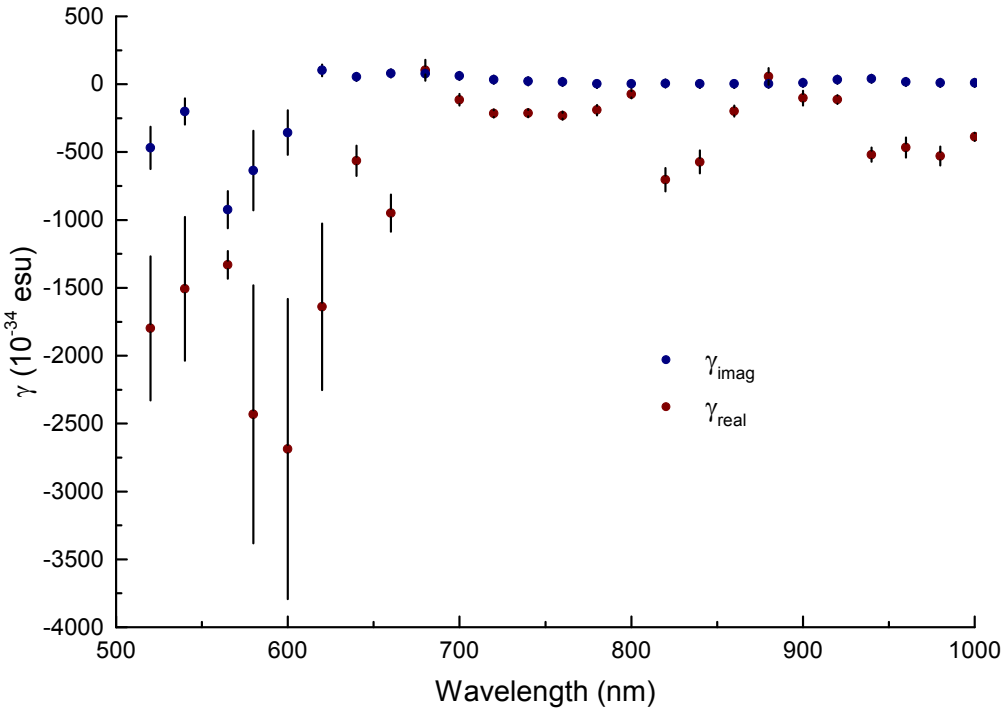

Figure S77. Plot of the real (red) and imaginary (blue) parts of the third-order hyperpolarizability of **6b**.

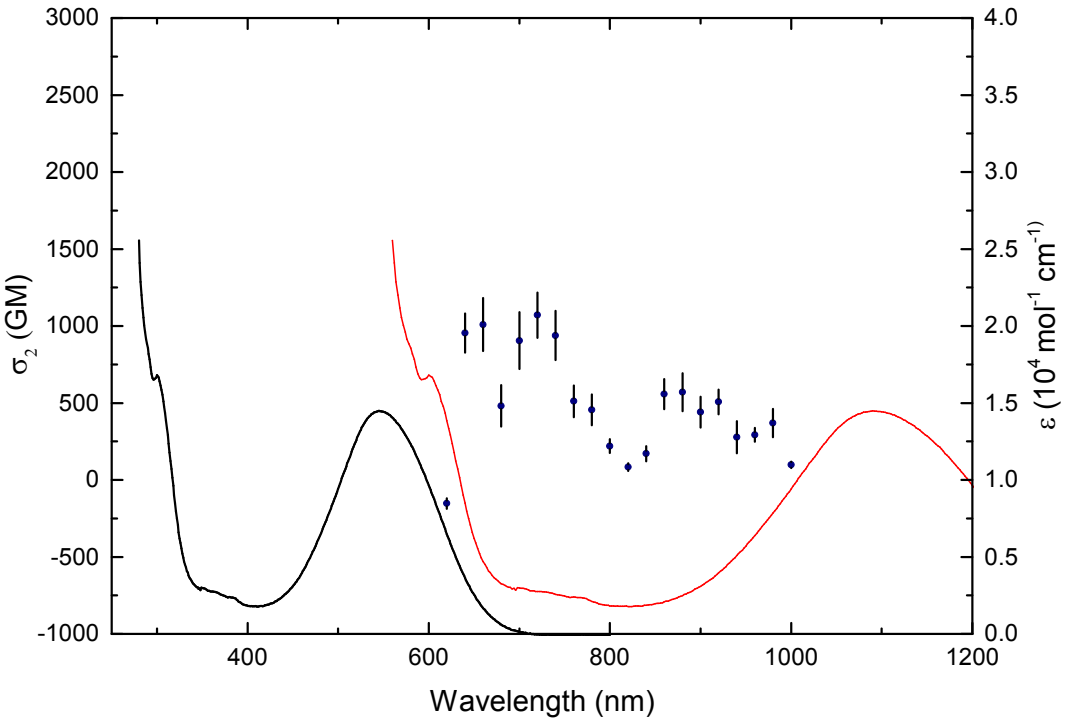

Figure S78. Plot of σ_2 (blue) for *trans*-[Ru(C≡C-10-$C_{14}H_8$-9-NO_2)Cl(dppe)$_2$] (**6c**) overlaid on the UV-visible spectrum (black), and including a plot of the UV-visible spectrum at twice the wavelength (red).

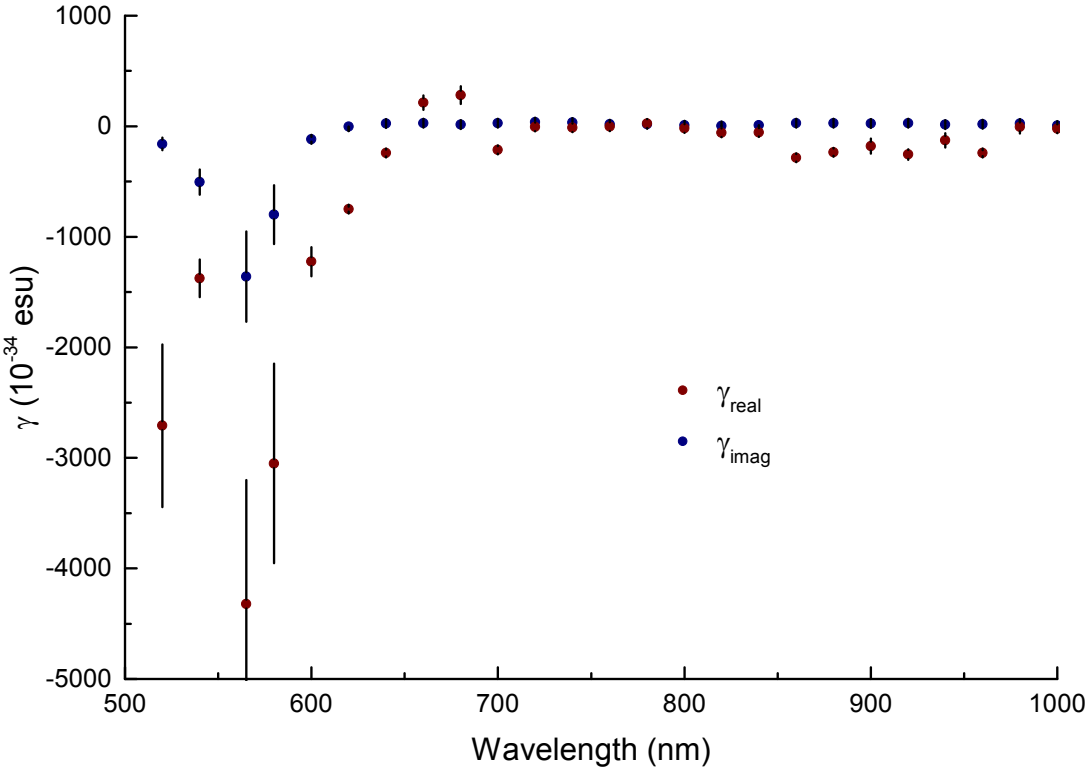

Figure S79. Plot of the real (red) and imaginary (blue) parts of the third-order hyperpolarizability of **6c**.

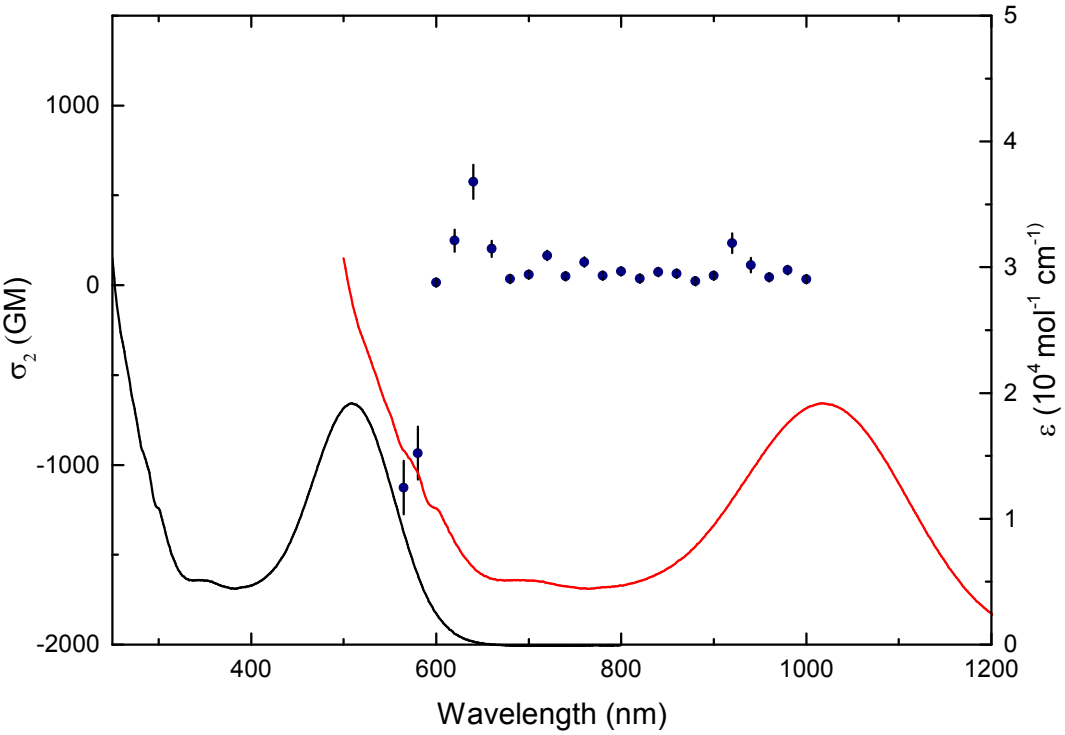

Figure S80. Plot of σ_2 (blue) for Ni(C≡C-4-$C_{10}H_6$-1-NO_2)(PPh_3)(η^5-C_5H_5) (**9b**) overlaid on the UV-visible spectrum (black), and including a plot of the UV-visible spectrum at twice the wavelength (red).

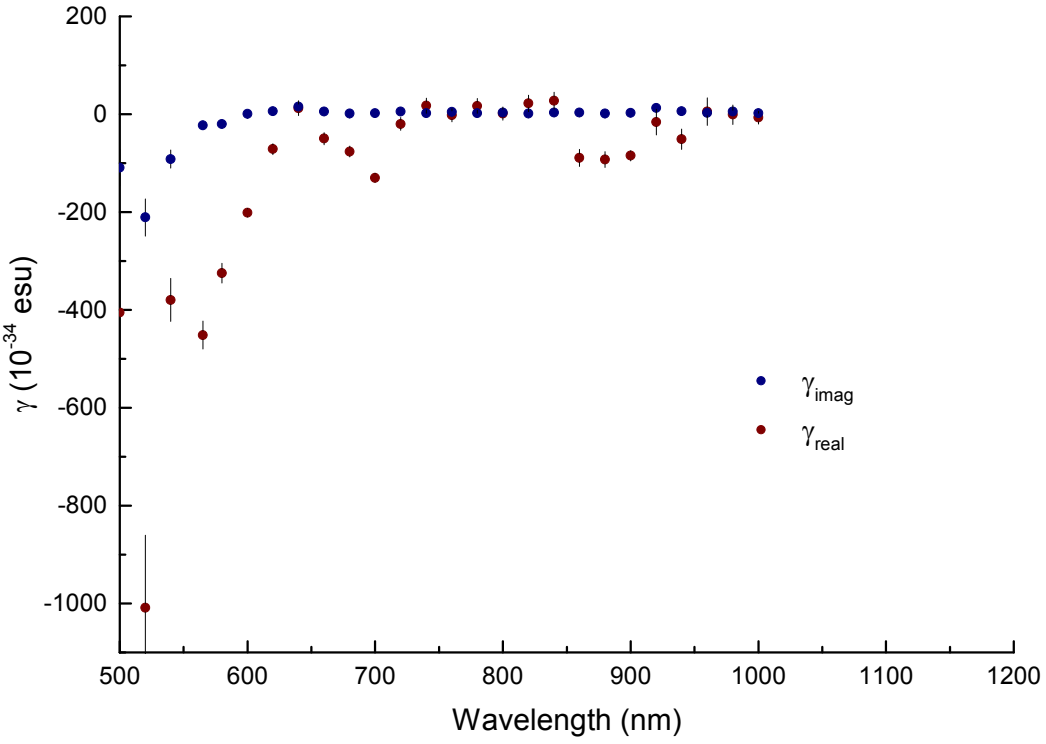

Figure S81. Plot of the real (red) and imaginary (blue) parts of the third-order hyperpolarizability of **9b**.

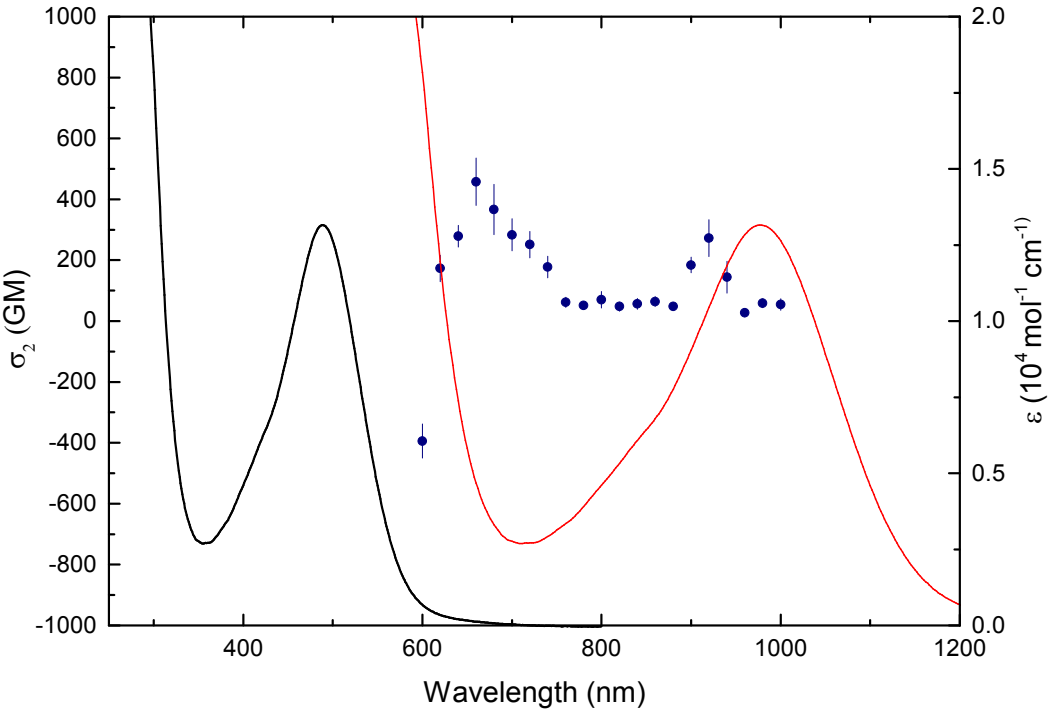

Figure S82. Plot of σ_2 (blue) for Ni(C≡C-10-$C_{14}H_8$-9-NO_2)(PPh_3)(η^5-C_5H_5) (**9c**) overlaid on the UV-visible spectrum (black), and including a plot of the UV-visible spectrum at twice the wavelength (red).

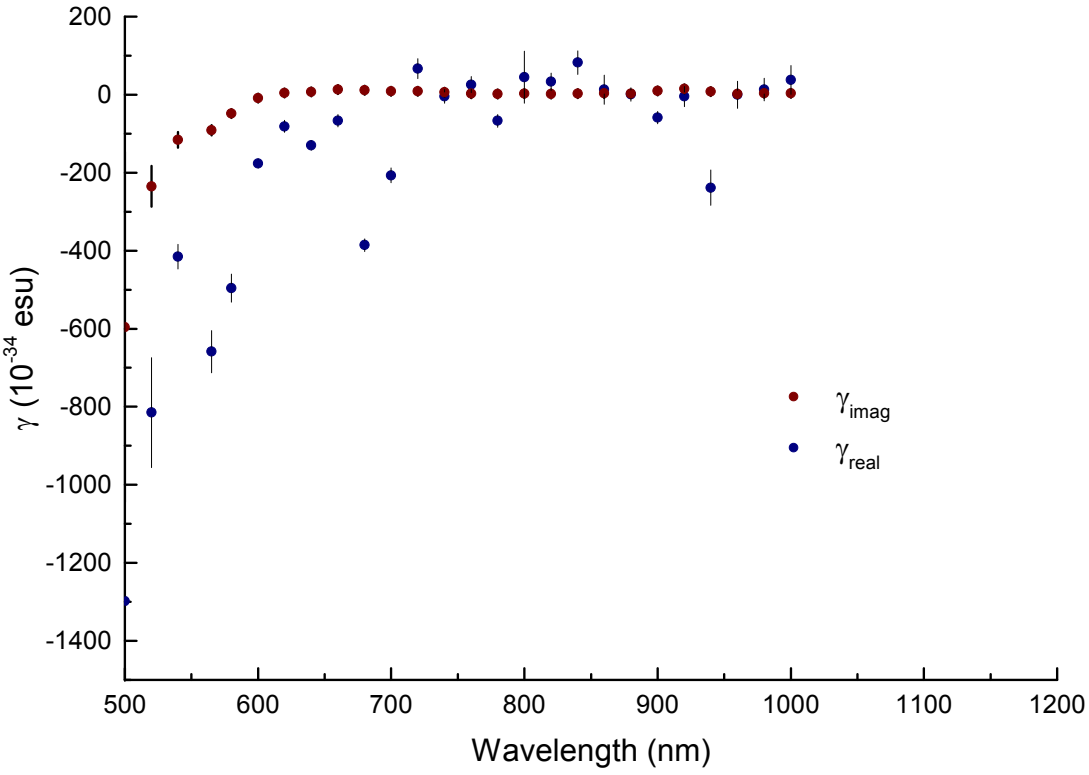

Figure S83. Plot of the real (red) and imaginary (blue) parts of the third-order hyperpolarizability of **9c**.

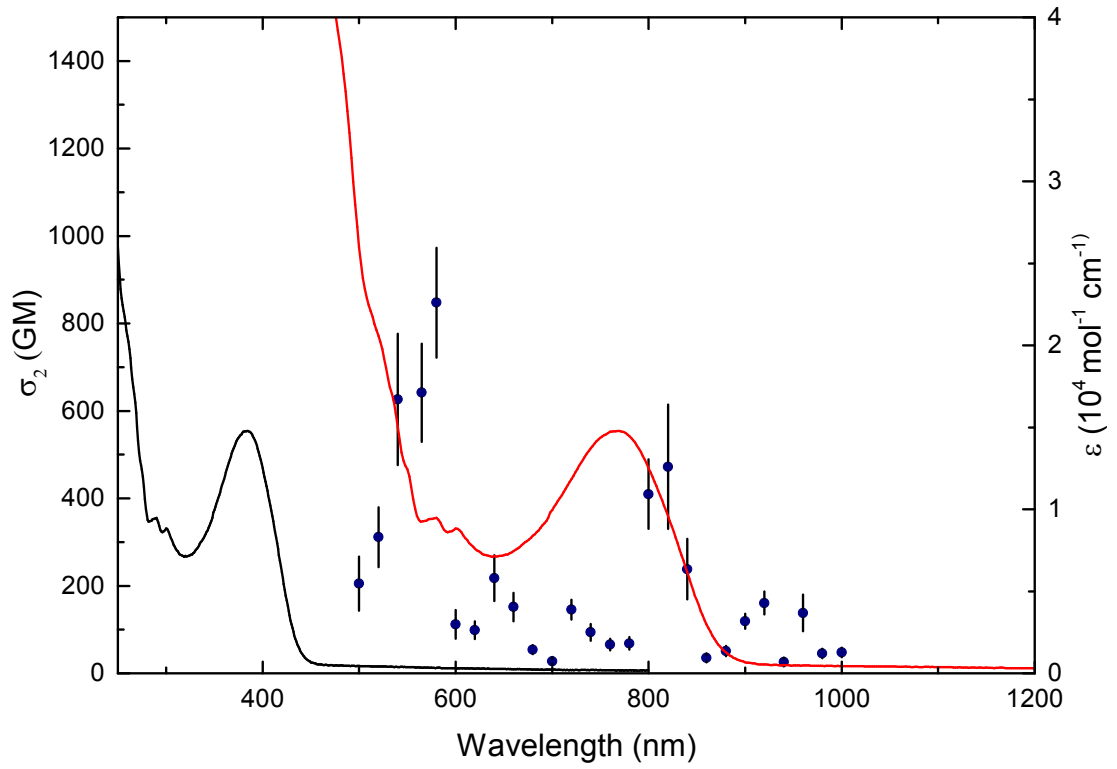

Figure S84. Plot of σ_2 (blue) for Au(C≡C-4-$C_{10}H_6$-1-NO_2)(PPh_3) (**10b**) overlaid on the UV-visible spectrum (black), and including a plot of the UV-visible spectrum at twice the wavelength (red).

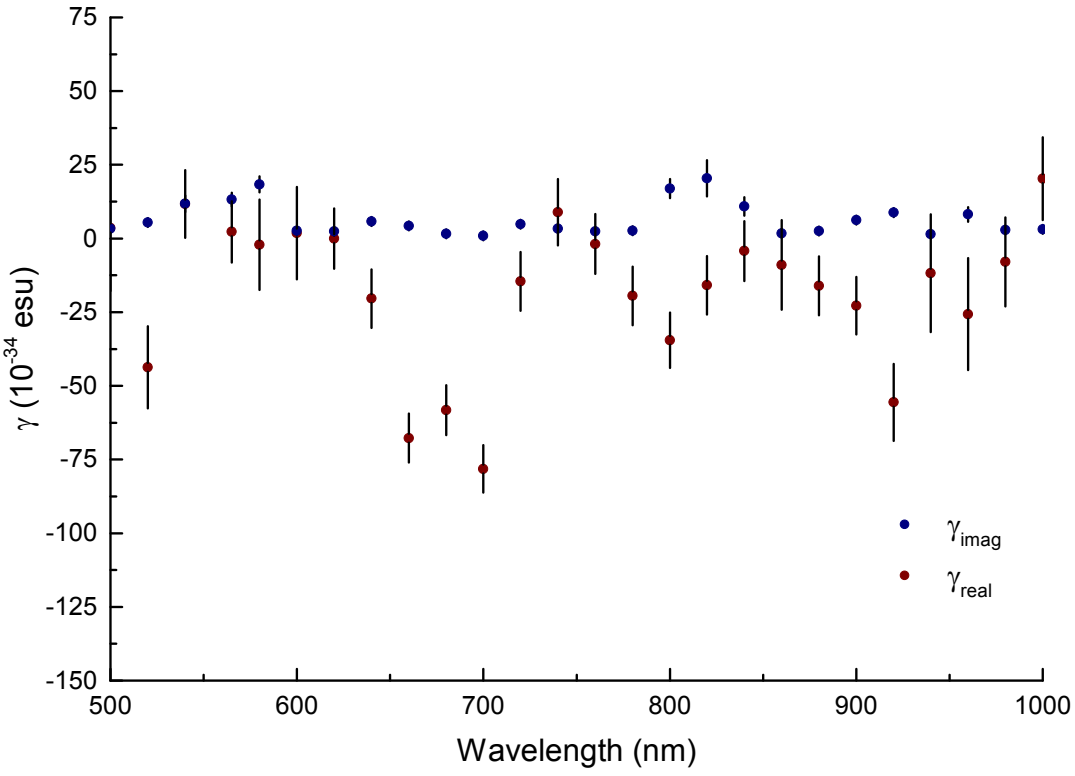

Figure S85. Plot of the real (red) and imaginary (blue) parts of the third-order hyperpolarizability of **10b**.

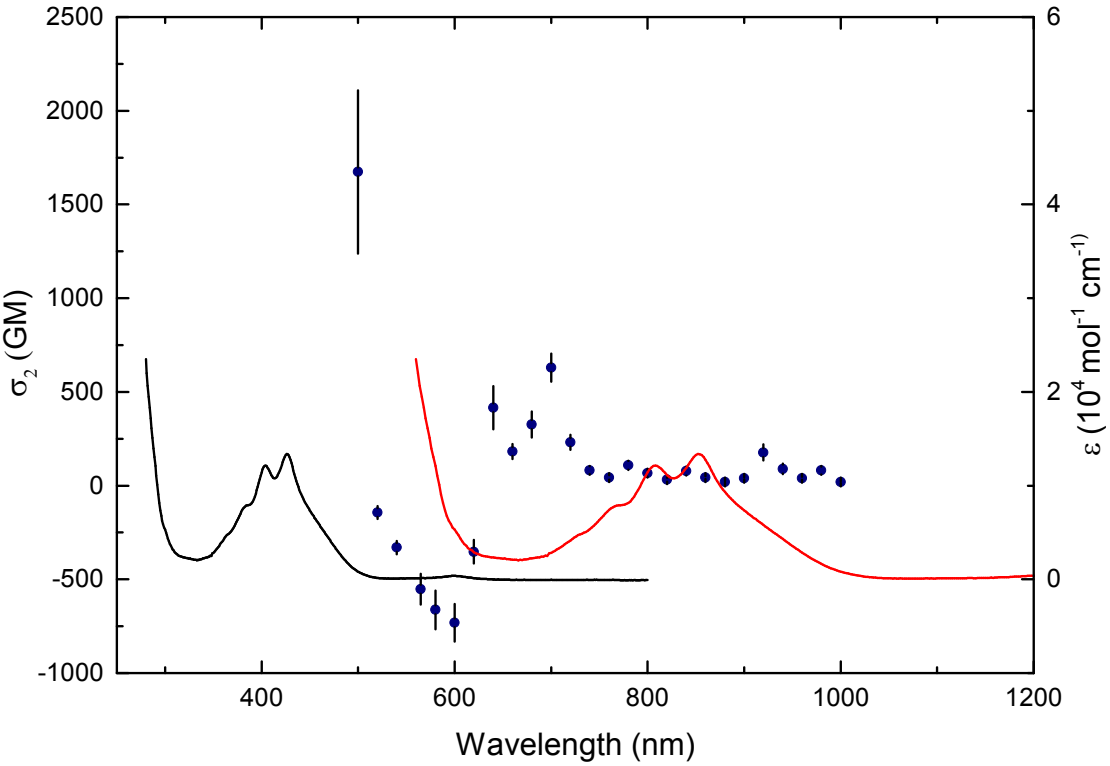

Figure S86. Plot of σ_2 (blue) for Au(C≡C-10-$C_{14}H_8$-9-NO_2)(PPh_3) (**10c**) overlaid on the UV-visible spectrum (black), and including a plot of the UV-visible spectrum at twice the wavelength (red)

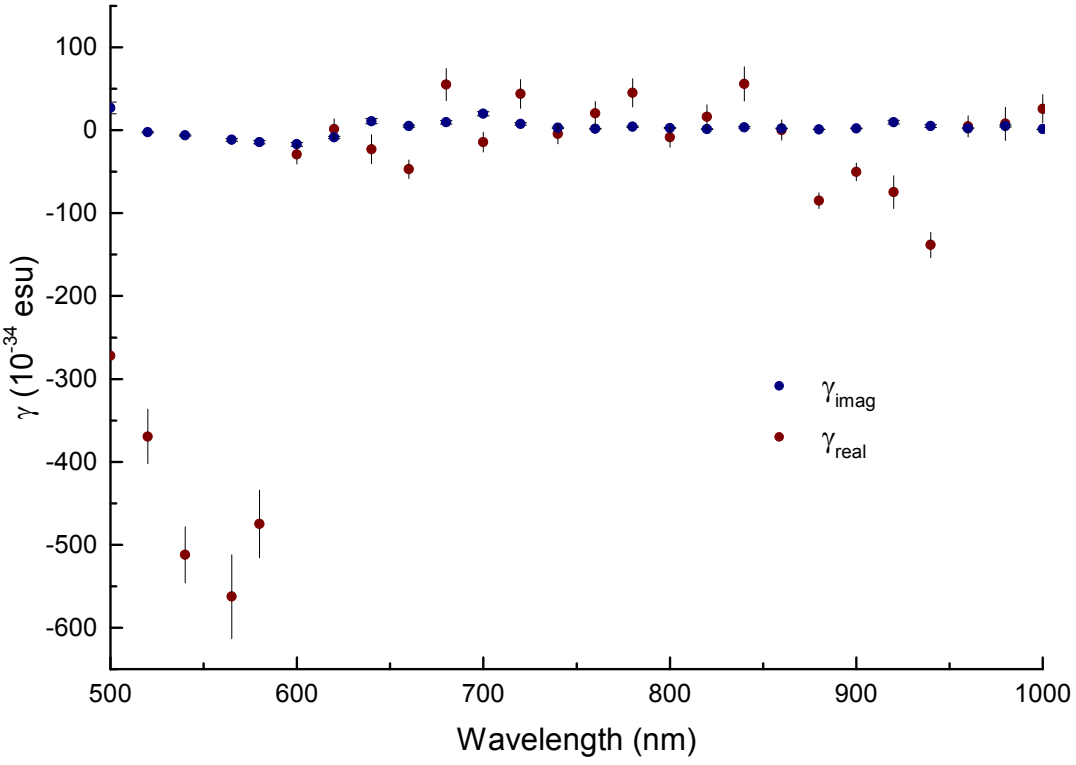

Figure S87. Plot of the real (red) and imaginary (blue) parts of the third-order hyperpolarizability of **10c**.

Theoretical Data

XYZ coordinates of the model complexes **7a′**, **7b′**, **7c′**, **8a′**, **9a′**, and **10a′**

7a′; E_h = –2830.9431628

Ru	0.00000	0.00000	1.51111
Cl	0.00000	0.00000	4.08277
P	1.39667	1.90944	1.61404
P	-1.39667	1.90944	1.61404
P	1.39667	-1.90944	1.61404
P	-1.39667	-1.90944	1.61404
C	0.00000	0.00000	-0.47374
C	0.00000	0.00000	-1.71188
C	0.00000	-3.07547	2.06973
H	0.00000	-4.05890	1.58439
H	0.00000	-3.21051	3.15696
C	0.00000	3.07547	2.06973
H	0.00000	4.05890	1.58439
H	0.00000	3.21051	3.15696
C	0.00000	0.00000	-3.12726
C	0.00000	1.21267	-3.86619
C	0.00000	-1.21267	-3.86619
C	0.00000	1.21760	-5.25143
H	0.00000	2.15409	-3.32523
C	0.00000	-1.21760	-5.25143
H	0.00000	-2.15409	-3.32523
C	0.00000	0.00000	-5.93955
H	0.00000	2.14284	-5.81493
H	0.00000	-2.14284	-5.81493
N	0.00000	0.00000	-7.39413
O	0.00000	-1.09118	-7.97410
O	0.00000	1.09118	-7.97410
C	2.16454	2.64425	0.10443
H	3.03405	2.04384	-0.18323
H	1.45088	2.60370	-0.72229
H	2.48427	3.67833	0.27557
C	-2.16454	2.64425	0.10443
H	-1.45088	2.60370	-0.72229
H	-3.03405	2.04384	-0.18323
H	-2.48427	3.67833	0.27557
C	2.16454	-2.64425	0.10443
H	1.45088	-2.60370	-0.72229
H	3.03405	-2.04384	-0.18323
H	2.48427	-3.67833	0.27557
C	-2.16454	-2.64425	0.10443
H	-3.03405	-2.04384	-0.18323
H	-1.45088	-2.60370	-0.72229

H	-2.48427	-3.67833	0.27557
C	2.69799	2.15747	2.89997
H	2.95938	3.21557	3.01378
H	2.32361	1.75757	3.84612
H	3.59777	1.60020	2.61692
C	-2.69799	2.15747	2.89997
H	-2.32361	1.75757	3.84612
H	-2.95938	3.21557	3.01378
H	-3.59777	1.60020	2.61692
C	2.69799	-2.15747	2.89997
H	2.32361	-1.75757	3.84612
H	2.95938	-3.21557	3.01378
H	3.59777	-1.60020	2.61692
C	-2.69799	-2.15747	2.89997
H	-2.95938	-3.21557	3.01378
H	-2.32361	-1.75757	3.84612
H	-3.59777	-1.60020	2.61692

7b′; E_h = –2984.5767798

Ru	0.01999	-1.94236	0.00000
Cl	-0.10028	-4.49939	0.00000
P	-1.88038	-1.78778	1.40091
P	-1.88038	-1.78778	-1.40091
P	1.92274	-2.20018	1.39720
P	1.92274	-2.20018	-1.39720
C	0.16843	0.03703	0.00000
C	0.27208	1.27243	0.00000
C	3.03328	-2.77412	0.00000
H	4.06430	-2.40037	0.00000
H	3.04417	-3.86949	0.00000
C	-3.07858	-1.42750	0.00000
H	-3.34371	-0.36400	0.00000
H	-4.00207	-2.01828	0.00000
C	0.46710	2.67216	0.00000
C	-0.64646	3.60010	0.00000
C	1.76209	3.20411	0.00000
C	-0.43436	5.02534	0.00000
C	-1.97155	3.09803	0.00000
C	1.98269	4.57859	0.00000
H	2.61073	2.52758	0.00000
C	-1.58698	5.86196	0.00000
C	0.93029	5.48366	0.00000
C	-3.06362	3.93653	0.00000
H	-2.09606	2.01993	0.00000
H	2.99111	4.97153	0.00000
C	-2.86014	5.33047	0.00000
H	-1.45033	6.93131	0.00000

H	-4.07144	3.52942	0.00000
H	-3.71423	6.00279	0.00000
N	1.31950	6.89129	0.00000
O	2.52832	7.15781	0.00000
O	0.44762	7.76955	0.00000
C	2.79416	-0.74942	2.13565
H	2.81219	0.07148	1.41455
H	2.23753	-0.40309	3.01286
H	3.81560	-1.00471	2.43927
C	2.79416	-0.74942	-2.13565
H	2.23753	-0.40309	-3.01286
H	2.81219	0.07148	-1.41455
H	3.81560	-1.00471	-2.43927
C	-2.14806	-0.43962	-2.63566
H	-1.81204	0.50889	-2.20803
H	-1.54623	-0.64282	-3.52816
H	-3.20072	-0.36373	-2.93060
C	-2.14806	-0.43962	2.63566
H	-1.54623	-0.64282	3.52816
H	-1.81204	0.50889	2.20803
H	-3.20072	-0.36373	2.93060
C	2.06714	-3.47991	-2.71964
H	3.11293	-3.66877	-2.98709
H	1.59767	-4.39884	-2.35891
H	1.53059	-3.13925	-3.61220
C	2.06714	-3.47991	2.71964
H	1.59767	-4.39884	2.35891
H	3.11293	-3.66877	2.98709
H	1.53059	-3.13925	3.61220
C	-2.57210	-3.26926	-2.25666
H	-2.48942	-4.13473	-1.59432
H	-3.61498	-3.11072	-2.55374
H	-1.97395	-3.47886	-3.14968
C	-2.57210	-3.26926	2.25666
H	-3.61498	-3.11072	2.55374
H	-2.48942	-4.13473	1.59432
H	-1.97395	-3.47886	3.14968

7c′; E_h = –3138.1965383

Ru	0.00000	0.00000	2.24504
Cl	0.00000	0.00000	4.79015
P	1.40696	1.91140	2.25665
P	-1.40696	1.91140	2.25665
P	1.40696	-1.91140	2.25665
P	-1.40696	-1.91140	2.25665
C	0.00000	0.00000	0.26057
C	0.00000	0.00000	-0.98103

C	0.00000	-3.14796	2.09517
H	0.00000	-3.62074	1.10636
H	0.00000	-3.93792	2.85545
C	0.00000	3.14796	2.09517
H	0.00000	3.62074	1.10636
H	0.00000	3.93792	2.85545
C	0.00000	0.00000	-2.39130
C	0.00000	1.23072	-3.11801
C	0.00000	-1.23072	-3.11801
C	0.00000	1.25283	-4.56226
C	0.00000	2.45108	-2.38298
C	0.00000	-1.25283	-4.56226
C	0.00000	-2.45108	-2.38298
C	0.00000	2.55979	-5.15845
C	0.00000	0.00000	-5.27480
C	0.00000	3.67464	-2.99930
H	0.00000	2.37311	-1.30196
C	0.00000	-2.55979	-5.15845
C	0.00000	-3.67464	-2.99930
H	0.00000	-2.37311	-1.30196
C	0.00000	3.71355	-4.40960
H	0.00000	2.64263	-6.22876
H	0.00000	4.59299	-2.41808
H	0.00000	-2.64263	-6.22876
C	0.00000	-3.71355	-4.40960
H	0.00000	-4.59299	-2.41808
H	0.00000	4.67024	-4.92588
H	0.00000	-4.67024	-4.92588
N	0.00000	0.00000	-6.73675
O	0.00000	-1.07291	-7.35943
O	0.00000	1.07291	-7.35943
C	-2.33716	-2.43910	3.76016
H	-2.63602	-3.49142	3.69355
H	-1.71260	-2.27231	4.64110
H	-3.23450	-1.82002	3.86550
C	-2.33716	2.43910	3.76016
H	-1.71260	2.27231	4.64110
H	-2.63602	3.49142	3.69355
H	-3.23450	1.82002	3.86550
C	-2.58377	2.32364	0.89326
H	-2.11619	2.10934	-0.07101
H	-3.47421	1.69213	0.98535
H	-2.89206	3.37444	0.93118
C	-2.58377	-2.32364	0.89326
H	-3.47421	-1.69213	0.98535
H	-2.11619	-2.10934	-0.07101
H	-2.89206	-3.37444	0.93118

C	2.58377	-2.32364	0.89326
H	2.11619	-2.10934	-0.07101
H	3.47421	-1.69213	0.98535
H	2.89206	-3.37444	0.93118
C	2.33716	-2.43910	3.76016
H	1.71260	-2.27231	4.64110
H	2.63602	-3.49142	3.69355
H	3.23450	-1.82002	3.86550
C	2.33716	2.43910	3.76016
H	2.63602	3.49142	3.69355
H	1.71260	2.27231	4.64110
H	3.23450	1.82002	3.86550
C	2.58377	2.32364	0.89326
H	3.47421	1.69213	0.98535
H	2.11619	2.10934	-0.07101
H	2.89206	3.37444	0.93118

8a'; E_h = –1723.0445408

Ru	-0.50165	-1.90365	0.00000
P	0.98606	-1.92845	1.75960
P	0.98606	-1.92845	-1.75960
C	-1.68027	-3.90810	0.00000
C	-2.06046	-3.14451	1.14858
C	-2.06046	-3.14451	-1.14858
H	-1.24897	-4.89989	0.00000
C	-2.67368	-1.93316	0.71731
H	-1.93483	-3.45455	2.17841
C	-2.67368	-1.93316	-0.71731
H	-1.93483	-3.45455	-2.17841
H	-3.07713	-1.15716	1.35337
H	-3.07713	-1.15716	-1.35337
C	-0.29208	0.07775	0.00000
C	-0.20128	1.31113	0.00000
C	-0.16506	2.72735	0.00000
C	-1.36282	3.48892	0.00000
C	1.06365	3.43688	0.00000
C	-1.33712	4.87415	0.00000
H	-2.31304	2.96442	0.00000
C	1.09823	4.82218	0.00000
H	1.99300	2.87534	0.00000
C	-0.10452	5.53512	0.00000
H	-2.25003	5.45736	0.00000
H	2.03512	5.36599	0.00000
N	-0.07265	6.99033	0.00000
O	1.03092	7.54605	0.00000
O	-1.15057	7.59381	0.00000
C	0.21669	-1.26990	3.31330

H	-0.66964	-1.85511	3.57536
H	0.91970	-1.29294	4.15411
H	-0.09855	-0.23830	3.13008
C	2.55105	-0.93914	1.74192
H	3.28951	-1.39604	1.07828
H	2.32647	0.06785	1.38112
H	2.97908	-0.87873	2.74863
C	1.61228	-3.58203	2.32408
H	2.21045	-4.03694	1.52806
H	2.22634	-3.49545	3.22839
H	0.76753	-4.24660	2.53018
C	1.61228	-3.58203	-2.32408
H	2.22634	-3.49545	-3.22839
H	2.21045	-4.03694	-1.52806
H	0.76753	-4.24660	-2.53018
C	0.21669	-1.26990	-3.31330
H	0.91970	-1.29294	-4.15411
H	-0.66964	-1.85511	-3.57536
H	-0.09855	-0.23830	-3.13008
C	2.55105	-0.93914	-1.74192
H	2.32647	0.06785	-1.38112
H	3.28951	-1.39604	-1.07828
H	2.97908	-0.87873	-2.74863

9a′; E_h = –1337.9096074

Ni	-1.80344	-1.64679	0.00000
C	-3.52678	-2.90221	0.00000
C	-3.62966	-2.07602	1.16841
C	-3.62966	-2.07602	-1.16841
H	-3.49684	-3.98507	0.00000
C	-3.62966	-0.74295	0.72592
H	-3.62300	-2.41739	2.19500
C	-3.62966	-0.74295	-0.72592
H	-3.62300	-2.41739	-2.19500
H	-3.63131	0.14254	1.34771
H	-3.63131	0.14254	-1.34771
P	-0.12844	-3.02697	0.00000
C	-0.62205	-0.23330	0.00000
C	0.17000	0.70777	0.00000
C	1.04834	1.82470	0.00000
C	2.45290	1.65139	0.00000
C	0.53984	3.14581	0.00000
C	3.31110	2.74113	0.00000
H	2.85889	0.64471	0.00000
C	1.39061	4.24135	0.00000
H	-0.53517	3.29299	0.00000
C	2.77142	4.02927	0.00000

H	4.38704	2.61660	0.00000
H	1.00935	5.25518	0.00000
N	3.67189	5.18004	0.00000
O	3.16846	6.30609	0.00000
O	4.88620	4.96166	0.00000
C	0.99511	-2.84381	1.44991
H	1.86504	-3.50500	1.36660
H	1.32187	-1.80264	1.50681
H	0.44767	-3.08178	2.36727
C	0.99511	-2.84381	-1.44991
H	1.32187	-1.80264	-1.50681
H	1.86504	-3.50500	-1.36660
H	0.44767	-3.08178	-2.36727
C	-0.49940	-4.83969	0.00000
H	0.42394	-5.43009	0.00000
H	-1.08539	-5.09866	0.88713
H	-1.08539	-5.09866	-0.88713

10a'; E_h = –1109.2386072

Au	-0.12723	-1.86776	0.00000
P	-0.29637	-4.20117	0.00000
C	0.01605	0.12156	0.00000
C	0.10204	1.34555	0.00000
C	0.19825	2.76456	0.00000
C	1.45889	3.40389	0.00000
C	-0.96586	3.56630	0.00000
C	1.55553	4.78840	0.00000
H	2.35699	2.79513	0.00000
C	-0.87743	4.95126	0.00000
H	-1.93701	3.08257	0.00000
C	0.38451	5.54879	0.00000
H	2.51530	5.29022	0.00000
H	-1.76189	5.57630	0.00000
N	0.48224	7.00948	0.00000
O	-0.56733	7.65641	0.00000
O	1.60862	7.51083	0.00000
C	0.48224	-5.03061	1.45015
H	0.01687	-4.66854	2.37175
H	0.36727	-6.11862	1.39119
H	1.54706	-4.78214	1.48673
C	-2.02184	-4.84985	0.00000
H	-2.55030	-4.48469	-0.88558
H	-2.03178	-5.94544	0.00000
H	-2.55030	-4.48469	0.88558
C	0.48224	-5.03061	-1.45015
H	0.36727	-6.11862	-1.39119
H	0.01687	-4.66854	-2.37175

H	1.54706	-4.78214	-1.48673

References

[1] J. Du, G. J. Moxey, *Acta Cryst.* 2015, **E71**, o311-o312.

[2] R. G. Gieling, *Sel. Org. React. Database* 2003.

[3] H. Zhao, P. V. Simpson, A. Barlow, G. J. Moxey, M. Morshedi, N. Roy, R. Philip, C. Zhang, M. P. Cifuentes, M. G. Humphrey, *Chem. Eur. J.* 2015, **21**, 11843 - 11854.

[4] B. Chaudret, G. Commenges, R. Poilblanc, *J. Chem. Soc., Dalton Trans.* 1984, 1635-1639.

[5] M. I. Bruce, C. Hamiester, A. G. Swincer, R. C. Wallis, *Inorg. Synth.* 1982, **21**, 78.

[6] K. W. Barnett, *J. Chem. Educ.* 1974, **51**, 422.

[7] M. I. Bruce, B. K. Nicholson, O. bin Shawkataly, *Inorg. Synth.* 1989, **26**, 324.

[8] D. Touchard, P. Haquette, S. Guesmi, L. L. Pichon, A. Daridor, L. Toupet, P. H. Dixneuf, *Organometallics* 1997, **16**, 3640-3648.

[9] A. M. McDonagh, I. R. Whittall, M. G. Humphrey, B. W. Skelton, A. H. White, *J. Organomet. Chem.* 1996, **519**, 229-235.

[10] I. R. Whittall, M. G. Humphrey, D. C. R. Hockless, B. W. Skelton, A. H. White, *Organometallics* 1995, **14**, 3970-3979.

[11] I. R. Whittall, M. P. Cifuentes, M. G. Humphrey, B. Luther-Davies, M. Samoc, S. Houbrechts, A. Persoons, G. A. Heath, D. Bogsanyi, *Organometallics* 1997, **16**, 2631-2637.

[12] I. R. Whittall, M. G. Humphrey, S. Houbrechts, A. Persoons, D. C. R. Hockless, *Organometallics* 1996, **15**, 5738-5745.

[13] A. L. Korich, T. S. Hughes, *Org. Lett.* 2008, **10**, 5405-5408.

[14] J. Rigaudy, A. M. Seuleiman, *Tetrahedron* 1982, **38**, 3157-3161.

[15] M. J. Frisch, G. W. Trucks, H. B. Schlegel, G. E. Scuseria, M. A. Robb, J. R. Cheeseman, J. A. Montgomery, Jr., T. Vreven, K. N. Kudin, J. C. Burant, J. M. Millam, S. S. Iyengar, J. Tomasi, V. Barone, B. Mennucci, M. Cossi, G. Scalmani, N. Rega, G. A. Petersson, H. Nakatsuji, M. Hada, M. Ehara, K. Toyota, R. Fukuda, J. Hasegawa, M. Ishida, T. Nakajima, Y. Honda, O. Kitao, H. Nakai, M. Klene, X. Li, J. E. Knox, H. P. Hratchian, J. B. Cross, C. Adamo, J. Jaramillo, R. Gomperts, R. E. Stratmann, O. Yazyev, A. J. Austin, R. Cammi, C. Pomelli, J. W. Ochterski, P. Y. Ayala, K. Morokuma, G. A. Voth, P. Salvador, J. J. Dannenberg, V. G. Zakrzewski, S. Dapprich, A. D. Daniels, M. C. Strain, O. Farkas, D. K. Malick, A. D. Rabuck, K. Raghavachari, J. B. Foresman, J. V. Ortiz, Q. Cui, A. G. Baboul, S. Clifford, J. Cioslowski, B. B. Stefanov, G. Liu, A. Liashenko, P. Piskorz, I. Komaromi, R. L. Martin, D. J. Fox, T. Keith, M. A. Al-Laham, C. Y. Peng, A. Nanayakkara, M. Challacombe, P. M. W. Gill, B. Johnson, W. Chen, M. W. Wong, C. Gonzalez, J. A. Pople, Gaussian Inc., Pittsburgh, PA, 2003.

[16] A. D. Becke, *J. Chem. Phys.* 1993, *98*, 5648-5652; bC. Lee, W. Yang, R. G. Parr, *Phys. Rev. B* 1988, **37**, 785-789.

[17] C. Adamo, V. Barone, *J. Phys. Chem.* 1999, **110**, 6158-6170.

[18] D. Andrae, U. Haeussermann, M. Dolg, H. Stoll, H. Preuss, *Theor. Chem. Acc.* 1980, **77**, 123-141.

[19] N. M. O'Boyle, A. L. Tenderholt, K. M. Langner, *J. Comp. Chem.* 2008, **29**, 839 - 845.

[20] J. Cosier, A. M. Glazer, *J. Appl. Cryst.* 1986, **19**, 105-107.

[21] P. Coppens, in *Crystallographic Computing* (Eds.: F. R. Ahmed, S. R. Hall, C. P. Huber), Munksgaard, Copenhagen, 1970, pp. 255-270.

[22] R. C. Clark, J. S. Reid, *Acta Crystallogr., Sect. A: Found. Crystallogr.* 1995, **51**, 887-897.

[23] CrysAlisPro, Agilent Technologies, Yarnton, England, 2013.

[24] G. M. Sheldrick, *Acta Cryst., A* 2008, **A64**, 112-122.

[25] G. M. Sheldrick, *Acta Crystallogr., Sect. A: Found. Crystallogr.* 2015, **C71**, 3-8.

[26] O. V. Dolomanov, L. J. Bourhis, R. J. Gildea, J. A. K. Howard, H. Puschmann, *J. Appl. Crystallogr.* 2009, **42**, 339-341.

[27] A. J. Hodge, S. L. Ingham, A. K. Kakkar, M. S. Khan, J. Lewis, N. J. Long, D. G. Parker, P. R. Raithby, *J. Organomet. Chem.* 1995, **488**, 205-210.

[28] I. R. Whittall, M. G. Humphrey, D. C. R. Hockless, *Aust. J. Chem.,* 1998, **51**, 219.

[29] K. Clays, A. Persoons, *Rev. Sci. Instrum.* 1992, **63**, 3285-3289.

[30] L. M. Tomalino, A. Voronov, A. Kohut, W. W. Peukert, *J. Phys. Chem.* 2008, **B112**, 6338-6343.

[31] M. Sheik-Bahae, A. A. Said, T. Wei, D. J. Hagan, E. W. van Stryland, *IEEE J. Quantum Electr.* 1990, **26**, 760-769.